MAGYAR ÁLLAMI
EÖTVÖS LORÁND
GEOFIZIKAI INTÉZET

EÖTVÖS LORÁND
GEOPHYSICAL INSTITUTE
OF HUNGARY

GEOFIZIKAI KÖZLEMÉNYEK

GEOPHYSICAL TRANSACTIONS

ВЕНГЕРСКИЙ
ГЕОФИЗИЧЕСКИЙ
ИНСТИТУТ
ИМ Л. ЭТВЕША

ГЕОФИЗИЧЕСКИЙ
БЮЛЛЕТЕНЬ

CONTENTS

VOL. 30. NO. 2. JULY 1984. (ISSN 0016—7177)

BUDAPEST

TARTALOMJEGYZÉK

СОДЕРЖАНИЕ

GEOPHYSICAL TRANSACTIONS 1984
Vol. 30. No. 2. pp. 121—139

SPECTRAL STRUCTURE OF REFLECTION SEISMOGRAMS FROM INSTANTANEOUS FREQUENCY DISPLAYS

J. G. SAHA*

The spectral characteristic of seismograms often resembles processes with mixed spectra. Such processes are usually nonstationary. Instantaneous phase/instantaneous frequencies derived from analytical signal technique enable one to detect the quasiharmonics present in a seismogram. The method is valid irrespective of whether the process is stationary or not. Time evolution and decay of such quasiharmonics can also be estimated with sufficient accuracy from instantaneous frequency displays.

d: theoretical seismograms, energy spectrum, instantaneous frequency, Hilbert transform

1. Introduction

A signal or a seismic trace (time series) can be described by certain parameters such as envelope, instantaneous phase and "instantaneous frequency" (IF). These parameters have been applied in geological interpretations [TANER et al. 1979]. The envelope of a signal is related to its strength and the phase may be understood by the number of accumulated cycles starting from a given time. The IF is defined as the derivative of instantaneous phase (or phase velocity which can also be negative). Although it can be defined clearly in mathematical terms, it is obviously not the same as that of Fourier frequency. In fact an IF that is present in a signal can fail to show up in the Fourier decomposition of the signal. In certain cases the IF will have values for which the Fourier spectrum of the signal vanishes [MANDEL 1974]. It has been pointed out that the frequency decomposition through the Fourier transform technique cannot describe the local non-stationarities in time whereas the IF plots emphasize these non-stationarities. We may state that IF plots represent a stochastic process where local non-stationarities in phase velocities are displayed. So, in general, one should be extremely cautious in associationg the IF with the usual frequency interpretation of seismic sections.

The derivatives of instantaneous phase (instantaneous frequency) with time of a reflection seismogram represent essentially a stochastic process. The term "instantaneous frequency" has been objected to by many authors for the reason that one cannot embrace simultaneously two mutually exclusive variables such as Fourier frequency and time. However, the so-called instantaneous frequency

* K.D.M. Institute of Petroleum Exploration, 9, Kaulagarch Road, Dehradun 248195, India
Manuscript received: 23 October, 1983

can be identified with Fourier frequency in certain cases and for narrow-band signals the mean square bandwidth is equal to the variance of the instantaneous frequency with appropriate weighting factor. This can be proved from signal energy distribution function with time and frequency. The distribution function directly leads to the well-known Fourier uncertainty and a short time spectrum can also be defined as proposed first by De Bruijn.

Most of the above aspects of IF are well-known. However one can show that statistical averages of Fourier frequency and IF, when appropriately weighted, are approximately equal (if the process has an envelope which is slowly varying with time). For example, the variance of IF with respect to Fourier mean frequency is related to the mean square bandwidth of the signal. We recall that when a wavemeter is tuned to a particular Fourier frequency with a modulated signal as input, we obtain a spike only when the IF runs through the Fourier frequency being measured [VAKMAN 1964]. From the principle of stationary phase it can be shown that the spectral density at any Fourier frequency is determined from the contributions of the integral during times when the IF coincides with the Fourier frequency. In this paper we will show that most of the relations connecting the IF and the Fourier frequency can be derived from the concept of signal energy density in time and frequency. Further, the spectral model of any complex process such as of a reflection seismogram can often be ascertained from its IF displays.

2. Signal representation

We represent a real signal or a seismic trace $f(t)$ by

$$f(t) = A(t)\cos\Theta(t) = A(t)\cos[\omega_0 t + \Phi(t)], \tag{1}$$

$A(t)$ and $\Theta(t)$ are the envelope and the phase respectively; may be termed as the slow part of the phase; ω_0 in the case of a seismic signal or seismic trace may be considered as the mean frequency about which the signal is centred in the frequency domain. In equation (1) the splitting of the signal into an amplitude part and an oscillatory part is obviously arbitrary and thus the representation is not unique. We consider next the complex representation of a signal:

$$\Psi(t) = f(t) + i\hat{f}(t) \tag{2}$$

$$= A(t)e^{i\Theta(t)} \tag{2a}$$

where

$$A(t) = \sqrt{f^2(t) + \hat{f}^2(t)} \tag{2b}$$

$$\Theta(t) = \arctan[\hat{f}(t)/f(t)] \tag{2c}$$

and "instantaneous frequency" is,

$$\omega(t) = \frac{\mathrm{d}\Theta(t)}{\mathrm{d}t} = \frac{f(t)\hat{f}'(t) - \hat{f}(t)f'(t)}{f^2(t) + \hat{f}^2(t)} \tag{2d}$$

To determine $\omega(t)$ we need not know $\Theta(t)$, if $\hat{f}(t)$ is known. We assume that $\hat{f}(t)$ is derivable through a linear operation on $f(t)$, viz. $\hat{f}(t) = \mathrm{L}f(t) = f(t) * k(t)$, where $k(t)$ is real operator and $*$ denotes convolution. It can be shown [MANDEL 1967] that $k(t)$ is uniquely determined when the signal is narrow band and is given by

$$k(t) = -\frac{1}{\pi} P\left(\frac{1}{t}\right) \tag{3}$$

or

$$\hat{f}(t) = \frac{1}{\pi} P \int \frac{f(\tau)}{\tau - \mathrm{t}} \mathrm{d}\tau \tag{4}$$

P denotes Cauchy's principal value. Henceforth limits of all integrals are from $-\infty$ to $+\infty$. The complex signal in equation (2) where $\hat{f}(t)$ is given by equation (4) is know as an analytic signal.

3. The "two frequencies"

Let us consider a vibration of the following form [VAKMAN 1973]:

$$f(t) = A_0 \sin^3 \omega_0 t \tag{5a}$$

The signal $\sin^3 \omega_0 t$ consist of two vibrations: $\sin \omega_0 t$ and $\sin 3\,\omega_0 t$. When we apply the analytic signal technique we obtain:

$$A(t) = A_0 \sqrt{\frac{5}{8} - \frac{3}{8}\cos 2\,\omega_0 t} \tag{5b}$$

$$\omega(t) = \frac{\frac{3}{4} - \frac{3}{4}\cos 2\,\omega_0 t}{\frac{5}{8} - \frac{3}{8}\cos 2\,\omega_0 t} \cdot \omega_0 \tag{5c}$$

We find that $A\,(t)$ changes from $1/2A_0$ to A_0 and $\omega(t)$ from 0 to $3/2\omega_0$ with a period of $1/2\omega_0$. We consider now a complex signal [MANDEL 1974]:

$$\Psi(t) = a_1 \exp\left[-i\left(\omega_0 - \frac{1}{2}\Delta\omega\right)t\right] + a_2 \exp\left[-i\left(\omega_0 + \frac{1}{2}\Delta\omega\right)t\right], \quad a_1 \neq a_2, \quad \Delta\omega \ll \omega_0 \tag{6a}$$

$\Psi(t)$ represents a combination of two sinusoidal oscillations with frequencies symmetrically placed with respect to ω_0. On application of the same technique:

$$\omega(t) = \omega_0 + \frac{1}{2}\Delta\omega\left(\frac{-a_1^2 + a_2^2}{a_1^2 + a_2^2 + 2a_1 a_2 \cos \Delta\omega t}\right) \tag{6b}$$

When $\cos \Delta\omega t = 1$,

$$\omega(t) = \omega_0 + \frac{1}{2}\Delta\omega\frac{a_2 - a_1}{a_2 + a_1} \tag{7a}$$

and for $\cos \Delta\omega t = -1$,

$$\omega(t) = \omega_0 + \frac{1}{2}\Delta\omega\frac{a_2 + a_1}{a_2 - a_1}. \tag{7b}$$

It is obvious that the deflections of $\omega(t)$ about ω_0 are not symmetrical and no Fourier components are present with frequencies as high as given by equation (7b). However the distributions of "instantaneous frequencies" of a signal and the spectral distributions of the signals are related by:

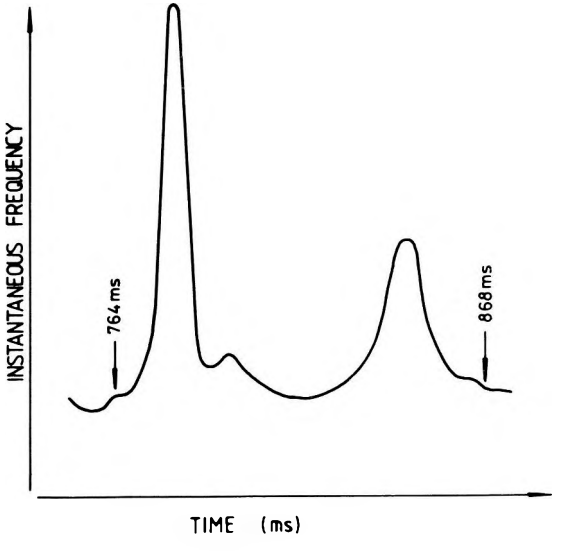

Fig. 1a. Instantaneous frequency of a segment of seismic trace: time window 764 ms—868 ms

1a. ábra. Egy szeizmogram szakasz pillanatnyi frekvencia függvénye. Időablak: 764 ms—868 ms

Рис. 1а. Мгновенная частота от сегмента сейсмической трассы: временное окно 764 мс—868 мс

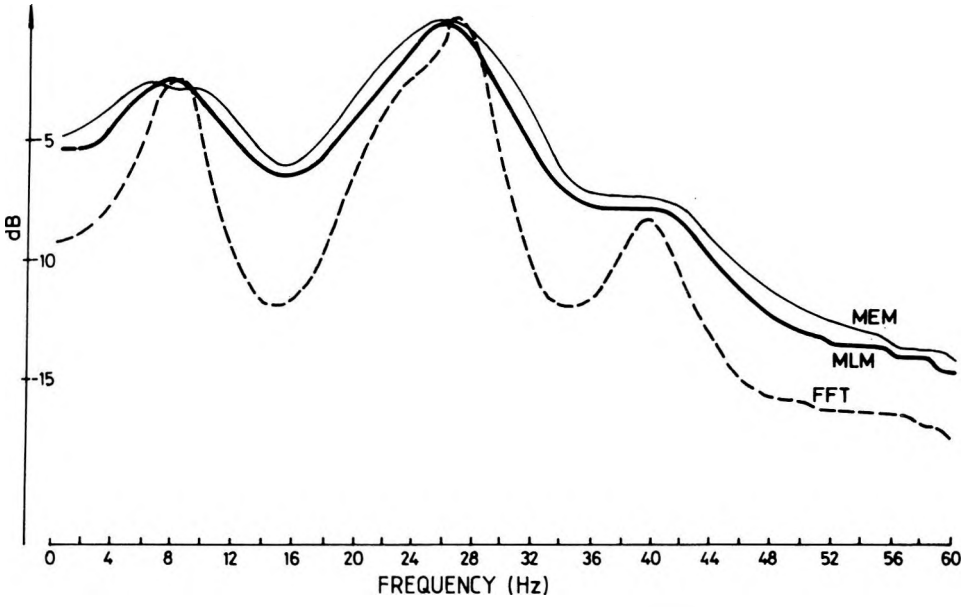

Fig. 1b. Spectral power estimate of the same segment of seismic trace FFT–Fast Fourier Transform; MLM–Maxiumum Likelihood Method; MEM–Maximum Entropy Method

1b ábra. Ugyanazon szeizmogram szakasz spektrális energia eloszlása

Рис. 1b. Оценка спектральной мощности по сегменту сейсмической трассы: временное окно 764 мс—868 мс

$$\int (\omega-\omega_0)^2 \Psi(\omega)\mathrm{d}\omega = \int [\omega(t)-\omega_0]^2 A^2(t)\mathrm{d}t \tag{8a}$$

$\Psi(\omega)$ is the spectral density,

$$\int \Psi^2(\omega)\mathrm{d}\omega = \int A^2(t)\mathrm{d}t, \quad \text{by Parseval's theorem} \tag{8b}$$

The left hand side of equation (8a) is the mean square bandwidth. For convenience we assume the integrals in (8b) are equal to unity. The relation in equation (8a) is approximately true. One has to assume here a slowly varying envelope. MANDEL [1974] has shown that this relation is also true for a stationary stochastic process. So there is no one to one relationship between these two "frequencies". This is because the two quantities are fundamentally different. *Figure 1a* shows sample by sample IF plots of a segment of one reflection seismic trace. The power spectral estimates for the same window are shown in *Figure 1b* where estimates have been calculated by different methods as per the

prescription of LACOSS [1971]. It is seen that the peak frequency where the spectral power becomes maximum is absent in all the IF values within the same time window.

4. Sturm—Liouville problem

We recall that solutions of certain non-linear differential equations of Mathieu—Hill type represent oscillations with modulation in time of both amplitude and frequency. However these equations are not suitable for describing a seismic trace. Solutions of such equations often show that the maximum amplitude and minimum "instantaneous frequency" (maximum apparent period of one oscillation) occur together in time. This is not generally true for a seismic trace. We now deal with solutions of the following type of linear second-order homogeneous differential equation of Sturm—Liouville (SL) type:

$$U'' + a(t)U = 0 \tag{9}$$

The solutions of equation (9) will have three different regimes and being interested in the oscillatory regime we assume $a(t) = g^2(t)$. If $g(t)$ is sufficiently large we can obtain an approximate solution by the WBK method:

$$U(t) = \frac{A_0}{\sqrt{g(t)}} \exp\left[\mathrm{i}\int g\,\mathrm{d}t - \Theta_0\right] \tag{10}$$

The solution shows that the amplitude is closely coupled with "instantaneous frequency". In fact it is true for a large class of signals and to quote Cornelius LANCZOS [1961] "the amplitude of the vibration is always inversely proportional to the square root of the IF. The law of zeros in the oscillations of Bessel functions, Laguerre or Hermite type of polynomials is not independent of the law according to which maxima of successive oscillations change". We should note that the solution is not unique and the separation of amplitude and frequency can occur in infinitely many ways. We next consider the following SL equation:

$$\frac{\mathrm{d}^2U(t)}{\mathrm{d}t^2} + [\omega(t) - \omega_0]^2 U(t) = 0 \tag{11}$$

where $U(t) = \Psi(t) \exp(-\mathrm{i}\omega_0 t)$ is the complex envelope. The assumption of the narrow band nature of signals means that the variation of $\left|\frac{\mathrm{d}U}{\mathrm{d}t}\right|$ should be as small as possible. We recall the connection between SL equations and calculus of variations and consider the following quadratic functional [BELLMAN 1970]:

$$J(U) = \int (U'^2 - g^2(t)U^2)\mathrm{d}t \tag{12}$$

where $g^2(t) = [\omega(t) - \omega_0]^2$.

Any solution of the SL equation is a stationary point for the functional $J(U)$. We search for that particular U which furnishes the absolute minimum of $J(U)$ and in turn will also furnish us with a unique solution of (11). We write (12) as:

$$J(U) = \int \left\{ \left| \frac{\mathrm{d}U}{\mathrm{d}t} \right|^2 - [\omega(t) - \omega_0]^2 A^2(t) \right\} \mathrm{d}t \tag{13}$$

Since the fluctuation of the envelope should be minimum, our extremization problem of $J(U)$ reduces to the problem of finding the conditions for which

$$\int [\omega(t) - \omega_0]^2 A^2(t)\mathrm{d}t \quad \text{is minimum.}$$

From equation (8a) we have:

$$\int [\omega(t) - \omega_0]^2 A^2(t)\mathrm{d}t \cong \int (\omega - \omega_0)^2 \Psi(\omega)\mathrm{d}\omega,$$

$A(t)$ varies slowly with time. The right hand side of the above equation is the variance of spectral density $\Psi(\omega)$ and it will be minimum when he deviation of ω from ω_0 is minimum. This is satisfied when ω_0 is the mean Fourier frequency:

$$\omega_0 \frac{\int \omega(t) A^2(t)\mathrm{d}t}{\int A^2(t)\mathrm{d}t} = \frac{\int \omega \Psi(\omega)\mathrm{d}\omega}{\int \Psi(\omega)\mathrm{d}\omega} \tag{14}$$

So the first moment of $(\omega - \omega_0)$ vanishes. To obtain a unique complex envelope function satisfying SL equation (11), the variational problem reduces to:

$$\int (\omega - \omega_0)^2 \Psi(\omega)\mathrm{d}\omega = \text{minimum} \tag{15a}$$

with the auxiliary condition

$$\int (\omega - \omega_0) \Psi(\omega)\mathrm{d}\omega = 0 \tag{15b}$$

Now $\Psi(\omega)$ is given by MANDEL [1967]:

$$\Psi(\omega) = \frac{1}{4} \Phi(\omega)[1 + \mathrm{i}K(\omega)]^2 \tag{15c}$$

$\Phi(\omega)$ is the spectral density of the real signal $f_a(t)$ and $K(\omega)$ is the Fourier

transform of $k(t)$. By applying standard variational technique, MANDEL [1967] has shown that the integral (15a) is indeed minimum if

$$K(\omega) = -\mathrm{i}\,\mathrm{sgn}\,\omega \tag{16}$$

or in time domain,

$$K(t) = -\frac{1}{\pi} P\left(\frac{1}{t}\right)$$

So we conclude that for a certain class of signals the complex envelope satisfying the SL equation possesses a unique solution when $\hat{f}(t)$ is the Hilbert transform of $f(t)$. Thus,

$$A(t) \approx \frac{A_0}{([\omega(t) - \omega_0]^2)\,\frac{\mathrm{i}}{4}}. \tag{17}$$

The validity of this relation is confined to within the reqime where the WBK soution is acceptable. The motivation of introducing the Sturm—Liouville problem in describing oscillatory processes with varying amplitude and "varying frequency" is now evident. Equation (17) shoes that when the deviation of IF from the mean Fourier frequency is maximum we should expect a minimum of the envelope at that instant. *Figure 2* shows a plot of the evenlope with IF derived from a reflection trace. It shows that the main maxima and minima of the envelope may be predicted with accuracy from a study of IF displays only. The so-called IF is not only a fundamentally different quantity from Fourier frequency, it is also closely coupled with the envelope of the process. In other words the instantenous phase/frequency is not a robust attribute of the signal strength. This follows also from analytic signal theory. When we represent a complex signal such as $\Psi(t) = A(t) \exp(\mathrm{i}\Theta(t)$, $\Psi(t)$ being regular and analytic in the upper half of the complex t plane, the phase and logarithm of the envelope are in quadrature. We also note that two random variables at any particular instant may be orthogonal. But it does not mean that the two processes are uncorrelated [PAPOULIS 1965]. We have a similar situation in the present case.

5. Signal energy distribution in frequency and time

The Fourier method is used to describe a signal either in frequency domain or in time domain, the two domains being mutually exclusive. Evidently a term like "freqency varying with time" is contradictory in the Fourier sense. To describe a signal energy density in frequency and time we attempt to combine

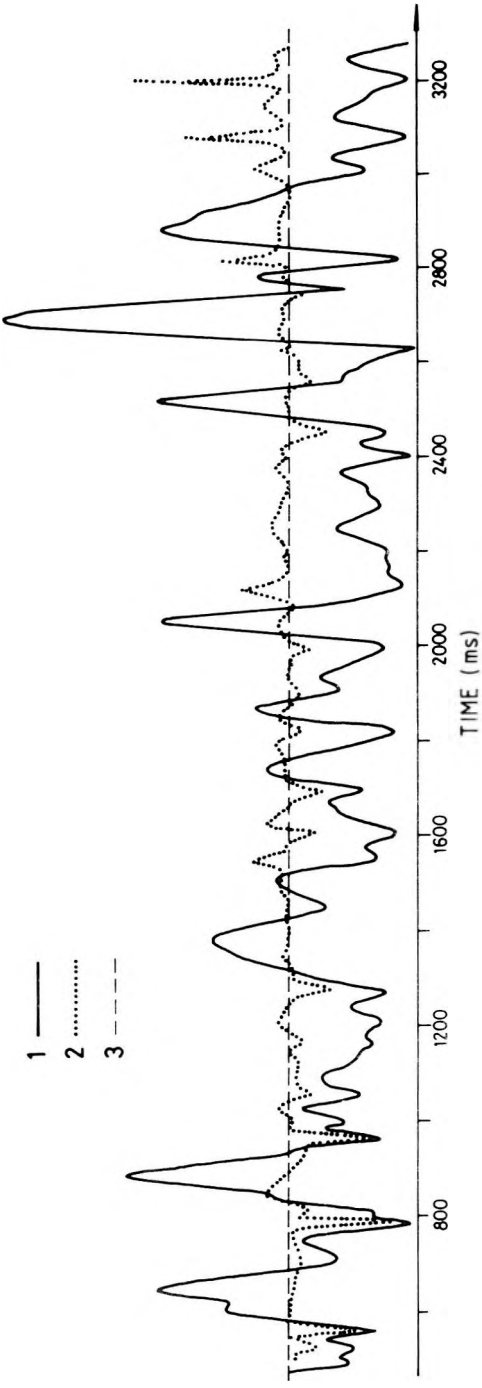

Fig. 2. Envelope and instantaneous frequency plot of a seismic trace
1—envelope; 2—instantaneous frequency; 3—mean Fourier frequency (20 Hz)

2. ábra. Egy szeizmikus jel burkolója és pillanatnyi frekvenciája
1—burkoló; 2—pillanatnyi frekvencia; 3—közepes Fourier frekvencia (20 Hz)

Рис. 2. Огибающая и диаграмма мгновенных частот сейсмической трассы
1—огибающая; 2—мгновенная частота; 3—средняя частота; Фурье (20 Гц)

these two mutually exclusive parameters. Be whatever it may, the existence of signal energy distribution in frequency and time is intuitively correct and a mathematical description of such a phenomenon was introduced by GABOR [1964]. Following RIHACZEK [1968] we define the signal energy density function in t and f as the two-dimensional Fourier transform of the combined autocorrelation function in time and frequency. This is similar to the auto-ambiguity function in Radar theory [VAKMAN 1964]. We take the symmetrical version of the auto-ambiguity function and the corresponding energy density function is:

$$p(t,\omega) = \int \Psi\left(t + \frac{\tau}{2}\right)\Psi^*\left(t - \frac{\tau}{2}\right)e^{-i\omega\tau}d\tau \tag{18}$$

The signal $\Psi(t)$ is given by equation (2a). $p(t, \omega)$ satisfies the following conditions:

$$\int p(t,\omega)d\omega = |\Psi(t)|^2 \tag{19a}$$

$$\int p(t,\omega)dt = |\Psi(\omega)|^2 \tag{19b}$$

$$\int p(t,\omega)dtd\omega = 2E, \tag{20}$$

E is the energy of the signal.
In can be proved that the first order conditional moment

$$\bar{\bar{\omega}} = \frac{\int \omega p(t,\omega)d\omega}{\int p(t,\omega)d\omega} = \frac{d\Theta(t)}{dt} = \omega(t) \tag{21a}$$

The variance of $p(t,\omega)$ at a particular instant

$$\bar{\bar{\omega}}^2 - (\bar{\bar{\omega}})^2 = -\frac{1}{2}\frac{\partial^2}{\partial t^2}[\log A(t)] \tag{21b}$$

From (21a) we infer that the IF provides a measure of Fourier frequency at which the energy/power of a signal acts at an instant of time t [ACKROYD 1970]. It can also be shown that the second conditional moment $\bar{\bar{\omega}}^2$ is related by:

$$\int \bar{\bar{\omega}}^2 A^2(t)dt = \int \frac{d\Psi}{dt}\cdot\frac{d\Psi^*}{dt}dt \tag{22a}$$

For a narrow band signal the right hand side is by definiton the mean square Fourier frequency [GABOR 1946]. So,

$$\int \bar{\bar{\omega}}^2 A^2(t)\mathrm{d}t = \int \omega^2(t)A^2(t)\mathrm{d}t = \omega^2 \tag{22b}$$

The appropriate weighting factor $A^2(t)$ is important. For Gaussian signals the mathematical expectation of IF may be infinite [STRÖM 1977] if the weight factor is not taken into account. Equation (18) for $p(t,\omega)$ is similar to Wigner's distribution function in quantum mechanics. The well known Fourier inequality $\Delta\omega\Delta t \geq \frac{1}{2}$ follows directly from equation (18) [MOYAL 1949]. By analogy with a piece of music, De Bruijn has termed the function $p(t,\omega)$ as the musical score or simply the score [DE BRUIJN 1967]. We recall that the instantaneous spectrum can be defined from the decompostion of the energy of singnals onto $t - f$ planes [LEVIN 1964]. Although $p(t,\omega)$ is real, one cannot define a physically realizable spectrum because $p(t,\omega)$ is not ≥ 0 for all t. For example, if $t\Psi(t) > 0$ for all t,$p(t,\omega)$ is negative. De Bruijn has shown that certain moving averages yield positive values and the local smoothing (double convolution) of the instantaneous spectrum of a process with the instantaneous spectrum of window function yields the physical spectrum of the process [MARK 1976]. The window function should be such that it is non-negative over $0 < t < \infty$ and its integral over the semiinfinite time domain is unity. We will not enter into details of spectral representation of non-stationary processes in the present article. The above points are mentioned here to stress the fact that a concept of signal energy density in time and frequency leads us not only to the concept of IF for narrow band signals, but with modifications the formulation can be used in defining the short period spectrum of any process. It is however quite complicated to generate a time-dependent spectrum as it is a function of two variables f and t.

6. Spectral dynamics of a seismogram

Classical spectrum analysis is based on the concept of the linear stationary model (at least to the order two). For non-stationary processes the covariance kernel in the Wiener—Khintchine integral is not independent of the time origin. Loynes [1968] while listing the desirable properties of the spectrum of any stochastic process shows that spectral characteristics in the Fourier sense do not exist for non-stationary processes. Other statisticians, notably PRIESTLEY [1965], and MARK [1976] do not agree with such a conclusion and are of the opinion that a local power-frequency distribution at each instant of time exists. From our basic assumption a reflection seismogram is a stationary stochastic process with a continuous spectrum. The sharp peaks and notches observed within a finite time window are attributed to layer thicknesses present within the window. From spectral studies of reflection seismograms it is however very difficult to make out whether the spectral peaks are separate harmonic quasi-harmonic

oscillations or are simply narrow peaks of a continuous spectrum. For processes with so-called mixed spectra we have discrete harmonics with a continuous coloured spectrum. Such a process is rarely stationary. If separate narrow band signals are superposed on a process with continuous spectra, due to the additive property of spectra it may appear similar to the spectrum of a reflection seismogram. This is always a non-stationary process. Further if we agree that there is a change of apparent periods of oscillations with time in a seismogram, the process is bound to be non-stationary. Let us consider a purely amplitude modulated process:

$$p(t) = A(t) \cos \omega_0 t$$

ω_0 is the peak Fourier frequency. The deterministic version of such a type of oscillation, known as a Berlage pulse, is given by:

$$f(t) = t^n e^{-\beta t} \sin \omega_0 t$$

n is any integer and β is a constant. Such analytical forms have been used in practice, particularly in simulation of earthquake coda [FARNBACK 1975]. In seismic exploration $\beta \approx \frac{\omega_0}{A}$. These are narrow band signals and from classical Fourier theory the spectra should contain an infinite number of frequencies. *Figure 3* shows the envelopes and spectra of such pulses. Following PRIESTLEY [1981] we can represent the vibration as of only two frequencies ω_0 and $-\omega_0$ each component having a time varying amplitude $A(t)$. Now if the envelope $A(t)$ and the oscillatory part cos ω_0 t are spectrally disjoint, from the product theorem of Bedrosian, the Hilbert transform in given by $A(t)$ sin $\omega_0 t$. This is true if the envelope is slowly varying with time and then the instantaneous phase is given by

$$\Theta(t) = \text{arc tan} \left[\frac{\text{H}\{p(t)\}}{p(t)} \right] = \omega_0 t$$

or IF is equal to ω_0; H denotes the Hilbert transform. Although the Hilbert operator is noncausal and equation (4) is computed by considering the integral over the entire range form $-\infty$ to $+\infty$, the value of $\text{H}\{p(t)\}$ depends very little on the character of random process beyond the duration of the quasiharmonic signal being detected and analysed [KHARCHENKO et al. 1973]. Such vibrations can be identified on a time scale where $\Theta(t)$ is linear or nearly linear. In IF displays we can detect and locate these frequencies where the IF is nearly constant, preferably for a period of time of the order of $f_0 T \approx 1$. Thus a study of instantaneous frequencies may be helpful to ascertain the dynamic change of frequencies (at least at certain discrete intervals of time) irrespective of the

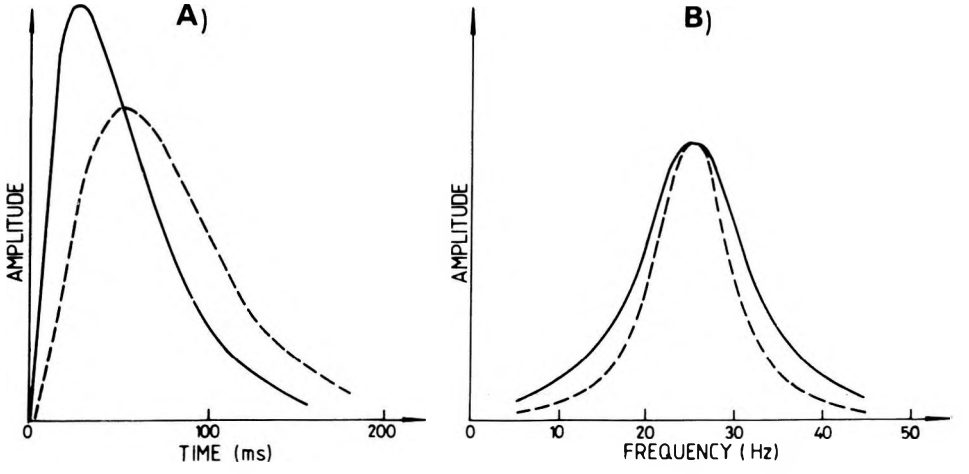

Fig. 3. Envelope (A) and spectrum (B) of Berlage pulse with peak frequency 25 Hz

3. ábra. Egy 25 Hz-es csúcsfrekvenciájú Berlage impulzus burkolója (A), és spektruma (B)

Рис. 3. Огибающая (А) и спектр (В) импульса Берлаж с пиковой частотой 25 Гц

fact that the random realization of a time series belongs to the non-stationary class. *Figures 4a* and *4c* show IF plots of a seismic trace for two different time windows. The trace is from a stacked section of land seismic data. The field seismograms (recording filter 8 Hz—124 Hz) after gain recovery have been stacked with appropriate spherical divergence and NMO corrections. No deconvolution of any kind has been applied. A band pass filter (8 Hz—60 Hz) has been used before obtaining the stacked output. The figures show the presence of two quasi-harmonics with frequencies 22 Hz and 27 Hz at about 1976 ms — 2021 ms and 2532 ms — 2592 ms respectively. Power spectral estimates by three different techniques (FFT, MLM and MEM) of the original seismic trace for the same time windows are shown in *Figures 4b* and *4d*. It is however observed that peak frequency values determined from IF plotes are nearer to peak values given by FFT or the Maximum Likelihood Method than values obtained from the Maximum Entropy Method. The peak freqency at a deeper level (Figure 4d) may sometimes be more than the peak frequency at a shallower level. This has been observed in many areas and was also mentioned earlier by other authors [TANER et al. 1979].

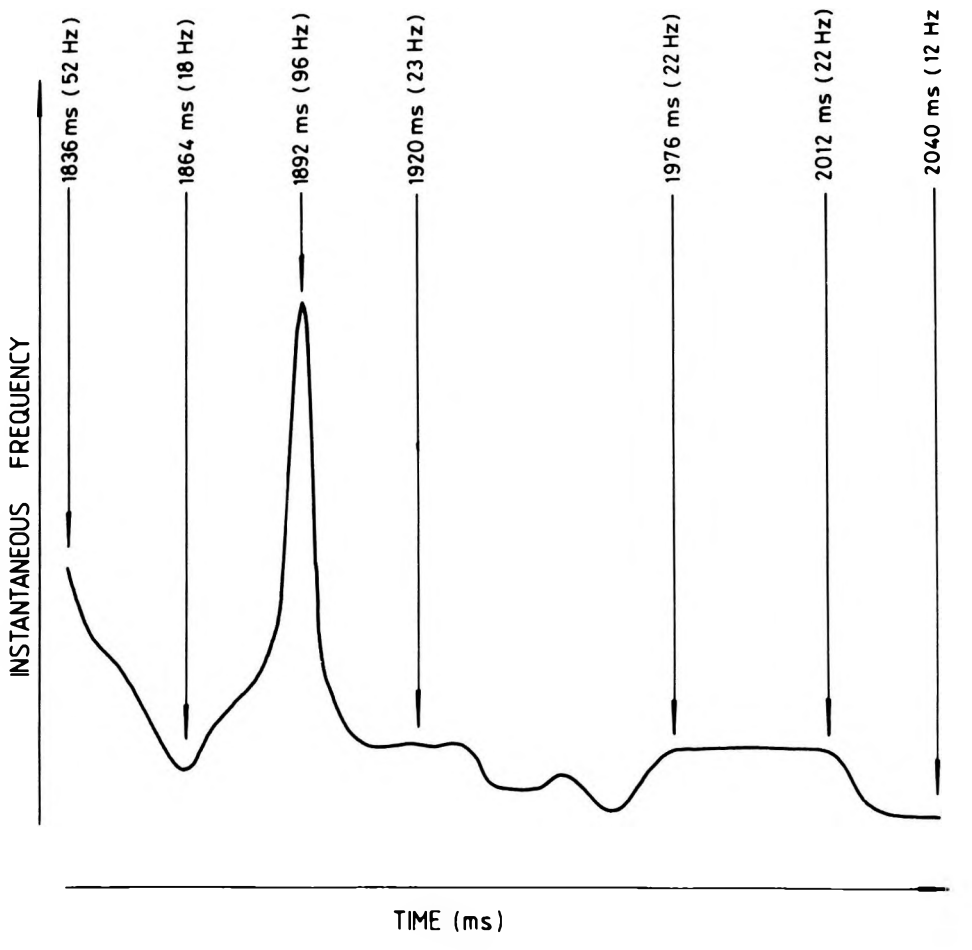

Fig. 4a. Instantaneous frequency plot of a seismic trace: time window 1836 ms—2040 ms

4a ábra. Egy szeizmogram szakasz pillanatnyi frekvencia függvénye. Időablak: 1836 ms—2040 ms

Рис. 4а. Диаграмма мгновенных частот по сейсмической трассе: временное окно 1836 мс—2040 мс

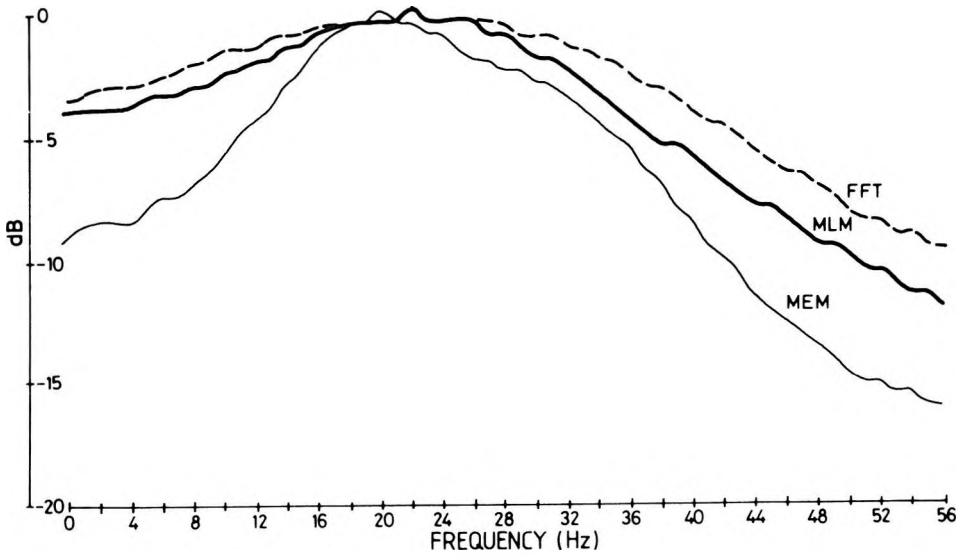

Fig. 4b. Spectral power estimate of a segment of seismic trace: time window 1976 ms—2012 ms

4b ábra. Egy szeizmogram szakasz spektrális energiaeloszlása. Időablak: 1976 ms—2012 ms

Рис. 4b. Оценка спектральной мощности по сегменту сейсмической трассы: временное окно 1976 мс—2012 мс

7. Conclusions

1. The Fourier frequency and instantaneous frequency are fundamentally different quantitites. However for a narrow band signal the variance of IF with respect to mean Fourier frequency is approximately equal to the band-width of the signal. This relation is true for stationary stochastic processes also. One should be cautious to use term by term IF values for the usual frequency interpretation of seismic section.

2. The complex envelope of a seismic envelope of a seismic trace can be determined uniquely by solving the appropriate Sturm—Liouville differential equation. The "instantaneous frequency" may often be strongly coupled with the envelope function. The location of maxima/minima of envelope (signal strength) can be predicted with fair accuracy from IF displays. The IF display may be helpful for seismic correlations where signal strengths are less.

3. An attempt has been made in this paper to "embrace" the two mutually exclusive parameters, Fourier frequency and IF, by utilizing the concept of signal energy density function in time and frequency. It is shown that IF is a measure of Fourier frequency at which the signal energy density is concontrated at a particular instant of time. The interpretation is meaningful if the energy density function is real and positive. This also explains the occasionally observed phenomenon where most of the signal energies are transmitted by filters with band-widths much narrower than the signal band-widths. The expression for energy density function considered in this paper, when suitably modified, can also be used to define a physically realizable short-time spectrum of any process (stationary or non-stationary).

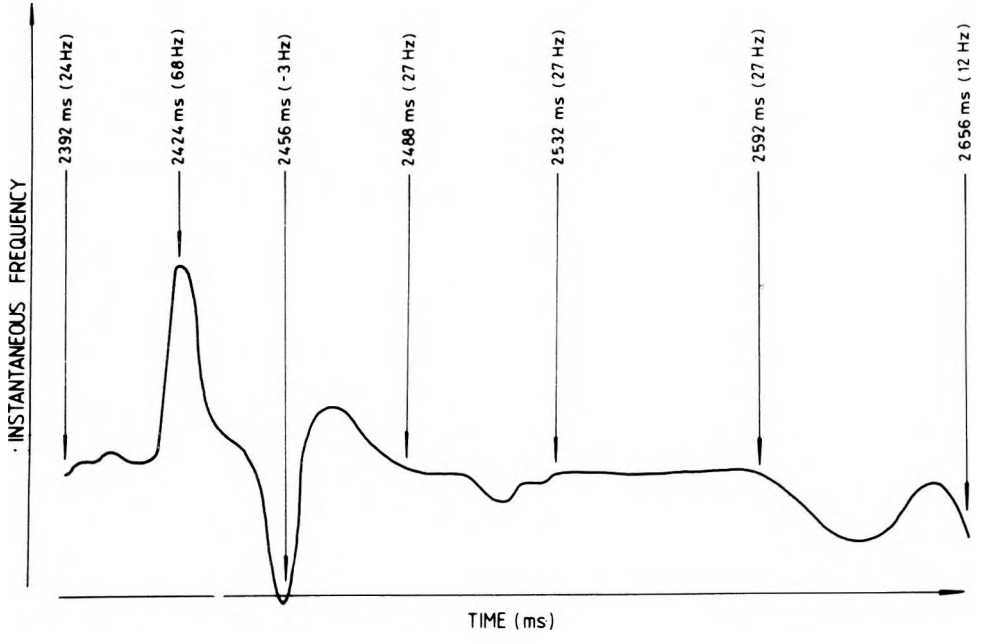

Fig. 4c. Instantaneous frequency plot of the same seismic trace as in Figure 4a; time window 2392 ms—2656 ms

4c ábra. A 4a ábrán szereplő szeizmogram pillanatnyi frekvencia függvénye a 2392 ms—2656 ms időablakban

Рис. 4с. Диаграммы мгновенных частот по сейсмической трассе, показанной на Рис. 4а: временное окно 2392 мс—2656 мс

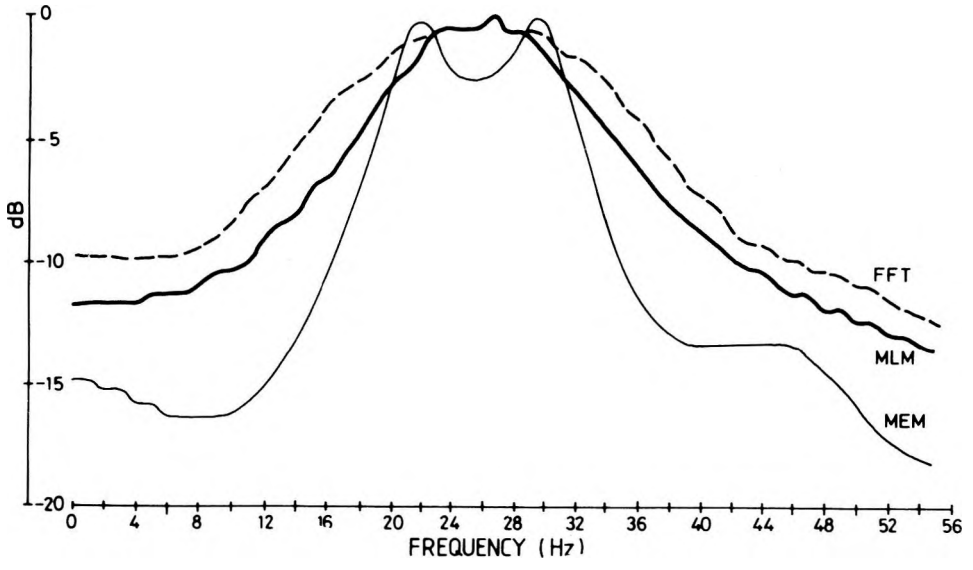

Fig. 4d. Spectral power estimate of the same seismic trace as in Figure 4a): time window 2532 ms—2592 ms

4d ábra. A 4a ábrán szereplő szeizmogram spektrális energiaeloszlása a 2532 ms—2592 ms időablakban

Рис. 4d. Оценка спектральной мощности по сеймической трассе, показанной на рис. 4а: временное окно 2532 мс—2592 мс.

4. The analytic signal technique can be exploited for decompostion of any random process into a number of quasi-harmonic oscillations at certain discrete time intervals of reflection seimograms. The peak Fourier frequencies determined from IF desplays may be used as additional information for ascertaining transition zones in a seismic section. The information obtained by this technique does not depend on the overall characteristics of the process.

Acknowledgements

I am thankful to Mr. V. C. Mohan, General Manager, Computer Services, KDMIPE, under whose guidance the relevant programs were developed by the Software Group of the Centre and also for his interest in the present study. I am specially indebted to Mr. P. N. Mukherjes for the efficient programming of the high resolution spectral estimate. Mr. L. P. Sati carried out the drawing work.

I am grateful to the Director of the Malaviya Institute of Petroleum Exploration for his permission to be present the paper.

REFERENCES

ACKROYD M. H., 1970: Instantaneous spectra and instantaneous frequency, Proc. IEEE, **58,** p. 141

BELLMAN R. 1970: Methods of nonlinear analysis, **1,** Academic Press

DE BRUIJN N. G., 1967: Uncertainty principles in Fourier analysis: Inequalities: pp. 57—71, Academic Press

FARNCBACK J. S., 1975: The complex envelope in seismic signal analysis. Bull. Seism. Soc. America, **65,** 4, pp. 951—962

GABOR D., 1946: Theory of communications, J. Inst. Elect. Engineer, part III, **93,** 26, pp. 429—441

KHARCHENKO N. F., WATSKI D. V., TOLMACHOV M. M., POLYKHIN A. T., 1973: Harmonic decomposition of a non-stationary random process realization, Radiotechnika i Elektronika, 18. no. 7 pp. 1507—1509 (in Russian)

LACOSS R. T., 1971: Data adaptive spectral analysis methods. Geophysics, 36, pp. 661—675

LANCZOS C., 1961: Linear differential operators, Van Nostrand

LEVIN M. J., 1964: Instantaneous spectra and ambiquity function, IEEE Trans. Inf. Theory, VII. 10. pp. 95—97

LOYNES R. M., 1968: On the concept of spectrum for nonstationary process. J. Roy. Statist. Soc. Ser. B, **30,** pp. 1—30

MANDEL L., 1967: Complex representation of optical fields in coherence theory, J. Opt. Soc. America, 57. No. 5. pp. 613—617

MANDEL L., 1974: Interpretation of instataneous frequencies, American J. Physics, 42. pp. 840—846

MARK W. D., 1976: Power spectral representation of nonstationary random processes defined over semi-infinite intervals, J.A.S.A, 59, No. 5, pp. 1184—1194

MOYAL J. E., 1949: Quantum mechanics as a statictical theory, Proc. Camb. Phil. Soc., pp. 99—124

PAPOULIS A., 1965: Probability, Random Variables and Stochastic Processes, McGraw-Hill

PRIESTLEY M. B., 1965: Evolutionary spectra and non-stationary processes, J. Roy. Statist. Soc., Ser B., 27, pp. 204—237

PRIESTLEY M. B., 1981: Spectral analysis and time series, 1. and 2, Acedemic Press

RIHACZEK A. W., 1968: Signal energy density distribution in time and freqency, IEEE Trans. Inf. theory, IT—14, pp. 369—374

STRÖM T., 1977: On amplitude weighted instataneous frequencies, IEEE Tran. Acc. Sp. Sig. Processing, ASSP—25, No. 4, pp. 351—352

TANER M. T., KOEHLER F., SHERIFF R. E., 1979: Complex seismic trace analysis. Geophysics, **44,** pp. 1041—1063

VAKMAN D. E., 1964: Sophisticated signals and the uncertainty principle in Radar, Acedemic Press

VAKMAN D. E., 1973: On the concept of amplitude, phase and frequency (Letter), Radartechnika i Elektronika, **18,** 8, pp. 1766—1768 (in Russian)

A REFLEXIÓS SZEIZMOGRAMOK SPEKTRÁLIS SZERKEZETÉNEK TANULMÁNYOZÁSA A PILLANATNYI FREKVENCIA VIZSGÁLATA ALAPJÁN

J. G. SAHA

A szeizmogramok spektrális jellemzői gyakran emlékeztetnek a kevert spektrumú folyamatok jellemzőire. Az ilyen folyamatok rendszerint nemstacionáriusak. A jelanalízis módszerével előállítható pillanatnyi fázis – pillanatnyi frekvencia függvények lehetővé teszik a szeizmogram kváziharmonikus tartalmának kimutatását. A módszer a folyamat stacionárius vagy nemstacionárius voltára való tekintet nélkül érvényes. A kváziharmonikusok kifejlődési és lecsengési folyamatai is kellő pontossággal követhetők a pillanatnyi frekvencia ismeretében.

СПЕКТРАЛЬНАЯ СТРУКТУРА СЕЙСМОГРАММ МОВ, ПОЛУЧЕННЫХ В РЕПРЕЗЕНТАЦИИ ПО МГНОВЕННОЙ ЧАСТОТЕ

Й. Г. САХА

Спектральная характеристика сейсмограмм часто похожа на процессы со смешанными спектрами. Фазовые/мгновенные частоты, выведенные путем техники анализа из сигналов, позволяют обнаружить присутствующие в сейсмограмме квази-гармонические частоты. Метод может найти применение независимо от того, носит ли процесс установившийся характер или нет. Временная эволюция и затухание таких квази-гармонических частот могут быть оценены с достаточной точностью по мгновенной визуализации частоты.

GEOPHYSICAL TRANSACTIONS 1984
Vol. 30. No. 2. pp. 141—155

APPLICATIONS OF STATISTICAL THEORY TO IMPROVEMENT OF TRACING OF REFLECTORS AND IDENTIFICATION OF ANOMALIES

F. M. HOLTZMAN**, E. A. KOZLOV*, O. A. POTAPOV*,
O. G. KUT'INA*, V. N. TROYAN**

The paper deals with identification of anomalies of parameters related to structural and lithological properties. Methods of tracing (classification) reflectors on seismic section are proposed. Some examples of utilizing algorithms to search for inhomogeneities on a seismic section and to specify the location of an oil reservoir based on the methods of multidimensional discriminant analysis are considered.

d: statistical analysis, inhomogeneity, wave attenuation, interval energy, resistivity, gravity anomaly

1. Introduction

The main task of modern geophysical prospecting for oil-promising zones for gas and other minerals is the location of areas with anomalous parameters in the geologic environment under study. The anomalies in question can be associated with structural or lithological peculiarities of the medium.

The search for structural anomalies is usually based on the methods of wave correlation: the detection of correlation breakpoints corresponding to an abrupt change in the reflecting properties of a boundary or tectonic faults. However, the problem of horizon tracing does not reduce to a simple determination of the structural features of a boundary; we should also consider the problem of tracing along the boundary those parameters which are correlatable with variations in the physical composition of rocks, e.g. layer velocity, amplitudes, wave attenuation, etc.

When searching for non-structural anomalies, the study of the distribution of a set of features and the search for areas where the statistical properties of the features essentially differ from each other becomes the main tool for dividing the section into blocks characterized by common properties.

* NPO Neftegeofizika, 103062 Moscow, Chernyshevskogo 22, USSR
** NIIF LGU 198904 Leningrad, St. Petergof, 1 Maya ul. 100, USSR
Paper presented at the 28th International Geophysical Symposium, Balatonszemes, Hungary, 28 September—1 October, 1983

The theory and algorithms for solving the mentioned tracing and grouping problems are thoroughly treated on the basis of mathematical statistics [Ed. HOLTZMAN 1981]. A short summary of the topic is to be found in Holtzman [1981], Practical applications are discussed in [KUT'INA 1982] snf [TROYAN 1982].

A set of arbitrary observational data can be regarded as a collection of realizations of random variables. Obviously conclusions drawn from observational data have also probabilistic character. The statistical interpretation theory postulates, as the most important requirement for evaluation algorithms, the possibility of checking the quality of their conclusions. As a measure characterizing the quality of conclusions may serve on of the statistical estimations on their information content, reliability, efficiency.

The present paper shows some application examples of tracing and grouping algorithms constructed on the above mentioned principles.

2. Defining the location of lithological anomalies

The problem of locating lithological anomalies can be solved together with the problem of horizon tracing or separately. In both cases, statistical analysis is based upon the values of the features (obtained during seismogram and time-section processing), that characterize a certain portion of a record covering usually 2—3 wave periods along T and 2—3 wavelengths along X. The main rule in selecting events is based on the signal-to-noise ratio in the analysis window; according to the assumed properties of the investigated material, the threshold value is selected from tables for distribution of random variables: normal, χ-square, Student's or Fischer's [KUT'INA 1982].

Figure 1 shows some examples of selecting events on a time section measured along one of the lines in the Aktyubinsk area. It can be seen that the widening of the time window for analysis (Fig. 1c) leads to better elimination of noise, improves the conditions of horizon traceablility and is useful for eveluating the integral characteristics of a record, for example, velocities. Determination of noise variance within the same time window as that of the signal energy (Fig. 1d) provides the possibility to emphasize wave behaviour in complicated wave zones (see parts of the section at $X = 4000$ m, $T = 2.1$ s).

Estimation of the parameters of selected events and subsequent tracing of the latter in time and along the line results in the creation of a field of features. Accumulation of features is performed at several successive stages of data processing: time, angle of wave arrival, signal-to-noise ratio, average amplitude and duration of basic peaks are determined from the time section while the velocity V_{CDP} from seismograms; tracing along the line permits one to determine the degree of wave regularity along X tracing in time allows one to determine

the frequency, attenuation, number of phases, intensity ratio of various phases, ratio of the times of events and degree of traceability along T.

The next stages of data processing and interpretation are the study of regularities of feature variation in various trends, determination of peculiarities of their behaviour, localization of anomalous portions of the section and interpretation of the obtained results, i.e. the main task is to decide on the physical nature of objects.

Fig. 1. Comparison of different processing schemes

1. ábra. A feldolgozási eljárások összehasonlítása

Рис. 1. Сопоставление различных режимов обработки

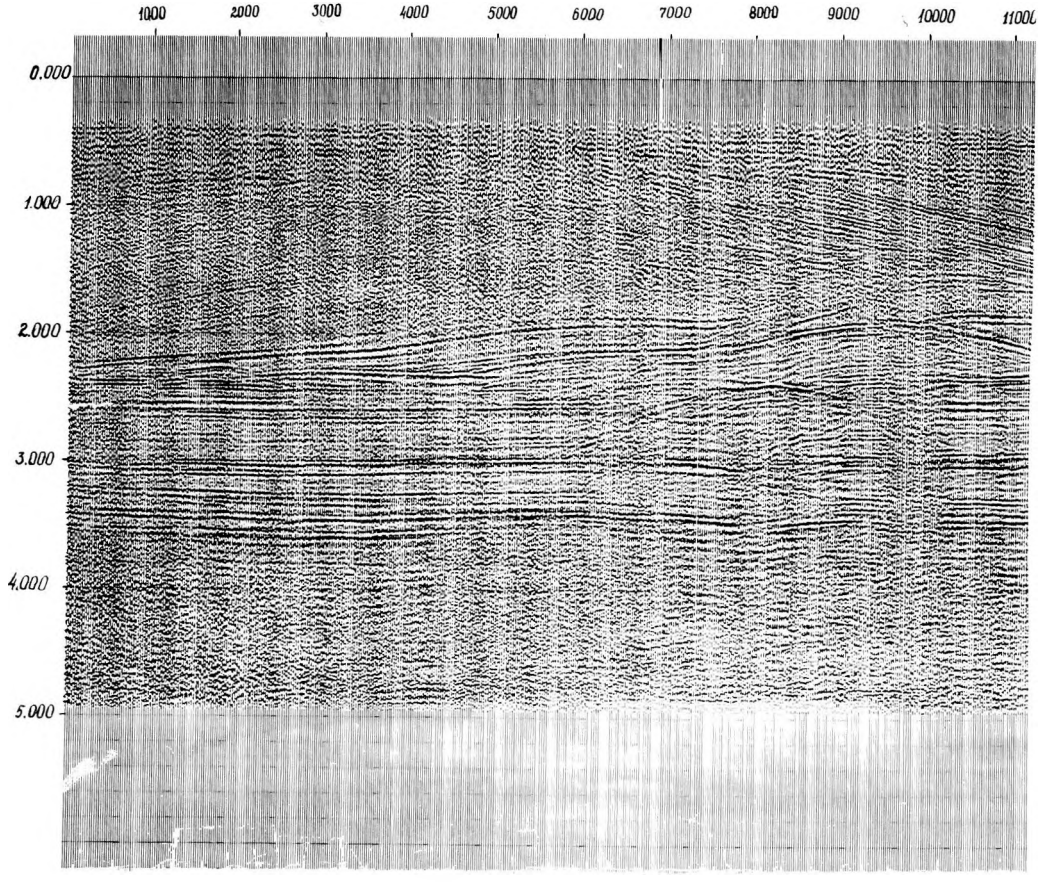

Fig. 1a. Standard processing

1a. ábra. Az időszelvény rutinfeldolgozása

Рис. 1а. Стандартная обработка

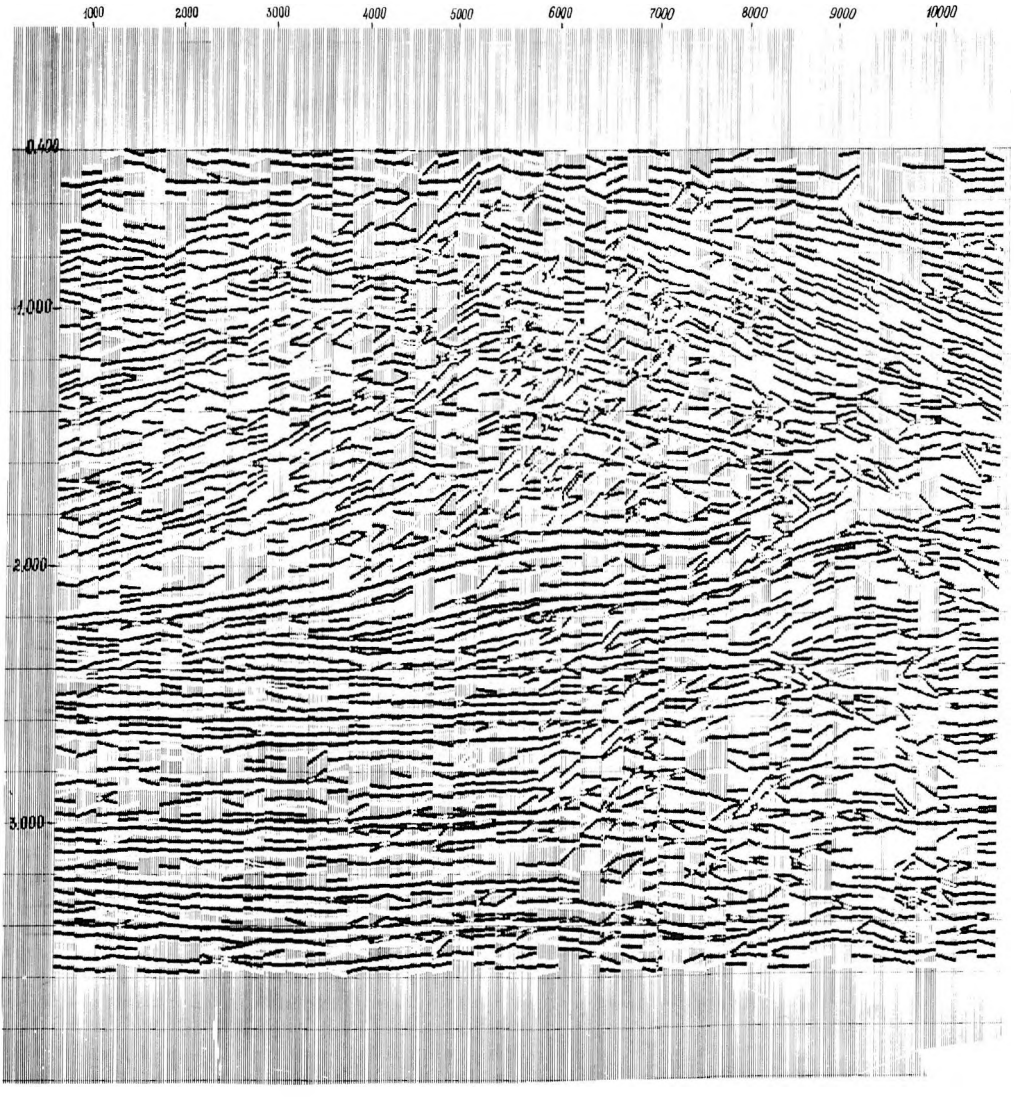

Fig. 1b. Results of signal enhancement in time sections (window of estimating noise dispersion is 1600 ms)

1b. ábra. Az időszelvény feldolgozása 1600 ms-os időablakban végzett zaj-szórás meghatározással

Рис. 1b. Результаты выделения волн по временному разрезу (оценка дисперсии помехи в окне 1600 мсек, сигнал во времени не суммируется)

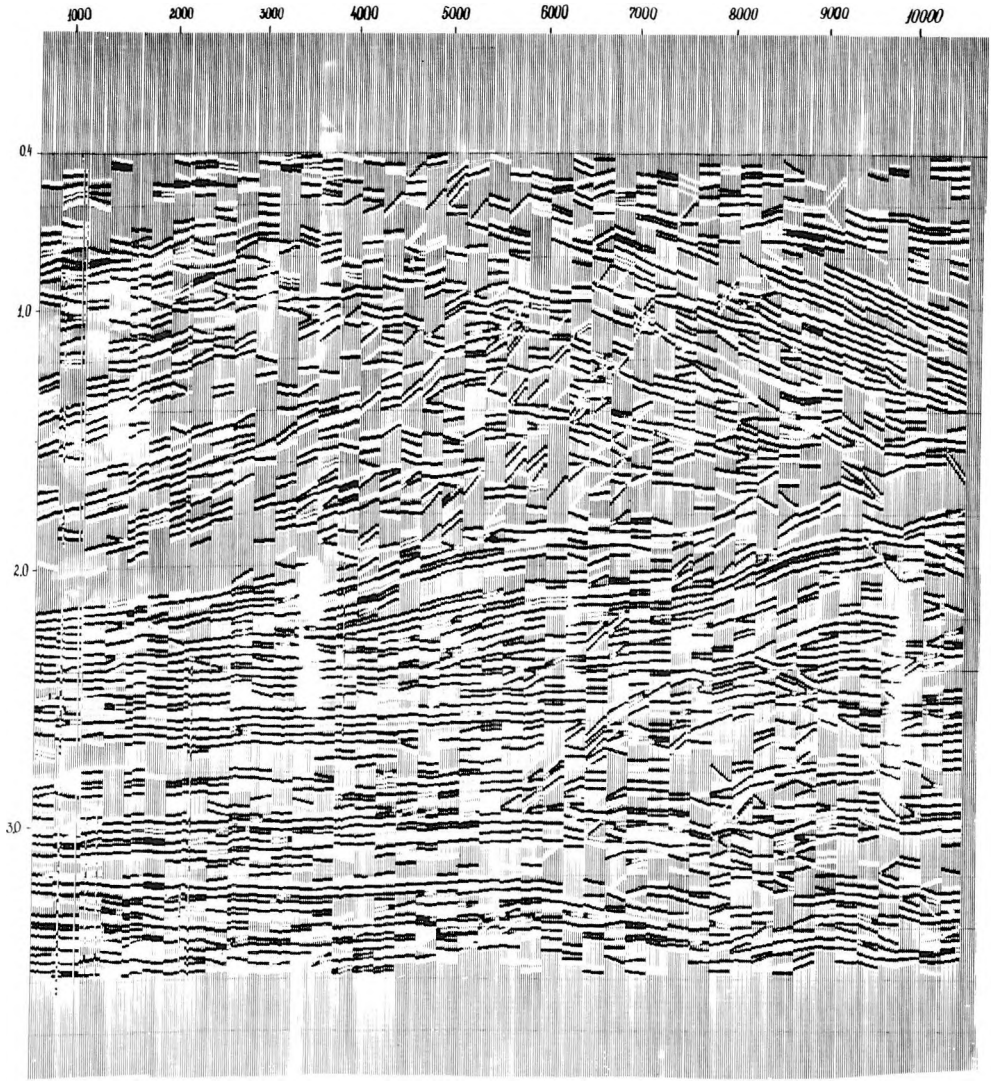

Fig. 1c. Results of signal enhancement in time sections (window of estimating noise dispersion is 1600 ms, window of signal summing is 40 ms)

1c. ábra. Az időszelvény feldolgozása 1600 ms-os időablakban végzett zaj-szórás meghatározással, valamint 40 ms-os ablakban végzett jelösszegezéssel

Рис. 1с. Результаты выделения волн по временному разрезу (оценка дисперсии помехи в окне 1600 мсек., окно суммирования сигнала: 40 мсек)

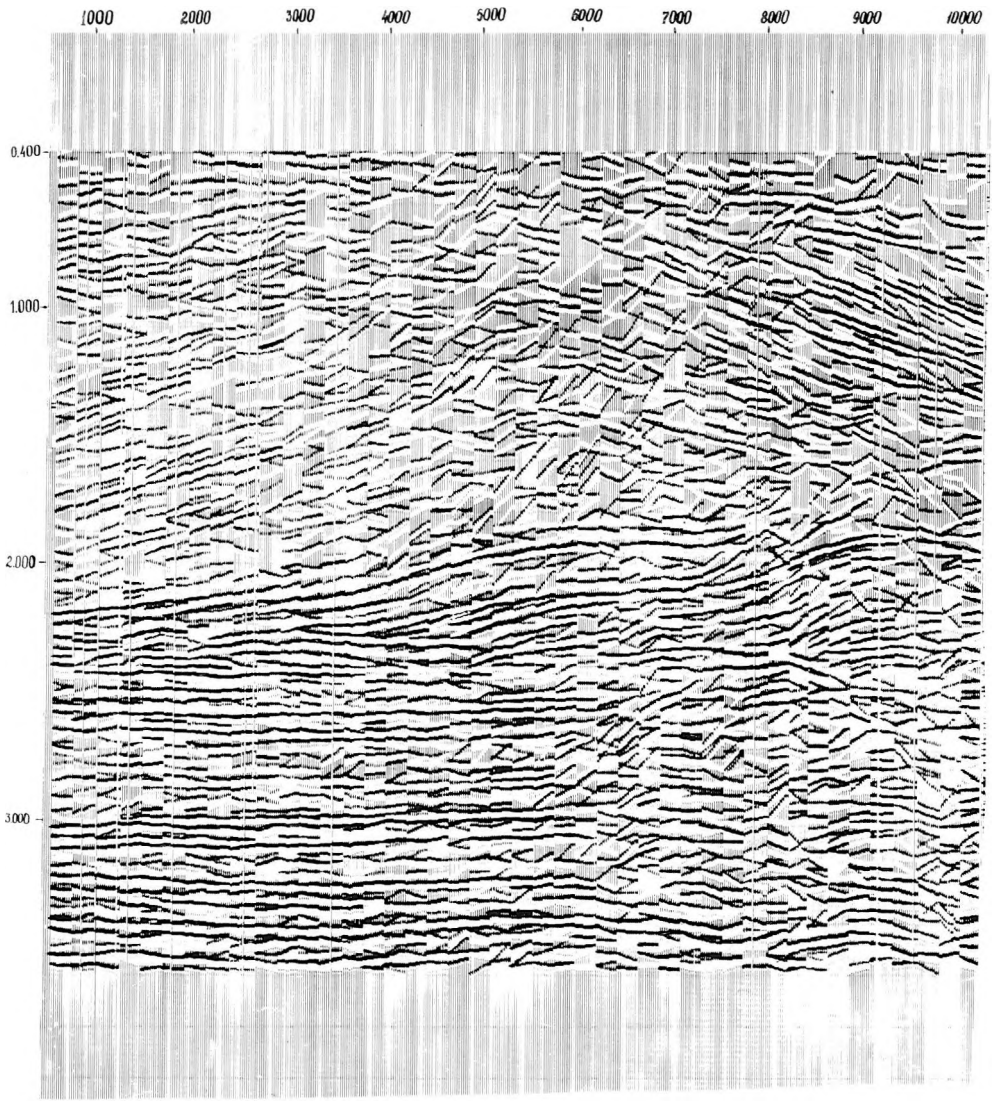

Fig. 1d. Results of signal enhancement in time sections (noise dispersion and signal energy are estimated in the same window 1600 ms)

1d. ábra. Az időszelvény feldolgozása 1600 ms-os időablakban végzett zaj-szórás és jelenergia meghatározással

Рис. 1d. Результаты выделения волн по временному разрезу (оценка дисперсии помехи и энергии сигнала в одном и том же временном окне; суммирование во времени не производится)

3. Determination of inhomogeneities in the section

In complicated geoseismic conditions, in the presence of noise the detection of inhomogeneity boundaries seems to be difficult. In this case, in order to determine the boundaries where the lithological composition changes, one needs, to search for the boundaries corresponding to the changes of integral characteristics of a record in various areas of the sequence under study. Accordingly, it is assumed that information on the properties of rocks is contained in seismograms not only from the boundaries where lithological composition changes but from the regions between the boundaries as well. The parameters essentially changing their values when crossing an interface are as follows: regular wave amplitude attenuation, ratio between time and amplitude of separate phases, duration of periods, velocities, etc. Variation in the values of these parameters may be obscured by noise and are shown only as various distributions of parameter values on both sides of the interface. The search for an interface can be accomplished by sorting out possible interface positions in a sequence, calculation of values of parameter distribution at each step on both sides of the interface and determination of the position corresponding to the greatest difference in distribution. Assuming equal covariance matrices for the distributions, the so called Machalonobis' distance can be used to express their difference. However, data analysis on the areas of inhomogeneities displays an essential difference in parameter variances and in correlation between separate parameters on both sides of the interface. Therefore, in order to estimate the degree of distribution variance when searching for inhomogeneities, it is advisable to apply probability measures regarding possible differences in covariance matrices. The methods of multivariate statistical analysis are often used in cases when learning samples with known classification are available. However, it seems impossible to create required learning samples (training sets) for solving the most important problems of subdividing objects into classes. Due to costly drilling and stripping work, objective identification of geophysical fields with mineral resources is possible only at some points of the territory; thus, the required typical learning samples cannot be ensured.

The frequency of correct attribution of an arbitrary spatial point to the areas being investigated can be considered as a measure allowing differences in covariance properties of distributions and not requiring samples with known classification (so called learning procedure without teacher). Establishment of the classes is performed using the rule elaborated with the help of the values of sample moments of distribution.

Let us consider an example of running the searching programme for inhomogeneities in some portions of the time section. The areas with relatively simple elliptical or partly hyperbolic boundaries served as models of anomalies. The search for an anomalous portion of the section was performed by means of the sorting out of all possible boundaries of the 2nd order. For each subdivision a decision rule was elaborated that effectively recognized in the par-

ameter space the alternative sets obtained at the current step of selecting and achieved degree of differentiation was calculated. The rule being elaborated in the course of learning is the optimum one among all possible types of decision rules for the case of arbitrary distributions with the two lowest moments coincident with their typical sample estimates from learning material.

The algorithm for the search for inhomogeneities includes:

– setting up the type of subdivision of observated space into alternative parts;

– calculation of statistical characteristics within these parts: sample mean and covariance matrices;

– calculation of coefficients of a linear discriminant function taking into account possible distinguishing of covariance matrices in alternative classes;

– calculation of frequencies of recognition errors of the 1st and 2nd types.

An example for one of the lines on the Jetybai oil field is shown in *Fig. 2*. The zone of seismic section, 10,000 m long (along the line) and 1000 m deep, included 882 observations of parameter vectors containing the following components: mean-interval coefficient of seismic wave attenuation, mean-interval energy, apparent electric resistivity, estimate of mean cross correlation between trace pairs of seismograms, gravity anomaly. Sample positions of boundaries (horizontal, inclined and curved) are shown in Fig. 2. Among the versions of the boundaries separating the section into left and right parts, two patterns having poor correlation with the geological data characterized by error probabilities of 0.43—0.49 are approaching an upper limit of 0.5. It means that the statistical distributions of features in such patterns hardly differ from one another and, consequently, cannot correspond to any inhomogeneities in the section. The boundary with a frequency estimate of 0.18 corresponds to one of the most abrupt changes in the set of parameters under consideration.

The obtained results are confirmed even in the case of a smaller number of samples as well as in the case of a reduced number of features. In the latter case, the efficiency of recognizing the alternative classes and, accordingly, the reliability of distinguishing the boundary corresponding to inhomogeneity decreases. However, there are some combinations of a small number of features for which the efficiency of recognition only slightly differs from the limiting one. For instance, the combinations of such parameters as mean energy and the estimate of mean cross correlation or apparent electrical resistivity and the estimate of mean cross correlation differ in efficiency from a complete set of features by 0.02 and less. It is clear that the majority of boundaries corresponding to increased values of differentiation efficiency are characterized by a certain persistence and repeated shape. It should be noted that the discriminant method of recognizing the inhomogeneities does not require a strict correlation between the parameters and the points on a section. Some shift of the values of a separate element in the distribution space (on a section plane) relative to the true distribution will lead to decreased correlation between a given feature and the features identified by other geophysical methods; as a consequence, the maximum difference between the features which is the basis for distinguishing the

physical object in question will be less pronounced. If the inhomogeneity is determined in spite of a shift, it can be said with confidence that it would also be determined using features better correlated with the particular points of the section. The above-mentioned facts supports the application of approximation methods when identifying features. Once an inhomogeneity is identified, specification of its position can be performed by means of the more precise processing of each geophysical method.

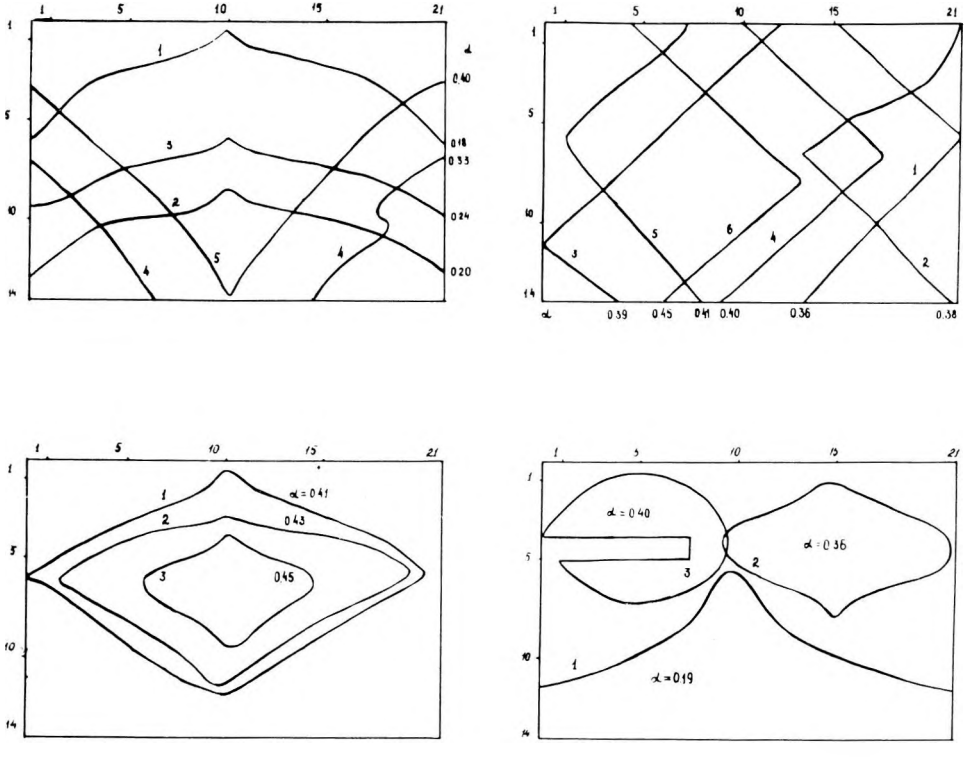

Fig. 2. Variants of dividing a cross-section into homogeneous zones
α — efficiency of dividing the cross-section into two zones (cummulative error probability)

2. ábra A heterogén szelvény zónákra osztása
α — a két zónára történő osztás hatékonysága (halmozott hibavalószínűség)

Рис. 2. Варианты разбиения участка разреза на зоны
α — эффективность разбиения (суммарная вероятность ошибки)

The absence of *a priori* information on the location of intervals possibly associated with lithological inhomogeneities necessitates subdivision of the whole medium to statistically homogeneous zones. It is difficult to carry out statistical analysis because neither the number of objects, nor their boundaries and statistical characteristics are known beforehand. Sometimes, a preliminary analysis of the obtained field of features can be performed by plotting a bar chart of their distribution on some selected intervals in a few portions of the line. If we do not know which elements form a class of objects and at the same time the average values are also unknown and can vary within the limits of a particular population of a single class, the procedure of gradual selection of elements assigned to the same class is required; this is performed by tracing [HOLTZMAN 1981, KUT'INA 1982]. Tracing reduces the problem of partitioning the space of features with unknown number of classes and unknown statistical characteristics to the problem of alternate scanning of possible combinations of feature values beginning with various reference points, calculation of the current average value and deciding about attributing alternative values of the features to one or another set of reference values. In more simple cases, when the characteristics of the objects are considered to be invariant within the limits of the classes and there is no restriction to attributing features to some local area of the space, only the problem of classification with an unknown number of classes remains. The most simple problem involves a known number of classes, namely two classes. The other problems are usually reduced to the above mentioned one, i.e. they are solved by means of multiple checking of two alternatives.

4. Localization of spatial anomalies

Localization of anomalies on the area is connected with the same problems but they are solved in the space of greater dimension. When tracing, the problems of approximation designed for calculating variable mean values, detection of a regular background, etc. are of particular importance [TROYAN 1982]. Tracing makes it possible to locate approximately the boundaries of spatial blocks having similar statistical properties. Then the problem concerning the specifying of object boundaries is to be solved: whether two objects under consideration belong to one or two classes (tracing through break, location of an inhomogeneous zone between the boundaries being identified, assignment of two separately traced phases to the same boundary etc.), whether a certain object could be subdivided into two (checking the uniformity of distribution of feature values), assignment of the remainder of single elements to one of the distinguished classes or neglecting these elements.

To a greater degree than the problem of distinguishing inhomogeneities on a section, the problem of localization of spatial anomalies is connected with the necessity to perform simultaneous analysis of the distribution of a great number

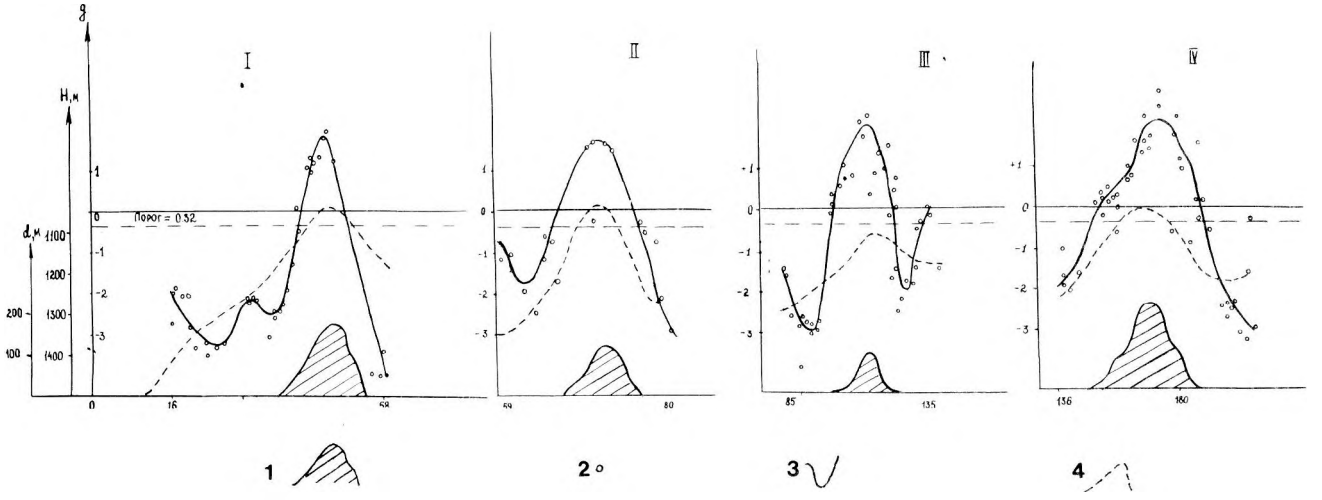

Fig. 3. Results of two-class grouping of data by discriminator function method
1 — reservoir thickness (d); 2 — values of discriminator function at separate points;
3 — smoothed values of discriminator function;
4 — depths of structures

3. ábra. A diszkriminátor-függvény módszerrel végzett kétosztályos felbontás eredményei
1 — tároló vastagság; 2 — a diszkriminátor függvény értékei; 3 — a diszkriminátor függvény simított értékei; 4 — a szerkezetek mélysége

Рис. 3. Результаты классификации по минимаксному решающему правилу
1 — мощность залежи (d); 2 — значения дискриминантной функции в отдельных точках;
3 — сглаженные зхачения дискриминантной функции; 4 — глубина залегания структуры

of feature values; this is too great a task for an interpreter. Application of discriminant functions for this problem allows one to reduce the whole set of multidimensional data into a one-dimensional file of discriminant function values. As in the previous case, the problem can be reduced to two alternatives assuming that the field under study could be subdivided into areas characterized by different statistical properties, discriminant function coefficients can be calculated and a chart of their values plotted. However, even the solution of this simple problem with known but different covariance matrices leads to quadratic rules which require a great number of operations for recognizing procedure, and they give unstable classification. A linear decision rule can be constructed only on the basis of an interation procedure [HOLTZMAN 1981].

Let us consider an example of formalized subdivision of territories into areas associated with the presence or absence of raw minerals. Complex studies with application of the methods of seismic, electric and gravity surveys as well as geochemical methods were carried out along the lines on the Jetybai field. The following elements were subjected to processing: mean value of an absorption coefficient of waves reflected from a reference boundary, number of reflections in a time interval, time of last reflection, density of events in time, value of apparent resistivity and its derivative, gravity anomaly, recalculated vertical gravity gradient, beta-activity from geochemical data.

Subdivision into alternative classes was performed according to preliminary geological interpretation on the basis of well data, and processed reflection data on structures resulted in the determination of the total thickness of the reservoir along individual lines. The total number of observation points was 175; for the learning process 12 points belonging to the class of reservoir and 27 points attributed to the area outside the reservoir were used. Using the values of sample moments, the coefficients of the linear minimax rule were calculated.

Figure 3 shows the results of recognizing all 174 points along individual lines. The resulting classification corresponds to the initial geological classification in 87% cases. The decision rule coefficients were varied in different combinations in the vicinity of obtained values with increments of ± 10%. Accordingly, empirical frequencies of correct recognition changed by not more than 2—3% thus pointing to the stable nature of the procedure for creating the decision rule.

Analysis of plots enables one to draw the following conclusions: 1) there are practically no errors when using the learning material; 2) recognition errors are generally present in a transition area between the reservoir and the outer part, in relation to the preliminary partitioning; 3) the decision rule values along the lines follow the behaviour of curves of the reservoir thickness and the depth of the structure and, hence, they could be used for approximate prediction of these values.

In *Figure 4* smoothed values of the decision rule are shown plotted as levels with similar values. It can be seen that recognition makes it possible to correct the prediction maps as well as to elaborate a quantitative measure of the degree of formal separability of the classes under consideration.

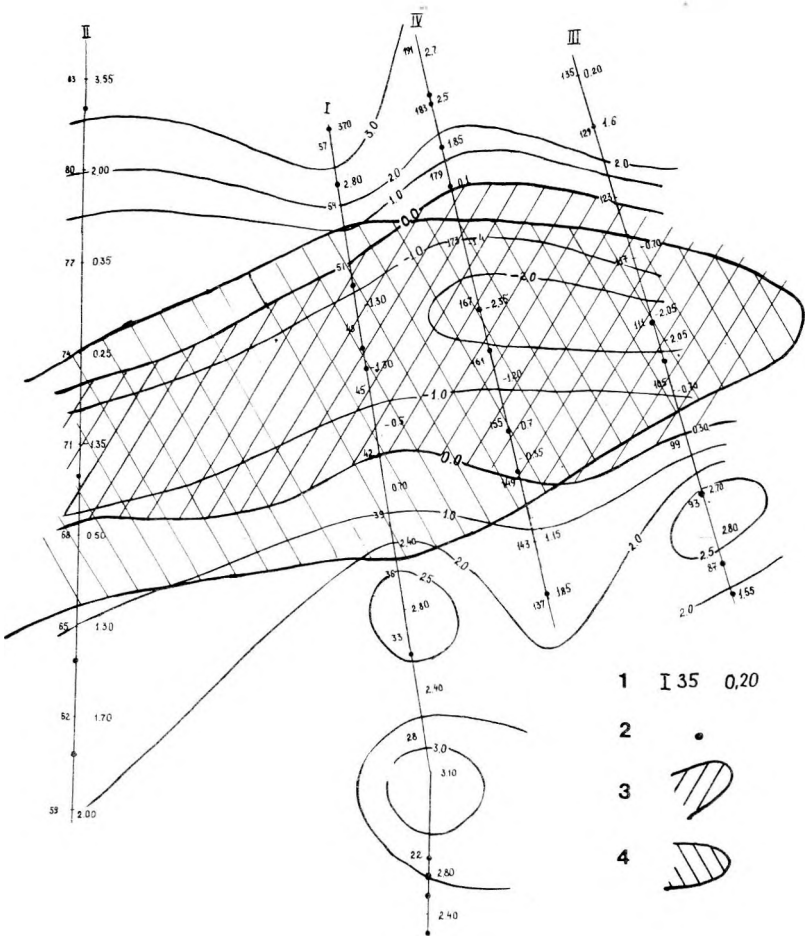

Fig. 4. Improvement of reservoir positioning
1 — pegmarks and values of discriminator function (g); 2 — points used for learning; 3 — reservoir outline from geological data; 4 — computed reservoir outline (zero level of discriminator function)

4. ábra. A tároló helyzetmeghatározásának javítása
1 — karószám, illetve a g diszkriminátor függvény értéke; 2 — a tanuláshoz használt pontok; 3 — a tároló határvonala fúrási adatok alapján; 4 — számított tároló határvonal (a diszkriminátor függvény zérus nívója)

Рис. 4. Уточнение положения залежи
1 — № № пикетов и зхачения дискриминантной функции; 2 — точки, использовавшиеся для обучения; 3 — контур залежи по геологическому прогнозу; 4 — рассчитанное положение контура залежи (нулевой уровень значений дискриминантной функции)

5. Conclusions

A study of the information capacity of various groups of features for separation of alternative sets was carried out. The values associated with the probability of correct separation of two sets with partly known distributions was considered as a measure of information capacity. Possible combinations of features for small extension of groups were studied. Groups of features with high efficiency of separation have been distinguished. The best combinations containing two or three features are based on all the types of prospecting. It can be seen that the high efficiency of integration is not connected with the predominant application of any single feature. When simultaneously using the data of electrical and seismic prospecting, both the number of reflections in a time interval and the time of the last reflection have the same efficiency. When combining seismic, gravity and geochemical methods, the above mentioned elements from seismic data or the density of events in time could be applied. In all cases, any combination of features which is sufficiently effective uses the data obtained from several geophysical methods.

REFERENCES

HOLTZMAN F. M. (Ed.) 1981: Statistical interpretation of geophysical data. L. LGU, 256 p.

HOLTZMAN F. M. 1981: Statistical algorithms for tracing and classification. Izv. AN SSSR, ser. Fizika Zemli, **4**, pp. 58—72

KUT'INA O. G. 1982: Elaboration of statistical algrithms for processing and interpretation of seismic data, 165 p., Nedra, Moscow

TROYAN V. N. 1982: Statistical methods for processing seismic information in interpretation of complicated areas. 202 p., Nedra, Moscow

REFLEKTOR-KIMUTATÁS ÉS ANOMÁLIA-AZONOSÍTÁS MINŐSÉGÉNEK JAVÍTÁSA STATISZTIKUS MÓDSZEREKKEL

F. M. Holtzman, E. A. Kozlov, O. A. Potapov, O. G. Kut'ina, V. N. Troyan

A szerzők szerkezeti és litológiai paraméterekben jelentkező anomáliák azonosításával foglalkoznak. Egy új módszert javasolnak az anomáliák helyének az időszelvényen történő meghatározására. Egy olajtároló meghatározásának példáján mutatják be a sokváltozós diszkriminátor analízis módszerével végzett időszelvény-feldolgozás eredményét.

ПРИМЕНЕНИЕ СТАТИСТИЧЕСКОЙ ТЕОРИИ ДЛЯ УЛУЧШЕНИЯ ПРОЦЛЕЖИВАНИЯ ОТРАЖАЮЩИХ ПОВЕРХНОСТЕЙ И ИДЕНТИФИКАЦИИ АНОМАЛИЙ

Ф. М. ГОЛЬЦМАН, Е. А. КОЗЛОВ, О. А. ПОТАПОВ, О. Г. КУТЬИНА, В. Н. ТРОЯН

В работе обсуждаются вопросы идентификации аномалий параметров, связанных со структурными и литологическими свойствами. Предлагаются способы прослеживания (классификации) отражающих поверхностей по сейсмическому разрезу. Приведены некоторые примеры применения алгоритмов для отыскивания неоднородностей по сейсмическому разрезу и для выделения местонахождений залежи нефти на основе методов многомерного дускриминасионного анализа.

GEOPHYSICAL TRANSACTIONS 1984
Vol. 30. No. 2. pp. 157—166

NEW FINITE DIFFERENCE SCHEMES FOR WAVE EQUATION MIGRATION

Róbert MÄRLE*

The paper describes some new difference schemes for wave equation migration. The favourable properties of these schemes from the point of view of the 3D problem will be pointed out.

d: wave equation migration, finite differences, 3D seismics

1. Introduction

In the last few years several publications have been devoted to wave equation migration. The problem of velocity inhomogeneities and of the appropriate boundary conditions have been dealt with in several places. Less attention has been given to the method of finite differences compared with the vast literature on frequency-domain migration. The initial successes achieved with ELGI's finite-difference migration programs and the new tasks which have arisen in 3D processing motivated our undertaking this study.

The research has centred around two tasks: ways to improve the treatment of greater dips, and novel possibilities for the execution of 3D migration in one step.

The first part of the paper will describe a negative result. The scheme to approximate the original equation will prove to be absolutely stable but not consistent. It will also be shown, heuristically, why we have not succeeded in finding a consistent scheme.

In the second part of the paper difference schemes will be introduced which can be used for the solution of the 3D migration in a single step.

2. Approximation of the full equation

CLAERBOUT [1976] derived the wave-equation

$$u_{xx} + u_{zz} + \frac{2}{v} u_{zt} = 0 \tag{1}$$

* Eötvös Loránd Geophysical Institute of Hungary, POB 35, Budapest, H-1440
Manuscript received: 15 February, 1984

Upon neglecting the u_{zz} term, we get the so-called "15° equation", which is very similar to the equation of heat conductivity. Claerbout introduced an absolutely stable, implicit difference scheme. While one has to stick to the requirement of absolute stability (since the ratio of the lattice constants (Δx, Δt, Δz) can be widely different), the requirement of the implicit difference schemes can be dropped. Since the 15° and 45° equations do not properly treat the very steep dips, it is reasonable to assume that if we could solve the complete equation, this would provide a better migration procedure for the very large dips.

For the equation of heat conduction quite a few difference schemes have been proposed, including explicit and absolutely stable ones, but even these are only conditionally consistent. To put it plainly, stability means that the numerical errors cannot accumulate during the solution so as to make the result quite useless, while consistency means that we are really approximating the same equation from which we have started out. Exact mathematical definitions can be found, for example, in the monograph of RICHTMYER and MORTON [1967]. Consider the equation of heat conduction

$$u_t = u_{xx} \tag{2}$$

The so-called Du-Fort—Frankel difference scheme will be:

$$\frac{u_k^{n+1} - u_k^{n-1}}{2\Delta t} = \frac{u_{k-1}^n - u_k^{n+1} - u_k^{n-1} + u_{k+1}^n}{(\Delta x)^2} \tag{3}$$

that is

$$\begin{aligned} u_k^{n+1} + a u_k^{n+1} &= a u_{k-1}^n + a u_{k+1}^n - a u_k^{n-1} - u_k^{n-1} \\ (1+a) u_k^{n+1} &= a(u_{k-1}^n + u_{k+1}^n) - (1-a) u_k^{n-1} \end{aligned} \tag{4}$$

with

$$a = \frac{2\Delta t}{(\Delta x)^2}$$

If we check the stability of this difference scheme by Neumann's method [cf. RICHTMYER and MORTON 1967], it turns out that it is stable independently of the value of a (if $a > 0$, but this obviously holds). Indeed, the amplification factor ξ of the Neumann method satisfies the equation

$$(1+a)\xi^2 - 2a \cos\varphi \cdot \xi - (1-a) = 0$$

from where

$$\xi_{1,2} = \frac{2a \cos\varphi \pm \sqrt{4a^2 \cos^2\varphi + 4 - 4a^2}}{2(1+a)}$$

If the discriminant is negative, ξ_1 and ξ_2 are complex conjugates of each other, i.e. their moduli are equal, and

$$|\xi_{1,2}|^2 = \frac{1-a}{1+a} < 1 \qquad a > 0$$

If the discriminant is positive, we can also easily prove that the moduli of ξ_1 and ξ_2 are less than 1.

The only problem with the difference scheme (3) is its consistency with the equation

$$u_t = u_{xx} - \frac{(\Delta t)^2}{(\Delta x)^2} u_{tt} \tag{5}$$

rather than with the original equation. If $\frac{\Delta t}{\Delta x}$ is sufficiently small, this does not cause serious errors.

The importance of consistency lies in the fact that the result obtained from the finite difference solution approximates the solution to that equation which is consistent with the difference scheme [Theorem of LAX, see RICHTMYER and MORTON op.cit.]. The consistency of a difference scheme can be studied by means of Taylor series. The absolute stability and conditional consistency of the Du-Fort—Frankel scheme are both due to the fact that in the approximation of u_{xx} the term $2u_k^n$ was substituted by the sum $(u_k^{n+1} + u_k^{n-1})$. Had they left the original terms as $2u_k^n$ the scheme would be consistent but by no means absolutely stable.

For some considerable time, the author has been attempting to find an absolutely stable difference scheme consistent with Eq. (1). Although these attempts have not been successful so far, the author has succeeded in finding an absolutely stable approximation (hereinafter we shall use the notation $u(n\Delta z, k\Delta t, l\Delta x) = u_{k,l}^n$):

$$\begin{aligned}
&\frac{1}{(\Delta z)^2}(u_{k,l}^{n+1} - u_{k,l+1}^n - u_{k,l-1}^n + u_{k,l}^{n-1}) + \\
&\frac{1}{2v\Delta z\Delta t}(u_{k+1,l}^{n+1} - u_{k-1,l}^{n+1} - u_{k+1,l}^{n-1} + u_{k-1,l}^{n-1}) = \\
&\quad - \frac{1}{(\Delta x)^2}((u_{k+1,l-1}^n + u_{k-1,l-1}^n)/2 - \\
&\quad - (u_{k-1,l}^{n-1} + u_{k-1,l}^{n+1} + u_{k+1,l}^{n-1} + u_{k+1,l}^{n+1})/2 + \\
&\quad + (u_{k+1,l+1}^n + u_{k-1,l+1}^n)/2)
\end{aligned} \tag{6}$$

It will be shown later that this scheme is absolutely stable; the consistency condition, however, is not met, for Eq. (6) is consistent with the equation

$$u_{zz} - \left(\frac{\Delta x}{\Delta z}\right)^2 u_{xx} + \frac{2}{v} u_{zt} = -u_{xx} + \left(\frac{\Delta z}{\Delta x}\right)^2 u_{zz} + \left(\frac{\Delta t}{\Delta x}\right)^2 u_{tt} \tag{7}$$

The applicability of this approximation for migration purposes has been checked by model experiments. The results obtained have generally met the expectations, though they have also revealed a few surprising features. The experiments were carried out on a mathematical model section, the obtained results were compared with that of a conventional 45° migration program. The model consists of dipping reflecting surfaces whose migrated picture can easily be constructed. On the whole, the 45° migration has put these reflecting surface elements in their proper place, with characteristic long "smiles" at their ends. On the other hand, scheme (6) has not put the surfaces in their proper place, they have only been displaced about half-way; their shortening however is exactly the same as theoretically expected. The lesson from the experiment is, of course, that this difference scheme cannot be applied for migration, though it should be added that when we selected Δz to be two times less than in the 45° equation, the result became much better and the time of computation was only about half that of the 45° migration. This latter phenomenon can easily be understood if we recall that the error of the consistency depends on Δz in an almost random manner, which makes the difference scheme practically inapplicable. The stability of the difference scheme can be established as follows. Multiplying Eq. (6) by $(\Delta z)^2$ and letting

$$a = \frac{(\Delta z)^2}{(\Delta x)^2} \qquad b = \frac{\Delta z}{2v\Delta t} \qquad \text{we obtain}$$

$$\begin{aligned} u^{n+1}_{k,l} - u^{n}_{k,l+1} - u^{n}_{k,l-1} + u^{n-1}_{k,l} + b(u^{n+1}_{k+1,l} - u^{n+1}_{k-1,l} - u^{n-1}_{k+1,l} + u^{n-1}_{k-1,l}) = \\ - a((u^{n}_{k+1,l-1} + u^{n}_{k-1,l-1})/2 - (u^{n-1}_{k-1,l} + u^{n-1}_{k+1,l} + u^{n+1}_{k-1,l} + u^{n+1}_{k+1,l})/2 + \\ + (u^{n}_{k+1,l+1} + u^{n}_{k-1,l+1})/2) \end{aligned} \tag{8}$$

Rearranging the equation with respect to the index n

$$\begin{aligned} u^{n+1}_{k,l} + a(u^{n+1}_{k-1,l} + u^{n+1}_{k+1,l})/2 + b(u^{n+1}_{k+1,l} - u^{n+1}_{k-1,l}) = \\ = u^{n}_{k,l+1} + u^{n}_{k,l-1} - a(u^{n}_{k+1,l-1} + u^{n}_{k-1,l-1} + u^{n}_{k-1,l+1} + u^{n}_{k+1,l+1})/2 + \\ + b(u^{n-1}_{k+1,l} - u^{n-1}_{k-1,l}) - a(u^{n-1}_{k-1,l} + u^{n-1}_{k+1,l})/2 - u^{n-1}_{k,l} \end{aligned} \tag{9}$$

and we get, by Neumann's method, the following equation for the amplification factor:

$$(1 - a\cos\omega\Delta t + 2ib\sin\omega\Delta t)\xi^2 = (2 - 2a\cos\omega\Delta t)\cos k_x\Delta x\xi - 1 - a\cos\omega\Delta t + 2ib\sin\omega\Delta t \tag{10}$$

With the further notations $C = 1 - a\cos\omega\Delta t$; $D = 2ib\sin\omega\Delta t$ we have

$$(C + iD)\xi^2 - 2C\cos k_x\Delta x\xi + C - iD = 0 \tag{11}$$

that is

$$\xi_{1,2} = \frac{2C\cos k_x\Delta x \pm \sqrt{4C^2\cos^2 k_x\Delta x - 4(C^2 + D^2)}}{2(C + iD)} = \frac{C\cos k_x\Delta x \pm i\sqrt{C^2 + D^2 - C^2\cos^2 k_x\Delta x}}{C + iD}$$

Upon multiplying both the numerator and denominator by the complex conjugate of the latter, we get

$$|\xi_{1,2}|^2 = \frac{C^2 + D^2}{C^2 + D^2} = 1 \tag{12}$$

that is, the difference scheme is stable.

Let us now consider a general scheme, based on the approximations

$$\begin{aligned}\hat{u}_{zz} = {} & a\,(u^{n-1}_{k-1,\,l-1} - 2u^{n}_{k-1,\,l-1} + u^{n+1}_{k-1,\,l-1}) + a_2\,(u^{n-1}_{k-1,\,l} - 2u^{n}_{k-1,\,l} + u^{n+1}_{k-1,\,l}) + \\ & + a_3(u^{n-1}_{k-1,l+1} - 2u^{n}_{k-1,l+1} + u^{n+1}_{k-1,l+1}) + a_4(u^{n-1}_{k,l-1} - 2u^{n}_{k,l-1} + u^{n+1}_{k,l-1}) + \\ & + a_5(u^{n-1}_{k,l} - 2u^{n}_{k,l} + u^{n+1}_{k,l}) + a_6(u^{n-1}_{k,l+1} - 2u^{n}_{k,l+1} + u^{n+1}_{k,l+1}) + \\ & + a_7(u^{n-1}_{k+1,l-1} - 2u^{n}_{k+1,l-1} + u^{n+1}_{k+1,l-1}) + a_8(u^{n-1}_{k+1,l} - 2u^{n}_{k+1,l} + u^{n+1}_{k+1,l}) + \\ & + a_9(u^{n-1}_{k+1,l+1} - 2u^{n}_{k+1,l-1} + u^{n+1}_{k+1,l+1})\end{aligned} \tag{13}$$

with $\sum_{i=1}^{9} a_i = 1$

$$\begin{aligned}\hat{u}_{xx} = {} & b_1(u^{n-1}_{k-1,l-1} - 2u^{n-1}_{k-1,l} + u^{n-1}_{k-1,l+1}) + b_2(u^{n-1}_{k,l-1} - 2u^{n-1}_{k,l} + u^{n-1}_{k,l+1}) + \\ & + b_3(u^{n-1}_{k+1,l-1} - 2u^{n-1}_{k+1,l} + u^{n-1}_{k+1,l+1}) + b_4(u^{n}_{k-1,l-1} - 2u^{n}_{k-1,l} + u^{n}_{k-1,l+1}) + \\ & + b_5(u^{n}_{k,l-1} - 2u^{n}_{k,l} + u^{n}_{k,l+1}) + b_6(u^{n}_{k+1,l-1} - 2u^{n}_{k+1,l} + u^{n}_{k+1,l+1}) + \\ & + b_7(u^{n+1}_{k-1,l-1} - 2u^{n+1}_{k-1,l} + u^{n}_{k-1,l+1}) + b_8(u^{n+1}_{k,l-1} - 2u^{n+1}_{k,l} + u^{n+1}_{k,l+1}) + \\ & + b_9(u^{n+1}_{k+1,l-1} - 2u^{n+1}_{k+1,l} + u^{n+1}_{k+1,l+1})\end{aligned} \tag{14}$$

with $\sum_{i=1}^{9} b_i = \frac{(\Delta z)^2}{(\Delta x)^2}$

and letting

$$\begin{aligned}\hat{u}_{zt} = {} & C_1(u^{n+1}_{k+1,\,l-1} - u^{n+1}_{k-1,\,l-1} - u^{n-1}_{k+1,\,l-1} + u^{n-1}_{k-1,\,l-1}) + \\ & + C_2(u^{n+1}_{k+1,\,l} - u^{n+1}_{k-1,\,l} - u^{n-1}_{k+1,\,l} + u^{n-1}_{k-1,\,l}) + \\ & + C_3(u^{n-1}_{k+1,\,l+1} - u^{n+1}_{k-1,\,l+1} - u^{n-1}_{k+1,\,l+1} + u^{n-1}_{k-1,\,l})\end{aligned} \tag{15}$$

with

$$C_1 + C_2 + C_3 = \frac{1}{2v\Delta z\Delta t}$$

This difference equation

$$\hat{u}_{zz} + \hat{u}_{xx} + \hat{u}_{zt} = 0$$

is consistent with the original full equation (1).

The difference scheme is general, if we restrict ourselves to the 27 lattice points around the point $u^n_{k,\,l}$. Let us now search for an absolutely stable scheme among these schemes. If we arrange the above equation with respect to the index n, the following terms will belong to index $(n+1)$:

$$\begin{aligned}& a_1 u^{n+1}_{k-1,\,l-1} + a_2 u^{n+1}_{k-1,\,l} + a_3 u^{n+1}_{k-1,\,l+1} + a_4 u^{n+1}_{k,\,l-1} + \\ & + a_5 u^{n+1}_{k,\,l} + a_6 u^{n+1}_{k,\,l+1} + a_7 u^{n+1}_{k+1,\,l-1} + a_8 u^{n+1}_{k+1,\,l} + \\ & + a_9 u^{n+1}_{k+1,\,l+1} + b_7(u^{n+1}_{k-1,\,l-1} - 2u^{n+1}_{k-1,\,l} + u^{n+1}_{k-1,\,l+1}) + \\ & + b_8(u^{n+1}_{k,\,l-1} - 2u^{n+1}_{k,\,l} + u^{n+1}_{k,\,l+1}) + b_9(u^{n+1}_{k+1,\,l-1} - 2u^{n+1}_{k+1,\,l} + u^{n+1}_{k+1,\,l+1}) + \\ & + C_1(u^{n+1}_{k+1,\,l-1} - u^{n-1}_{k-1,\,l-1}) + C_2(u^{n+1}_{k+1,\,l} - u^{n+1}_{k-1,\,l}) + \\ & + C_3(u^{n+1}_{k+1,\,l+1} - u^{n+1}_{k-1,\,l+1})\end{aligned} \tag{16}$$

The same terms appear for $(n-1)$, only the signs of the c_i-s will be opposite and b_1, b_2, b_3 will figure. For the index n the c_i-s will be missing, b_4, b_5, b_6 will figure and the a_i-s will appear with coefficient (-2).

By Neumann's method, the amplification factor is the root of the second-order equation

$$(A + B_1 + C)\xi^2 - (2A - B_2)\xi + A + B_3 - C = 0 \tag{17}$$

If we choose the a_i-s symmetrically to a_5, the number A will be real. The number C is pure imaginary. Two cases should be distinguished: either $B_2 = 0$ and $B_1 = B_3$, or $B_2 = B_1 + B_3 = 2B_1$. In the first case the equation for the amplification factor assumes the form

$$(A+B+iF)\xi^2 - 2A\xi + (A+B-iF) = 0 \tag{18}$$

from where

$$\xi_{1,2} = \frac{2A \pm \sqrt{4A^2 - 4(A^2+B^2+2AB+F^2)}}{2(A+B+iF)} \tag{19}$$

In this case we shall have $|\xi| > 1$ for certain values of k_x, k_z, ω since the numbers A, B, F are functions of k_x, k_z, ω that is, the difference scheme is not stable for these values.

In the second case the equation becomes

$$(A+B_1+iF)\xi^2 - (2A-2B_1)\xi + (A+B_1-iF) = 0 \tag{20}$$

that is,

$$\xi_{1,2} = \frac{A-B_1 \pm \sqrt{(A-B_1)^2 - (A+B_1)^2 + F^2}}{A+B+iF} \tag{21}$$

The same situation is encountered as with Eq. (19), that is the difference scheme is not stable in either of the cases. We have not proved, of course, that there exists no absolutely stable difference scheme which would be consistent with the full equation: however, if it exists, its construction will certainly not be an easy task (and it will become more difficult with the incorporation of more lattice points).

3. Approximation of the 15° and 45° equations

CLAERBOUT and JOHNSON [1971] proposed the following approximation in their solution of the 15° equation:

$$u_{k+1}^{n+1} - u_k^{n+1} - u_{k+1}^n + u_k^n = a\mathrm{T}(u_{k+1}^{n+1} + u_k^{n+1} + u_{k+1}^n + u_k^n) \tag{22}$$

where $\mathrm{T}u = u_{l-1} - 2u_l + u_{l+1}$ is the operator of the second difference with respect to x, and

$$a = \frac{v\Delta z \cdot \Delta t}{4(\Delta x)^2} .$$

This scheme is absolute stable, and consistent with the 15° equation. It has been widely used for 2D migration and its properties are well known. If we try to use it, however, for 3D migration, we face the obstacle that the arising system of equations will have a block-tridiagonal, rather than tridiagonal, matrix which

causes a substantial increase in computation time. It would be very important to find new absolutely stable and consistent difference schemes for which there are corresponding linear systems with diagonal matrices. A possible difference scheme arises from the equation

$$u_{k+1}^{n+1} - u_{k-1}^{n+1} - u_{k+1}^{n} + u_{k-1}^{n} = a\mathrm{T}(u_k^{n+1} + u_k^n) \tag{23}$$

Let us first determine the amplification factor:

$$u_{k+1}^{n+1} - a\mathrm{T}u_k^{n+1} - u_{k-1}^{n+1} = u_{k+1}^{n} + a\mathrm{T}u_k^n - u_{k-1}^{n} \tag{24}$$

$$u_k^{n+1}(-a\mathrm{T} + 2i \sin \omega \Delta t) = u_k^n(a\mathrm{T} + 2i \sin \omega \Delta t) \tag{25}$$

$$u_k^{n+1} = \frac{A + iB}{-A + iB} u_k^n \tag{26}$$

$$\xi = \frac{A + iB}{-A + iB} \qquad |\xi|^2 = \frac{A^2 + B^2}{A^2 + B^2} = 1 \tag{27}$$

which proves the stability of the scheme.

In 3D migration, derivatives with respect to y must also be taken into account, i.e. the scheme should be correspondingly modified. In the actual execution of the 3D migration by means of this scheme, we have to simultaneously store 6 vectors as against the 4 vectors needed in Claerbout's scheme. This apparent drawback is counterbalanced by the fact that if we were to carry out 3D migration in a single step by Claerbout's method, the number of operations would increase proportionally to the number of parallel profiles. For example, for an areal survey consisting of 78×85 CDP traces, the migration would require 78 times as much time. One way to circumvent this difficulty is the two-step migration [Ristow and Houba 1979], which, however, causes further inaccuracies in the solution. An additional advantage of the one-step migration is that it saves a great deal of data transfers and requires fewer operations. The 45° equation can also be approximated by difference schemes of the same properties as scheme (23).

A possible choice is:

$$\begin{aligned} &\frac{\mathrm{T}}{a}(u_{k+1}^{n+1} - u_{k+1}^{n} + u_k^{n+1} - u_k^n) - \frac{1}{b}(u_{k+2}^{n+1} - u_{k+2}^{n} + \\ &\quad u_{k+1}^{n} - u_{k+1}^{n+1} - u_k^{n+1} + u_k^n + u_{k-1}^{n+1} - u_{k-1}^{n}) = \\ &\qquad = \frac{\mathrm{T}}{c}(u_{k+1}^{n} - u_k^n + u_{k+1}^{n+1} - u_k^{n+1}) \end{aligned} \tag{28}$$

where

$$a^{-1} = \frac{1}{(\Delta x)^2 \Delta z}, \; b^{-1} = \frac{4}{v^2 \Delta x (\Delta t)^2}, \; c^{-1} = \frac{2}{v(\Delta x)^2 \Delta t} \tag{29}$$

It can be shown that the difference scheme (28) is consistent with the so-called 45° equation:

$$u_{xxz} = \frac{4}{v^2} u_{ztt} + \frac{2}{v} u_{xxt} \tag{30}$$

The proof of consistency has been omitted as it is quite lengthy and does not require any original thoughts beyond the usual manipulations. This difference scheme also has the drawback that more data should be stored, and the same advantageous property: during solution the system of equations decomposes into independent subsystems.

Stability can be shown as follows. Rearranging Eq. (28) with respect to index k we get

$$\begin{aligned} \frac{\mathrm{T}}{a}(u_{k+1}^{n+1} + u_k^{n+1}) - \frac{1}{b}(u_{k+2}^{n+1} - u_{k+1}^{n+1} - u_k^{n+1} + u_{k-1}^{n+1}) - \\ \frac{\mathrm{T}}{c}(u_{k+1}^{n+1} - u_k^{n+1}) = \frac{\mathrm{T}}{a}(u_{k+1}^n + u_k^n) - \\ - \frac{1}{b}(u_{k+2}^n - u_{k+1}^n - u_k^n + u_{k-1}^n) + \\ + \frac{\mathrm{T}}{c}(u_{k+1}^n - u_k^n) \end{aligned} \tag{31}$$

By Neumann's method, the amplification factor ξ will assume again the form

$$\xi = \frac{A - iB}{A + iB} \tag{32}$$

that is, $|\xi| = 1$, which proves stability.

It should finally be noted that these new difference schemes have not yet been checked on actual seismic data: their applicability, advantages and disadvantages, will only be proved by practice.

REFERENCES

CLAERBOUT J. F., 1976: Fundamentals of geophysical data processing. McGraw Hill, New York
CLAERBOUT J. F., JOHNSON A. G., 1971: Extrapolation of time dependent waveforms along their path of propagation. Geophys. J. R. Astron. Soc. **26**, 14, pp. 285—295
LOEWENTHAL D., LU L., ROBERTSON R., SHERWOOD J., 1976: The wave equation applied to migration. Geophys. Prosp. **24**, pp. 380—399
RICHTMYER R. D., MORTON K. W., 1967: Difference methods for initial value problems. John Wiley, New York
RISTOW D., HOUBA W., 1979: 3 D finite difference migration. Paper presented at the 41st EAEG Meeting, Hamburg

ÚJABB DIFFERENCIA-SÉMÁK A HULLÁMEGYENLET MIGRÁCIÓHOZ

MÄRLE Róbert

A cikk olyan differencia-sémákat ír le, amelyeket eddig nem használtak a hullámegyenlet migrációhoz. Ismerteti az új sémák tulajdonságait, különös tekintettel azokra, amelyek a 3 D migráció szempontjából jelentősek.

НОВЫЕ ДИФФЕРЕНЦИАЛЬНЫЕ СХЕМЫ ДЛЯ МИГРАЦИИ ПО ВОЛНОВОМУ УРАВНЕНИЮ

Р. МЭРЛЕ

В работе дается описание дифференциальных схем, которые до сих пор не были использованы для миграции по волновому уравнению. Обсуждаются особенности новых схем, причем особое внимание придается тем, которые считаются важными с точки зрения пространственной миграции.

GEOPHYSICAL TRANSACTIONS 1984
Vol. 30. No. 2. pp. 167—176

MULTI-OFFSET VERTICAL SEISMIC PROFILING

J. KNIGHT*, L. HOROWICZ**

A Vertical Seismic Profile (VSP) was made, using a vibroseis source, in a well in Austria owned by OEMV-AG. Seven offset source seismic profiles were also made, using a vibroseis source. Normal moveout corrections, based on the velocity model from the zero offset VSP, were applied during processing of the offset seismic profiles. Using five of the offset profiles in one direction from the well, a processing technique was developed to produce a combined, multi-offset common depth point display. Interpretation was based on ray-trace modelling, and production of synthetic VSP's. A quantitative estimate of the dip of a dominant reflector was made, and it was possible to infer lateral structural changes.

d: vertical seismic profiling (VSP), offset, vibroseis

1. Introduction

Vertical Seismic Profiling (VSP) consists of using a surface seismic source placed near a borehole, and recording the seismic response of the earth at a receiver placed at different depths over an interval in the borehole. The receiver consists of a set of geophones (four for example) in a downhole tool which is coupled to the side of the borehole by a caliper arm. The signal is recorded digitally and processed in a similar way to surface seismic signals. The basic advantages of such borehole seismic profiling over surface seismic profiling are:

1. The detector is closer to reflecting layers
2. The downgoing wavefield can be studied separately from the upgoing wavefield, giving better information on reverberations (multiples)
3. A better deconvolution operator can thus be designed
4. The true depth of any reflector intersecting the borehole is directly determined

VSP can be divided into a) Vertical ray-path VSP
b) Offset source (non-vertical ray-path) VSP

In the case of offset VSP the seismic source is placed a significant distance away from the top of the borehole, to provide lateral subsurface coverage away from the borehole as the receiver is moved up the borehole.

In both cases, separation of up and downgoing wavefields is then achieved by applying a "velocity filter" which discriminates on the basis of the difference in apparent velocity (or moveout) of up and downgoing events as seen by the spread of detector positions (set of levels) in the borehole.

* Société de Prospection Electrique Schlumberger, Koninginnegracht 15, Den Haag, Holland
** Société de Prospection Electrique Schlumberger, 12, Place des Etats Unis, Montrouge, Paris
Paper presented at the 28th International Geophysical Symposium, Balatonszemes, Hungary, 28 September—1 October, 1983

In the example described in this paper a vertical ray-path VSP was carried out with the source close to the well (30 metres offset), and five additional VSP's were made with the source at increasing offsets away from the borehole in one direction, up to 1662 metres. Two more offset profiles were made in other directions from the well. The same acquisition parameters were used for all source positions, namely, a Mertz Vibrator source, 3 upsweeps per level, 9—100 Hz in 13 seconds, with a level separation of 5 milliseconds giving a spatial aliasing frequency of 100 hertz. The downhole tool was a lightweight (70 kg) prototype with positive pressure coupling.

The final result of this survey was the development of software to produce a combined multioffset VSP, using the five offset data sets in one direction from the borehole. A ray-path modelling program was used to interpret the results.

2. Single offset VSP processing

The vertical ray-path VSP was processed using a standard VSP processing chain (including velocity filtering and deconvolution). The result is shown in *Figure 1* where the VSP can be compared with the sonic and density logs, the acoustic impedance curve, and the synthetic seismograms. The velocity information at the borehole from this VSP was used as a basis for a model to derive normal moveout (NMO) corrections for the offset VSP data, before applying the velocity filter to each data set. For each VSP data set, the raw data were redisplayed and edited before stacking to produce a single trace at each receiver level in the borehole. The stacks were normalized, band-pass filtered and a True Amplitude Recovery consisting of an exponential gain was applied to correct for geometrical spreading. A static correction was applied to the vertical ray-path VSP first break times to reference them to the chosen seismic reference datum.

Fig. 1. Zero-offset VSP after wave shaping

1. ábra. Lyukszáji VSP jelalak formálás után
1 — összegzés kivágással; 2 — elsődleges reflexiók; 3 — csak többszörösök; 4 — elsődleges és többszörös reflexiók; 5 — csillapitás menet; 6 — intervallum-sebesség; 7 — idő—mélység görbe; 8 — akusztikus impedancia; 9 — reflexiós koefficiensek; 10 — sűrűség; 11 — akusztikus karotázs

Рис. 1. ВСП с нулевым смещением после формирования сигнала
1—накапливание с вырезом; 2—первычные отражения; 3—только многократные; 4—первычные и многократные отражения; 5—ход затухания; 6—интервальная скорост; 7—крывая время-глубина; 8—акустический импеданс; 9—коеффициенты отражения; 10—плотность; 11—акустический каротаж

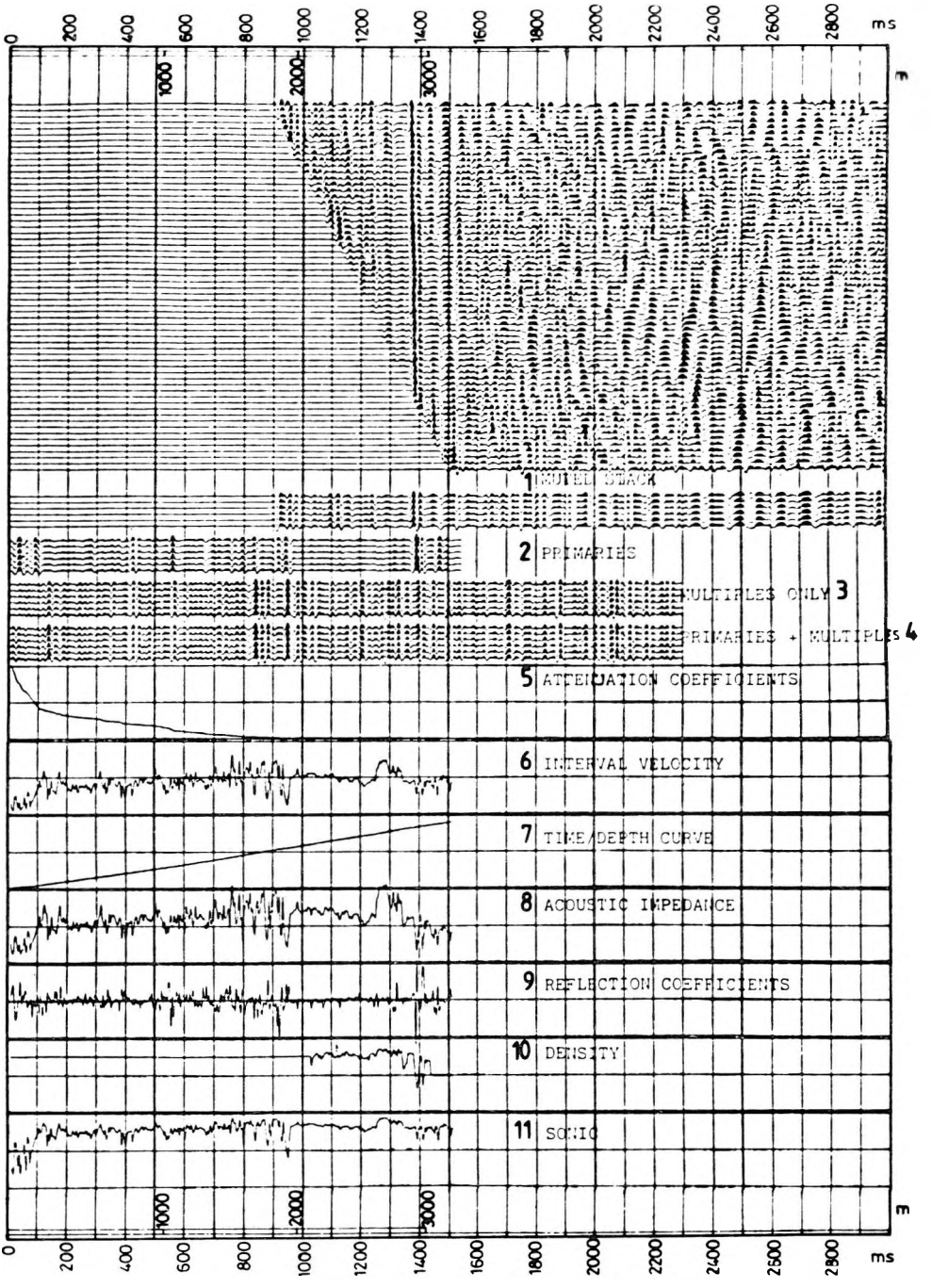
0
200
400
600
800
1000
1200
1400
1600
1800
2000
2200
2400
2600
2800
ms
1000
2000
3000
m
1 MODEL STACK
2 PRIMARIES
3 MULTIPLES ONLY
4 PRIMARIES + MULTIPLES
5 ATTENUATION COEFFICIENTS
6 INTERVAL VELOCITY
7 TIME/DEPTH CURVE
8 ACOUSTIC IMPEDANCE
9 REFLECTION COEFFICIENTS
10 DENSITY
11 SONIC
0
200
400
600
800
1000
1200
1400
1600
1800
2000
2200
2400
2500
2800
ms
1000
2000
3000
m

A normal moveout (NMO) correction was then applied to each set of offset data, using the velocity function derived from the first break time/depth curve of the vertical ray-path VSP. This NMO correction has the effect of replacing the oblique reflector travel times from the source to the receiver by the corresponding vertical two-way travel times between the surface datum and the reflection point. The corrections are determined by assuming a horizontally layered model, and using the ray tracing program to model reflection transit

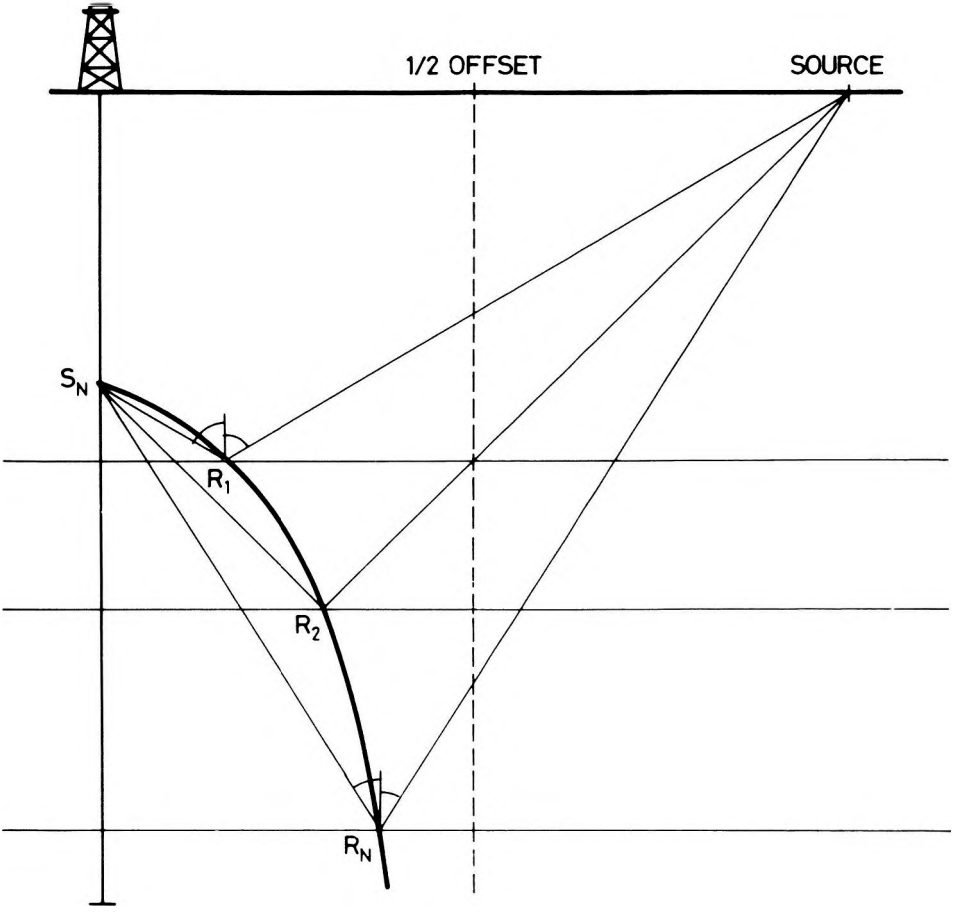

Fig. 2. Hyperbola of mirror points

2. ábra. A reflektáló pontok hiperbolája

Рис. 2. Гипербола зеркальных точек

times. This program is based on an iterative process to find the correct Fermat ray-paths from source to receivers, within a 2-dimensional velocity layer model which can be created interactively on a visual display unit. A further static correction was applied to each offset data set to tie it to the time/depth curve of the vertical ray-path VSP.

After application of this NMO correction each offset data set was then processed with the velocity filter to separate upgoing from downgoing wavefields. The upgoing wavefields were deconvolved using a filter designed and applied firstly on the downgoing wavefield, with a band width limited zero phase output wavelet. At this stage the offset VSP data can be overlain with a set of equi-offset lines (at 50 metre offset intervals), which indicate the lateral offset of any reflecting points from the borehole. Naturally these lines are not parallel with the time axis since the reflection points at different reflectors for any pair of offset source and receiver positions lie on a parabola (see *Figure 2*). These lines are determined from ray tracing using the velocity model on which the NMO corrections were based. The 491 m offset data set has been illustrated at this stage of processing in *Figure 3*.

The final step on each data set is to produce a "corridor stack" of the data between adjacent equi-offset lines to produce constant offset traces similar to surface seismic data. The averaging implicit to this procedure is justified on the basis of the Fresnel zones associated with wave propagation. These "corridor stacks" are shown in *Figure 4*.

3. Multi-offset VSP processing

It is now possible to consider consolidating all the data to produce a multi-offset common depth point (CDP) stack from all the deconvolved data. This is achieved simply by combining all the constant offset traces to produce a single profile. The result of this is also shown in Figure 4.

4. Interpretation

The following reflections can be correlated across all the offset VSP out to 996 m with their probable significance indicated.

A) 1.12 s (velocity decrease)
B) 1.26 s (velocity increase)
C) 1.29 s (velocity decrease)
D) 1.38 s (velocity decrease)

Between 1.45 and 1.56 seconds a series of positive and negative reflections are observed. Below 1.6 seconds it is difficult to make a common positive correlation between VSP while the low frequency events observed below 2.2 s are probably shear wave reflections.

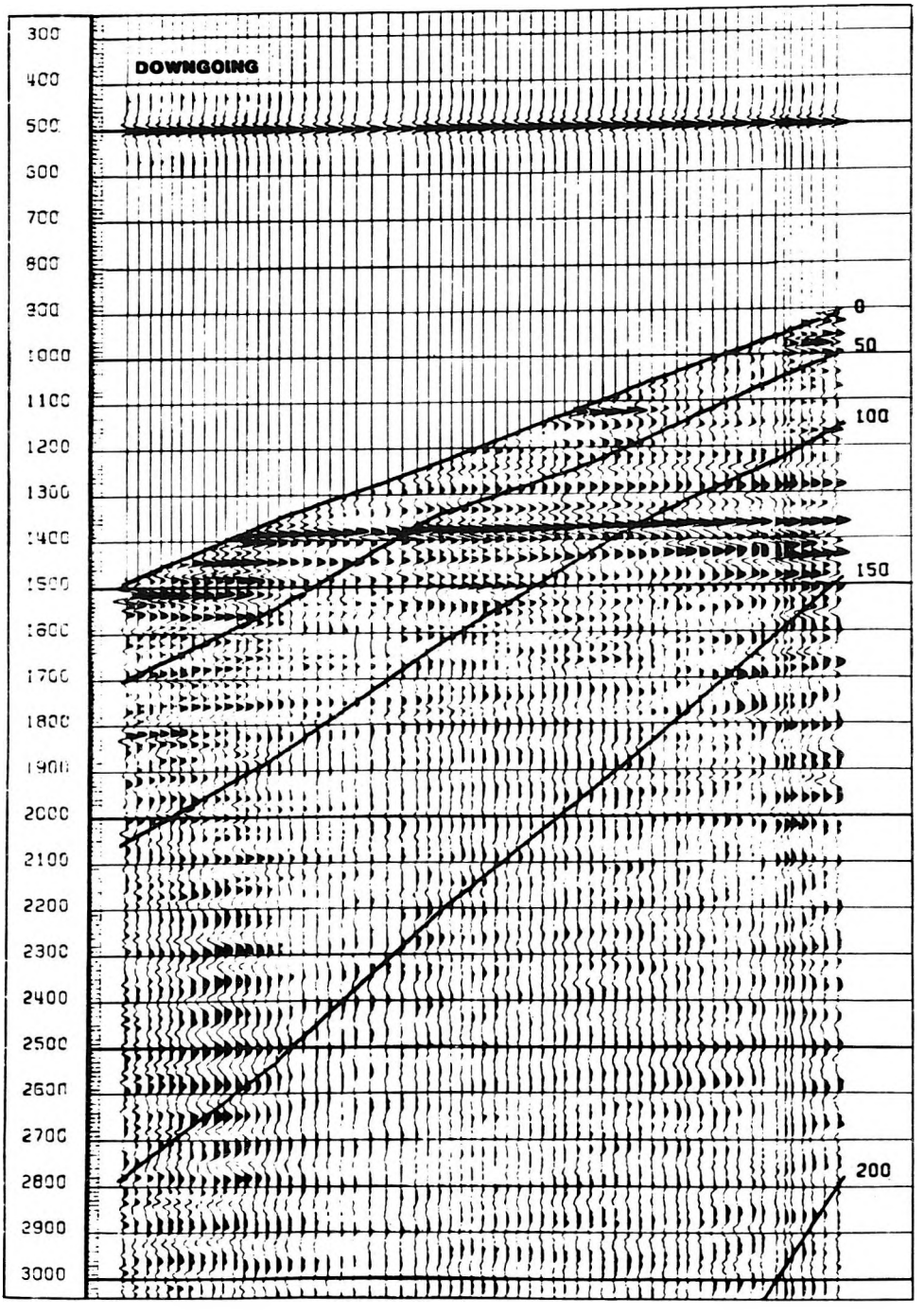
DOWNGOING
0
50
100
150
200
300
400
500
600
700
800
900
1000
1100
1200
1300
1400
1500
1600
1700
1800
1900
2000
2100
2200
2300
2400
2500
2600
2700
2800
2900
3000

The dominant reflection D at 1.38 seconds is observed on all the offset VSP's except that at 2612 m it corresponds to a velocity decrease at 2880 m observed on the time-depth curve. It dips upwards towards the South-East. The assembly of single offset CDP stacks in this direction indicate that the apparent dip decreases with offset. When these are summed to form the multi-offset CDP stack the net effect is to give a convex form to the updip trend. Although this ties well with the seismic section, the fact that we have based the NMO correction on a horizontal model means that the actual reflection offsets are greater than indicated by the equi-offset curves. This effect is more pronounced for the short offset VSP's which will thus have greater apparent dips. *Table 1* shows the corresponding model and measured delta times and indicates that a 10° dip is a reasonable estimate.

5. Conclusions

The survey described in this paper has shown that:

a. Offset VSP surveys reveal lateral structure;
b. Larger offsets give better resolution away from the borehole, but introduce shear wave problems;
c. Single offset VSP data sets (one source, many receivers) can be combined to produce a multi-offset profile.

The technique of offset VSP allows the reconstruction of the subsurface model in the vicinity of the borehole, in a deterministic way. This implies that the model must be known, so it is at least a way of validating surface seismic structural interpretation. In addition, however, the sonic log and check shot calibration (from VSP first breaks), provides a velocity model at the borehole. Therefore the aim of the modelling is largely to resolve structure away from the well. Although the VSP NMO correction method is relatively insensitive to changes in the dip in the models, the positions of actual reflection points are very sensitive to dip. Thus there must be some knowledge of structural dips (from surface seismic and borehole dipmeter interpretation) if the results of the corridor stacking process are to be meaningful. Where the lateral coverage is large, dips can be more readily determined directly from an offset VSP profile.

Fig. 3. 491 m offset VSP upgoing waves after deconvolution to 8—64 Hz signal and 50 m equi-offset lines

3. ábra. 491 m gerjesztési távolsággal felvett VSP felfelé haladó hullámai 8—64 Hz-es vibro-dekonvolúció után, az azonos fúrás—reflektáló ponttávolság vonalaival

Рис 3. Поднимающиеся волны ВСП при смещении 491 м после деконволюции сигналов 8—64 Гц и изолиниями смещения через 50 м

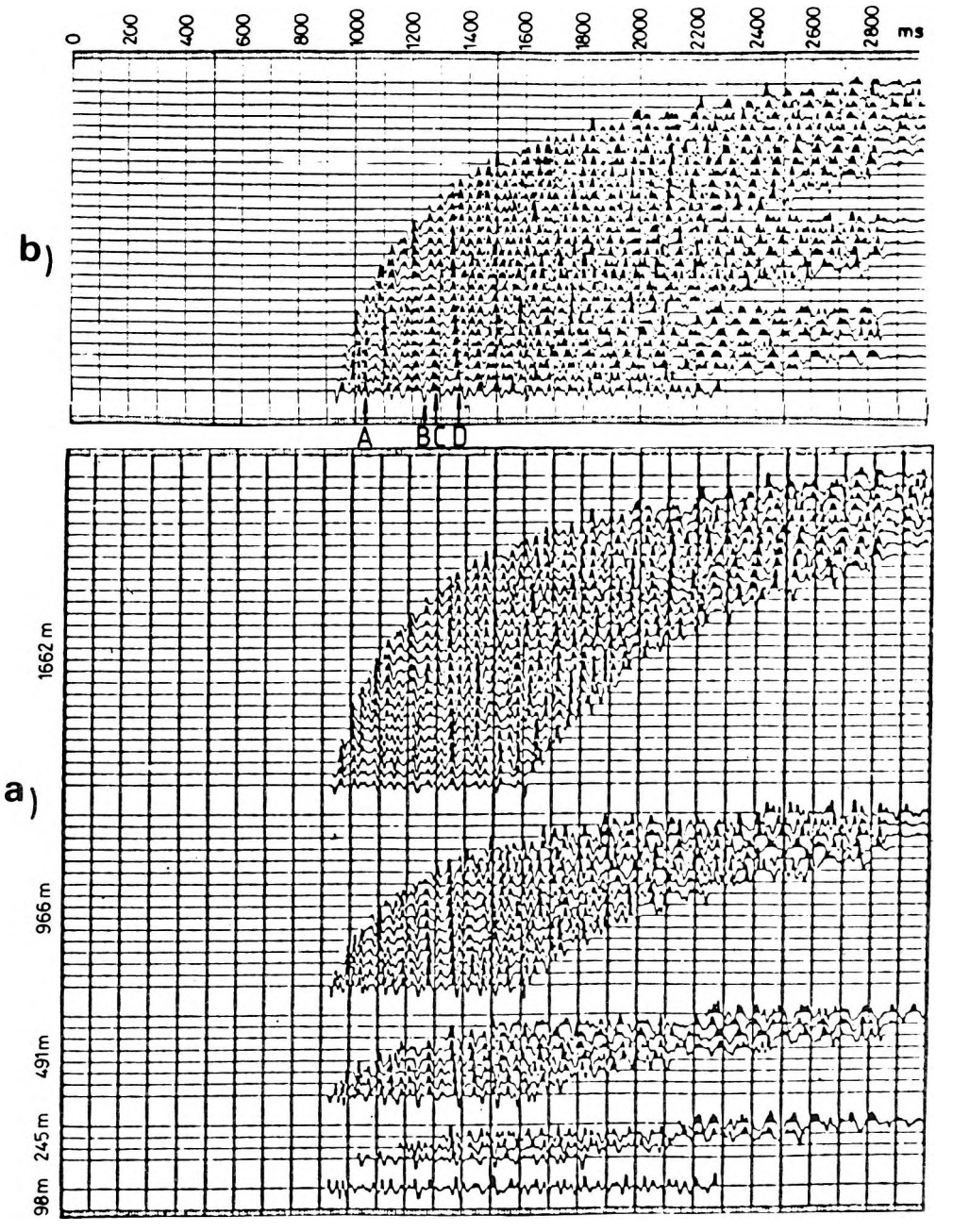
0
200
400
600
800
1000
1200
1400
1600
1800
2000
2200
2400
2600
2800
ms
b)
A
B
C
D
a)
1662 m
966 m
491 m
245 m
98 m

The approach used in this study of inversion through ray-tracing theory is probably limited to fairly simple structural dip models. Such approaches as "Dip Analysis", using the known velocities and an increase in the redundancy of data to provide a means of compiling "residual surface consistent" statics, are now being investigated.

Acknowledgment

We would like to extend our appreciation to the management of OEMV-Aktiengesellschaft, for permitting the publication of this paper.

VÁLTOZÓ IRÁNYÚ ÉS TÁVOLSÁGÚ GERJESZTÉSSEL VÉGZETT VERTIKÁLIS SZEIZMIKUS SZELVÉNYEZÉS (VSP)

J. KNIGHT, L. HOROWICZ

A szerzők vibroseis-gerjesztéssel vertikális szeizmikus szelvényezést (VSP) végeztek egy ausztriai mélyfúrásban. A szokásos felvételen kívül hét, különböző távolságú gerjesztést is alkalmaztak. A lyukszáji gerjesztéssel kapott sebesség-modell alapján végezték az eltolásos felvételek dinamikus korrekcióját. Eljárást dolgoztak ki különböző eltolású gerjesztéssel kapott szelvények közös mélységpontos szelvénnyé történő egyesítésére, amelyet öt, közös egyenes mentén eltolt gerjesztéssel felvett szelvényre alkalmaztak. Az interpretációt sugár-vezetéses modellezés és a szintetikus VSP-k készítése segítségével végezték. Kvantitatíve meghatározták egy domináns reflektor dőlését, és oldalirányú szerkezeti változásokat is sikerült kimutatniuk.

Fig. 4. Processing of VSP seismograms
a) corridor stacks after wave shape filter
b) combined multi-offset VSP
98—245—491—1662 m offsets

4. ábra. VSP szeizmogramok feldolgozása
a) VSP szeizmogramok transzformálása az $x—t_0$ síkra
b) A transzformált szeizmogramok összegzése

Рис. 4. Обработка сейсмограмм ВСП
а) преобразование сейсмограмм ВСП на плоскость $x—t_0$
b) накапливание сейсмограмм ВСП при смещении

ВЕРТИКАЛЬНОЕ СЕЙСМИЧЕСКОЕ ПРОФИЛИРОВАНИЕ С МНОГОКРАТНЫМ СМЕЩЕНИЕМ ИСТОЧНИКА

Й. НАЙТ, Л. ГОРОВИЦ

Было проведено вертикальное сейсмическое профилирование (ВСП) с использованием вибросейсмического источника в скважине фирмы OEMV-AG (Австрия). Были также изготовлены семь сейсмических профилей при смещении вибрационного источника. Кинематическая поправка, основанная на скоростной модели с нулевым смещением ВСП, была введена при обработке смещенных сейсмических профилей. С использованием пяти из смещенных профилей по одному направлению от скважины была разработана техника обработки с целью комбинированного изображения по общей глубинной точке с многократным смещением. Интерпретация была основана на моделировании траекторий и создании синтетических ВСП. Была проведена количественная оценка наклона опорной отражающей поверхности и были сделаны выводы о продольных структурных изменениях.

GEOPHYSICAL TRANSACTIONS 1984
Vol. 30. No. 2. pp. 177—200

INTEGRATED INTERPRETATION OF SEISMIC AND WELL LOGGING DATA IN THE DETAILED PHASE OF OIL AND GAS EXPLORATION AND IN THE SEARCH FOR STRATIGRAPHIC TRAPS

G. N. GOGONENKOV*, S. S. ELMANOVICH*, V. V. KIRSANOV*, Yu. A. MIKHAILOV*

A description is given of the case history of a western Siberian oil field where the technique of seismic stratigraphy was combined with the most up-to-date dynamic processing of seismic profiles. All geological information, well logs, seismic and petrophysical parameters were integrated to produce a reliable assessment of the hydrocarbon potential of the area.

d: seismic surveys, well logging, integrated interpretation, seismic stratigraphy, oil and gas fields, stratigraphic traps, western Siberia

1. Introduction

In recent years the rapid development of seismic methodology and technology has greatly contributed to the sharp increase in depth range, accuracy and detailedness of the studies of geological sections, particularly in hydrocarbon prospecting. Also, the increased possibilities of the seismic method suggest that these techniques should have an important role in the later stages of the geologic-exploratory process as well, namely, in the stage of the detailed exploration and industrial exploitation of the deposits. It is expected that seismic prospecting in combination with well logging data would help us to achieve substantial cuts in costs and deadlines when opening up new reservoirs. One only needs to recall that usually most of the enormously expensive exploratory drilling is done during the detailed exploration phase. A drastic reduction in the number of exploratory drillings at the expense of deeper interpretation of the available seismic material is one of the most important tasks of exploration geophysics from the economic viewpoint. We foresee a particularly important effect of the more precise determination of the structure of reservoirs. Complex analysis of all available data could also be useful in the planning of post-exploration work, and in the detection of associated deposits, including non-anticlinal traps.

Our study is based on seismic sections, processed by the PGR program package (the Russian abbreviation stands for Prognozirovanie Geologiches-

* Central Geophysical Expedition of the Oil Ministry, 123298 Moscow, ul. Narodnogo Opolcheniya 4o. korp. 3, USSR
Manuscript received: 15 July, 1983

kogo Razreza = Prediction of the (lithologic properties of) Geological Sections, see GOGONENKOV [1981 a, 1981 b]), and subsequently analysed by the methods of seismic stratigraphy [PAYTON 1977]. We also carried out facies analysis on the well log data. The present work describes the methodological foundations of the integrated interpretation and illustrates its effectiveness through a case history dealing with the post-exploration for hydrocarbon reservoirs on a western Siberian exploration site.

2. Scheme of the integrated interpretation of geological–geophysical data on the basis of seismic stratigraphy

The sequence of, and interconnections between the individual stages of the whole procedure — from the preparation and editing of the input data to the

Fig. 1. Schematic flow-chart of processing of geological–geophysical data by seismic stratigraphy

1. ábra. A szeizmikus sztratigráfiai adatfeldolgozás folyamatábrája

1—BEMENŐ INFORMÁCIÓK; 2—pillanatnyi amplitúdók, frekvenciák és fázisok; 3—időszelvények; 4—pszeudo-akusztikus szelvények; 5—kőzettani adatok akusztikus, gamma-gamma és egyéb karotázs görbék alapján; 6—geológiai információk (a priori szedimentációs modell, fúrási adatok); 7—karotázs adatok (látszólagos ellenállás, PS, neutron-gamma stb.); 8—próbaüzemi adatok, olaj/víz határ meghatározása; 9—AZ ADATOK EGYBEVETÉSE; 10—időszelvények és pszeudo-akusztikus szelvények a karotázs-adatokkal; 11—reflexiók sztratigráfiai korrelációja; 12—karotázs-adatok idő-léptékben; 13—SZEIZMIKUS SZTRATIGRÁFIAI ÉRTELMEZÉS; 14—időszelvények és pszeudo-akusztikus szelvények rekonstrukciója az eredeti síkban; 15—szeizmikus sztratigráfiai analízis; 16—fácies analízis; 17—szeizmikus fácies térképek; 18—szeizmikus litofácies szelvények; 19—karotázs fácies térképek; 20—szedimentációs modell; 21—a hullámtér paramétereinek kvantitatív becslése; 22—a dinamikai paraméter- és akusztikus impedanciatérképek szerkesztése; iteratív modellezés; 23—izokron térképek, szerkezeti és paleo-szerkezeti térképek; 24—EREDMÉNYEK; 25—a perspektivikus objektumok kiválasztása; 26—javaslatok részletes szeizmikus kutatásra; 27—javaslatok a fúrási tervhez; 28—javaslatok a termelő fúrási program módosítására

Рис. 1. Схема комплексной интерпретации геолого-геофизических данных на сейсмостратиграфисеской основе

1—исходная информация; 2—мгновенные амплитуды, мгновенные частоты, мгновенные фазы; 3—временные разрезы; 4—разрезы ПАК; 5—петрофизические данные по АК, ГГК, СК и др.; 6—геологическая информация (исходная модель, осадконаколления, данные анализа керна); 7—каротажные данные (КС, ПС, ГК, НГК, КВ и др.); 8—результаты опробования СКВ, положение ВНК; 9—комплексирование данных; 10—временные разрезы и разрезы ПАК в комплексе с каротажными данными; 11—стратиграфическая привязка отражений; 12—каротажные данные во временном масштабе; 13—сейсмостратиграфическая интерпретация; 14—палеореконструкции временных разрезов и разрезов ПАК; 15—сейсмостратиграфический анализ; 16—фациальный анализ; 17—карты сейсмических фаций; 18—сейсмолитофациальные разрезы; 19—карты каротажных фаций; 20—модель осадконакопления; 21—количественная оценка параметров волнового поля; 22—построение карт динамических параметров и карт акустических жесткостей, моделирование (ПМС); 23—карты изохрон, структурные и палеоструктурные карты; 24—результаты; 25—выделение перспективных объектов; 26—рекомендации на проведение детальных сейсмических исследований; 27—рекомендации на бурение скважин; 28—рекомендации на изменение проекта эксплуатационного бурения

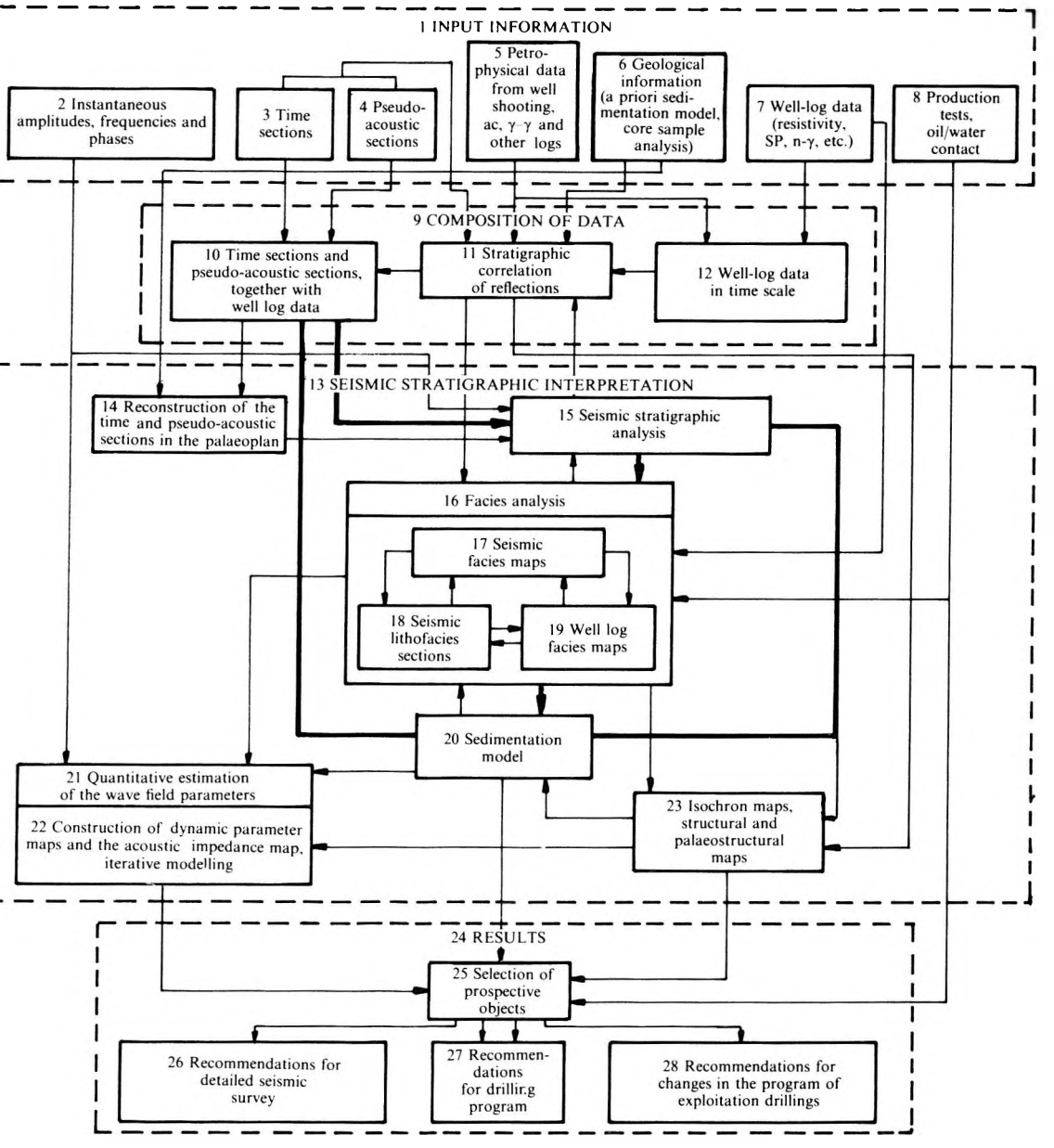
1 INPUT INFORMATION
2 Instantaneous amplitudes, frequencies and phases
3 Time sections
4 Pseudo-acoustic sections
5 Petro-physical data from well shooting, ac, γ-γ and other logs
6 Geological information (a priori sedi-mentation model, core sample analysis)
7 Well-log data (resistivity, SP, n-γ, etc.)
8 Production tests, oil/water contact
9 COMPOSITION OF DATA
10 Time sections and pseudo-acoustic sections, together with well log data
11 Stratigraphic correlation of reflections
12 Well-log data in time scale
13 SEISMIC STRATIGRAPHIC INTERPRETATION
14 Reconstruction of the time and pseudo-acoustic sections in the palaeoplan
15 Seismic stratigraphic analysis
16 Facies analysis
17 Seismic facies maps
18 Seismic lithofacies sections
19 Well log facies maps
20 Sedimentation model
21 Quantitative estimation of the wave field parameters
22 Construction of dynamic parameter maps and the acoustic impedance map, iterative modelling
23 Isochron maps, structural and palaeostructural maps
24 RESULTS
25 Selection of prospective objects
26 Recommendations for detailed seismic survey
27 Recommen-dations for drilling program
28 Recommendations for changes in the program of exploitation drillings

final conclusions and recommendations — are schematically shown in *Fig. 1.* Input data can include all kinds of geological–geophysical information about the study site: seismic data (both in the usual presentation and transformed into instantaneous frequency-, amplitude- and phase sections as described in PTETSOV and GOGONENKOV [1982], or into pseudo-acoustic impedance sections, [cf. GOGONENKOV et al. 1980]; well logging data of exploratory boreholes and analysis of core samples; all available geological information (sedimentation models, stratigraphy, lithology, descriptions of the core samples and of the mud, etc.); and all relevant petrophysical relationships and data, primarily as regards velocities and bulk densities, these having the greatest influence on the seismic wave field.

A few remarks should be made on preliminary seismic data processing, for all subsequent steps basically depend on this very important stage. The preliminary processing should transform the recorded seismograms into a time section that could be considered as an undistorted model of the wave field. The time section should contain only primary reflections from plane-wave sources within the medium, the elastic signal should have zero-phase characteristics in the useful frequency range. Using state-of-the-art processing packages for multiple-coverage seismic data [KOZLOV et al. 1973], and the novel possibilities of true amplitude recovery [AVERBUKH 1982], this goal can always be achieved under favourable seismogeological conditions. Since the final interpretation will have been based on the dynamic parameters of the reflected waves, unusually high requirements should be imposed on the completeness and thoroughness of the processing, both in the design of the processing flow-chart and in the selection of the parameters for the individual steps. The main criteria against which processing quality should be matched is, how does the resulting time section fit to the above-described models? The agreement has to be checked by wave-field analysis, which has become an integral part of all up-to-date seismic processing systems.

The first, and crucial step of integrated interpretation is the juxtaposition of the seismic and well log data to the same scale. In order to do this, the well logs should be rescaled from depth to two-way travel time, by means of the proper velocity function, and superimposed on the seismic sections. (Or, alternatively, we transform the seismic time sections into depth, and use both kinds of data in depth scale). An example of the composite display of seismic data and SP logs is shown in *Fig. 2.* In lack of marker horizons and if the velocity distributions and temporal tie-ins are not accurately known, the combination of seismic and well log data could be an intricate and uncertain task whose proper solution calls for the utilization of all available geological–geophysical information.

Having constructed an intercorrelating network of seismic and well log data, we can proceed to the central part of the investigation, to seismic stratigraphy, where we construct the sedimentation model, and estimate the geological nature and petrophysical properties of the different sedimentary sequences with a degree of resolution allowed by the seismic material.

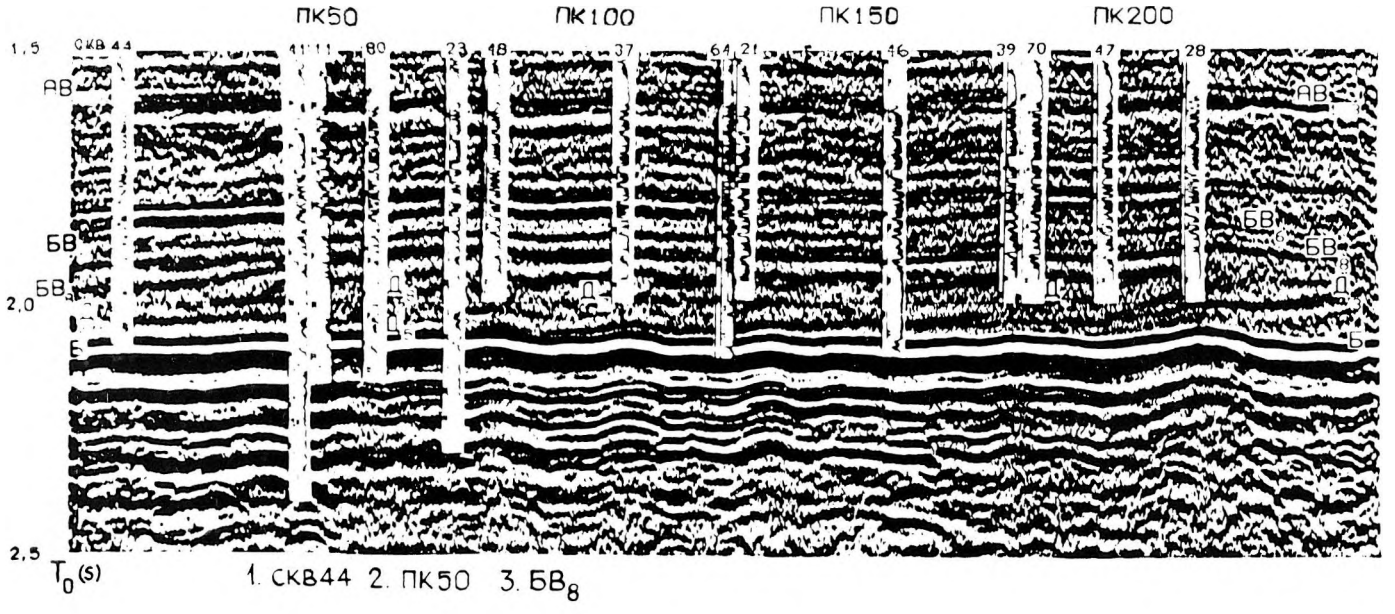

Fig. 2. Composite display of the seismic and well log data (SP log) for Profile 3 of the Pokacheva area
1—borehole; 2—pegmark; 3—payzone

2. ábra. A szeizmikus és karotázs (PS) adatok együttes ábrázolása a Pokacseva terület 3. számú szelvényén
1—mélyfúrás; 2—karószám; 3—termelő réteg

Рис. 2. Совместное изображение сейсмической и промыслово-геофизической (кривые ПС) информации по профилю 3 Покачевской площади

The basic task of seismic stratigraphy is to be able to create geological hypotheses about the sedimentation models of the target (productive and prospective strata). We start out from *a priori* hypotheses, and these are gradually improved as we iteratively proceed through more and more refined variants of the sedimentation model, and by a composite study of the seismic and well log facies.

The following are the basic tasks of seismic stratigraphy in the detailed phase of seismic prospecting:

a) To delineate and analyse the large stratigraphic units (seismic sequences) of the seismic time section, corresponding to long periods (of a few million years) in the development of the palaeo-basin, each of them corresponding to different palaeotectonic conditions of sedimentation.

b) To delineate and study the seismic facies belonging to these sequences.

c) To predict the source rocks.

After performing these tasks we predict the sedimentation conditions and the lithology, delimit the reservoirs and sealing formations, and map the prospective CH-bearing objects. *Figure 3* illustrates the subdivision of a west Siberian time section into seismic sequences. If we have to confine ourselves to the relatively short sections of the detailed survey, we often face a particular problem: the seismic profiles reveal only parts of the sequences so that their structural regularities and their extension cannot be fully clarified. To circumvent this problem, the stratigraphic analysis of local areas should be supplemented by seismic facies analysis.

In order to construct the seismic facies map, the relative positions of the fragments of the analysed time sections should exactly repeat the configuration of seismic profiles (as shown in *Fig. 4*, where the elements of the facies map were taken from a series of E—W profiles of the given area).

In order to decipher the genetic nature of the seismic facies we use the seismic lithofacies sections and the well log facies maps. The seismic lithofacies sections are constructed from a combined interpretation of the time sections, core samples, grain-size analyses and the whole complex of geophysical well log data. For the analysis, the vertical scale of the sections is transformed to that of the well logs while the horizontal scale will be that of the seismic sections. In the correlation between lithostratigraphic units the well log data should be matched with the seismic sections. In spite of the significant differences between the resolution power of the two methods, we can still avoid the pitfalls in the correlation of the well log information and we shall more accurately represent the geological build-up even at those places where no boreholes were available *(Fig. 5)*.

The seismic lithofacies sections can also be constructed on the palaeoplan. *Figure 6* shows the section of Fig. 5, reconstructed in the palaeoplan. Usually, we take the roof of the thick shale formation as the datum plane in palaeo-reconstructions, because of its good lateral correlation. The palaeo-reconstruction of the seismic lithofacies sections reveals the palaeotectonic development

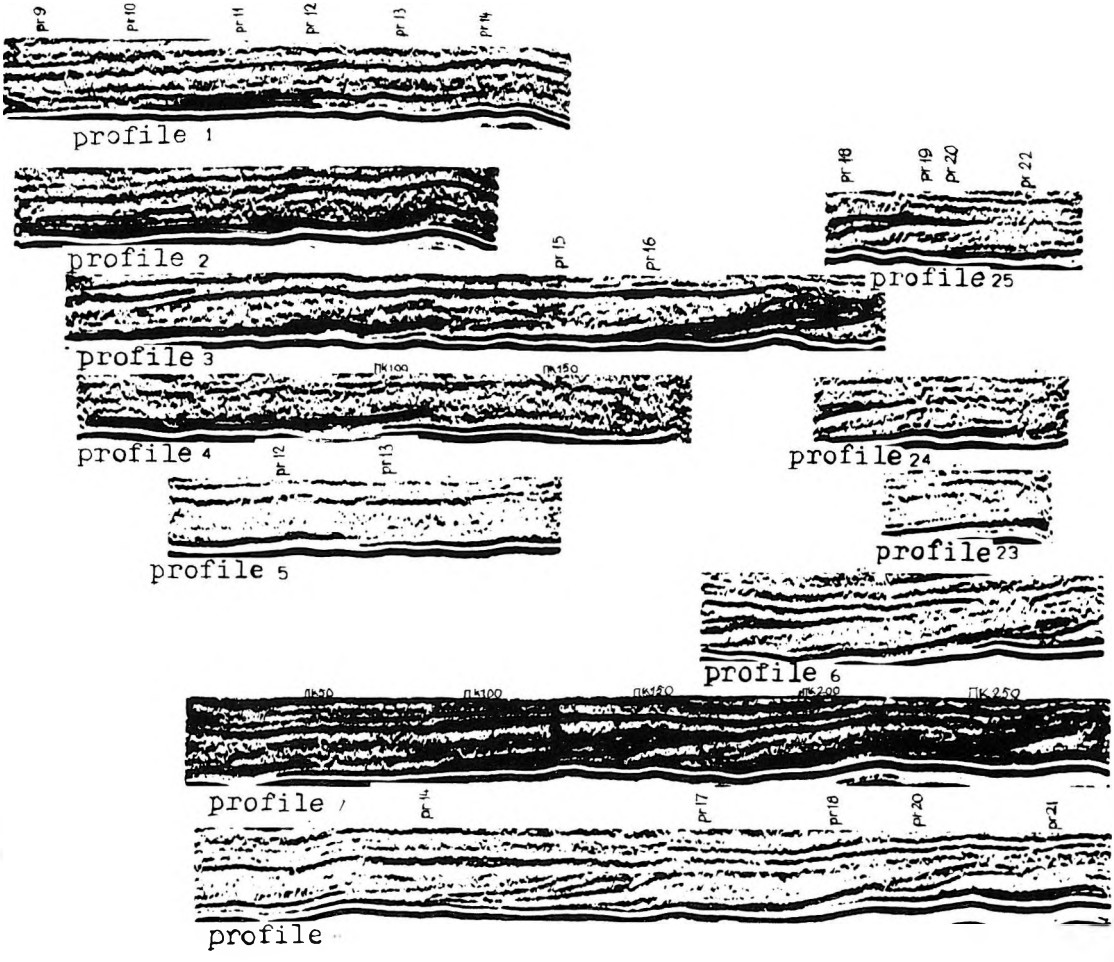

Fig. 4. Elements of the seismic facies map. E–W profiles, Pokacheva area

4. ábra. A szeizmofacies térkép elemei. Pokacseva terület, K–Ny-i szelvények

Рис. 4. Элемент карты сейсмических фаций. Профили широтного простирания. Покачевская площадь

Fig. 3 can be found on the last page

A *3. ábra* a füzet utolsó oldalán található

Рис. 3 приведен на последней странице

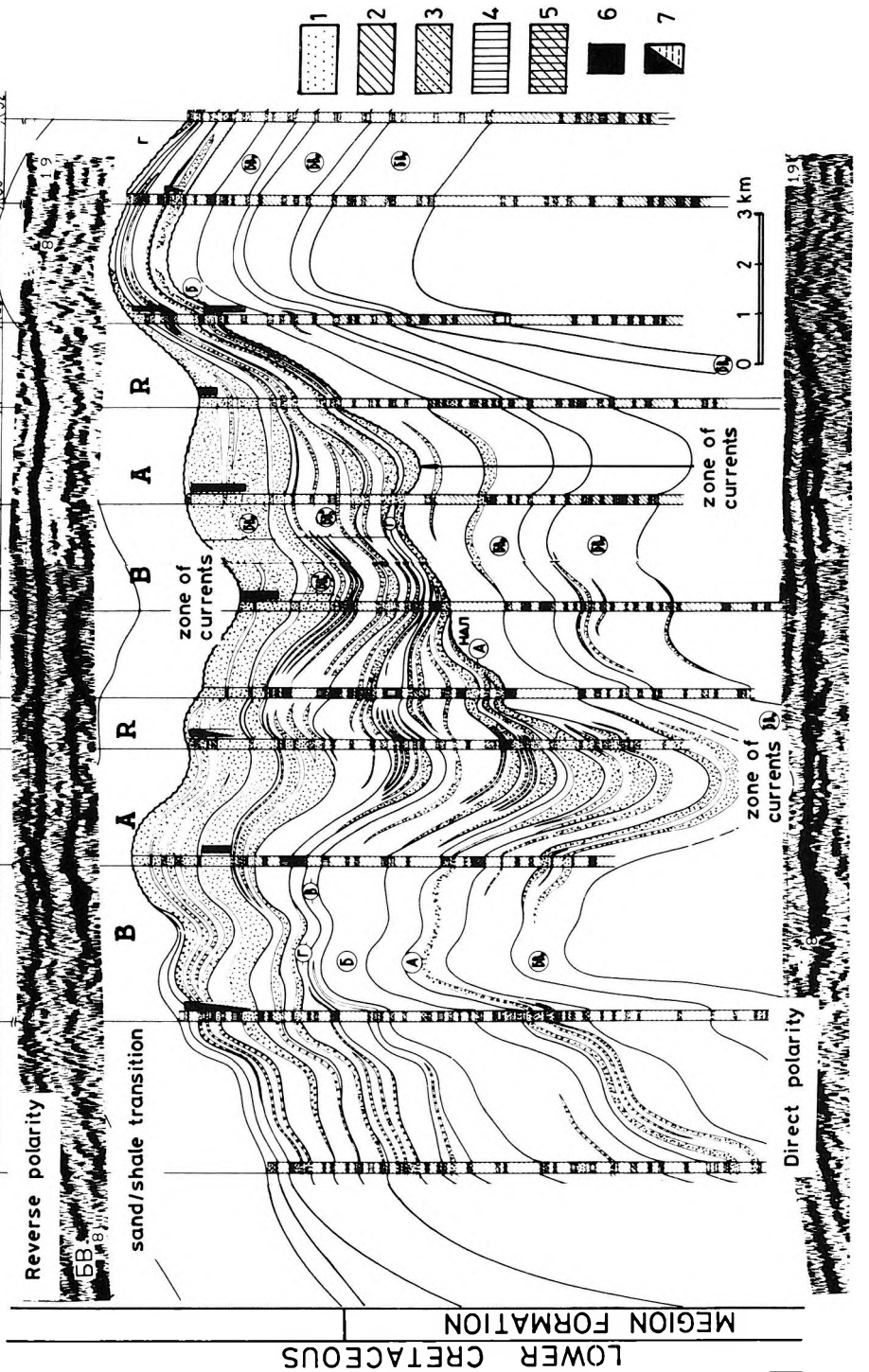
LOWER CRETACEOUS
REGION FORMATION
Reverse polarity
sand/shale transition
Direct polarity
zone of currents
zone of currents
zone of currents
0 1 2 3 km
1 2 3 4 5 6 7

of the territory, the development history of synsedimantary structures and their connection with the reservoirs or sand/shale transitions.

The well log facies map serves for a division of the territory according to the type and character of the genetically different facies. The well log facies analysis is based on the changes of the SP patterns reflecting variations of grain size. Changes in the lithologic composition and rock-physical properties — recorded by SP logs — are essential indicators of the sedimentation conditions [TAYLOR 1980]. On the maps, constructed for the given stratigraphic intervals, we also display the corresponding SP pattern *(Fig. 7)*. From its form one can conclude to the genetic nature of the sand bodies. Because of the close connection between certain types of facies and the morphologically pronounced negativ and positive features of the palaeorelief of the basin floor, the genetic interpretation of SP curves should be corroborated by palaeo-morphologic data.

Making use of seismic stratigraphy and facies analyses, and of the correlation of the lithologic parameters to the seismic facies and of lithofacies conditions, we can construct the well log facies map supplemented with data of grain-size analysis. Based on this map, we can form an idea on the sedimentation model, clarify the genetic nature of the sedimentary units and conduct a search for zones of possible reservoirs, for stratigraphic and combined traps.

To estimate the dimensions of the traps, to trace the contours of a deposit, to pick the most promising location of a borehole, etc., we carry out special wave-field analyses by means of the PGR package. The quantitative estimation of wave-field parameters is based on the dynamic analyses (instantaneous amplitudes and frequencies) and on pseudo-acoustic transformation. We construct maps of the dynamic and (pseudo-) velocity parameters along the reflecting horizons corresponding to the prospective pay zones; and establish a correlational dependence between the seismic (amplitude, frequency, acoustic impedance) and geological–petrophysical characteristics (porosity, sand/shale ratio, oil saturation, productivity, etc.). The choice between different models and the solution of some particular questions arising in the analysis of the anomalous wave field are facilitated by seismic modelling techniques.

Fig. 5. Seismic lithofacies section in the present plane (vertical exaggaration 1:100) for Profile 3 of the Pokacheva area
1 — different sands and aleurolites (productive rocks, reservoirs); 2 — shale, argillite; 3 — shaly sandstone; 4 — aleurolite; 5 — shaly aleurolite; 6 — oil; 7 — oil + water

5. ábra. Pokacseva–3 szeizmikus litofacies szelvény (100-szoros vertikális kimagasítással)
1 — homok és aleurolit (termelő rétegek, tárolók); 2 — agyag; 3 — agyagos homokkő; 4 — aleurolit; 5 — agyagos aleurolit; 6 — olaj; 7 — olaj + víz

Рис. 5. Сейсмолитофациальный разрез в современном плане по профилю 3 Покачевской площади
1 — песчано-алевролитовые разности (проницаемые породы, коллекторы); 2 — глины; 3 — глинистые песчаники; 4 — алевролиты; 5 — глинистые алевролиты; 6 — нефть; 7 — нефть + вода

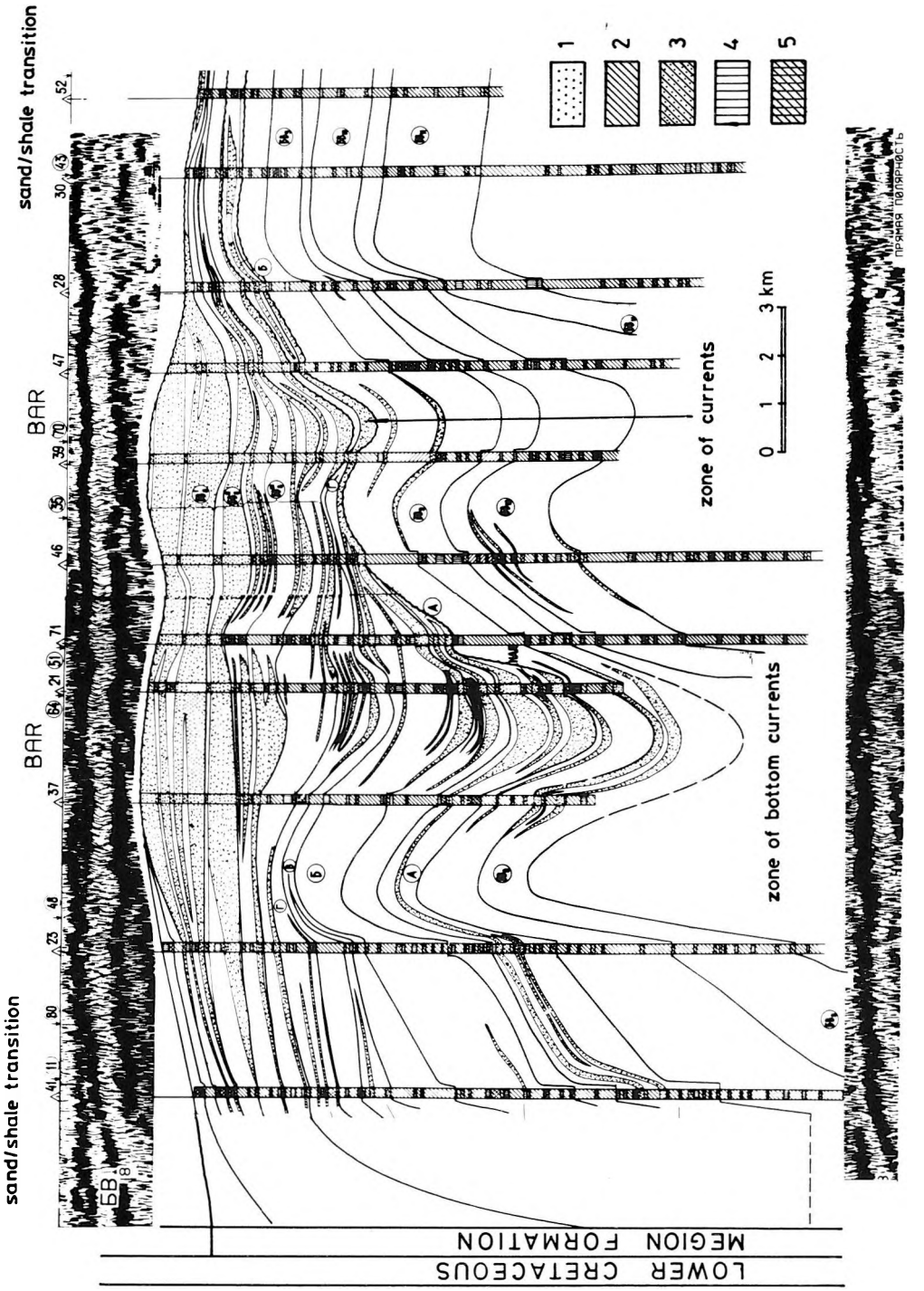
sand/shale transition
BAR
BAR
sand/shale transition
zone of currents
zone of bottom currents
0 1 2 3 km
1
2
3
4
5
LOWER CRETACEOUS
REGION FORMATION

The final stage of interpretation is based on the analysis of all data: based on this analysis we make recommendations for additional exploratory boreholes and for the correction of the drilling program of the production wells.

3. Application of integrated interpretation of geological–geophysical data in the post-exploration phase

The effectiveness of the method will be illustrated on the example of a project involving the Pokacheva deposit of the west Siberian CH-bearing province, on the NW side of the lower Vartovo arch. The large, multilayered, Jurassic and lower Cretaceous oil beds had previously been revealed by seismic and well log surveys and prepared for exploitation, some oil producing wells are already operating. In 1981 a detailed seismic survey was carried out as post-exploration of the site, it was interpreted according to the above-described methodology. The exploration was focused on the deposits of the Megion Formation, which was already sufficiently known from exploratory boreholes. While the occurrence of industrial amounts of oil in these deposits has proved the regional presence of oil, general disagreement still existed among geologists as to the regularities of the structure and conditions of development of these deposits. Due to the complicated build-up of the formation and to its lithological inhomogeneity the correlation between well log sections is very uncertain, which explains the existence of different sedimentation models. The top of the Megion Formation contains the productive bed $БВ_8$ which extends all over the lower Vartovo arch and is the basic oil-producing layer of the ocality. In the Pokacheva deposit, the oil-bearing layer is inhomogeneous: both in the western and eastern part of the site sand/shale transition zones were found by drilling. Also, a low yield of oil is obtained from the sandstones of the so-called Achimovy member, which is usually in the lower Megion Formation. Consequently, the structural position of the reservoirs in the Achimovy member and the location of the traps within it have remained unsolved problems in spite of the large number of wells, because of the very complex nature of the logging material.

Fig. 6. Seismic lithofacies section in the palaeoplane for Profile 3 of the Pokacheva area (vertical exaggeration 1 : 100)
1 — sandy-aleurolithic clastics (permeable rocks, reservoirs). Sealing rocks: 2 — shale, argillite; 3 — shaly sandstone; 4 — aleurolite; 5 — shaly aleurolite

6. ábra. Pokacseva–3 szeizmikus litofacies szelvény az eredeti síkban (100-szoros vertikális kimagasítással)
1 — törmelékes homokkő és aleurolit (tárolók). Zárórétegek: 2 — agyag; 3 — agyagos homokkő; 4 — aleurolit; 5 — agyagos aleurolit

Рис. 6. Сейсмолитофациальный разрез в палеоплане по профилю 3 Покачевской площади
1 – песчано-алевролитовые разности (проницаемые породы, коллекторы); 2 – глины; 3 – глинистые песчаники; 4 – алевролиты; 5 – глинистые алевролиты

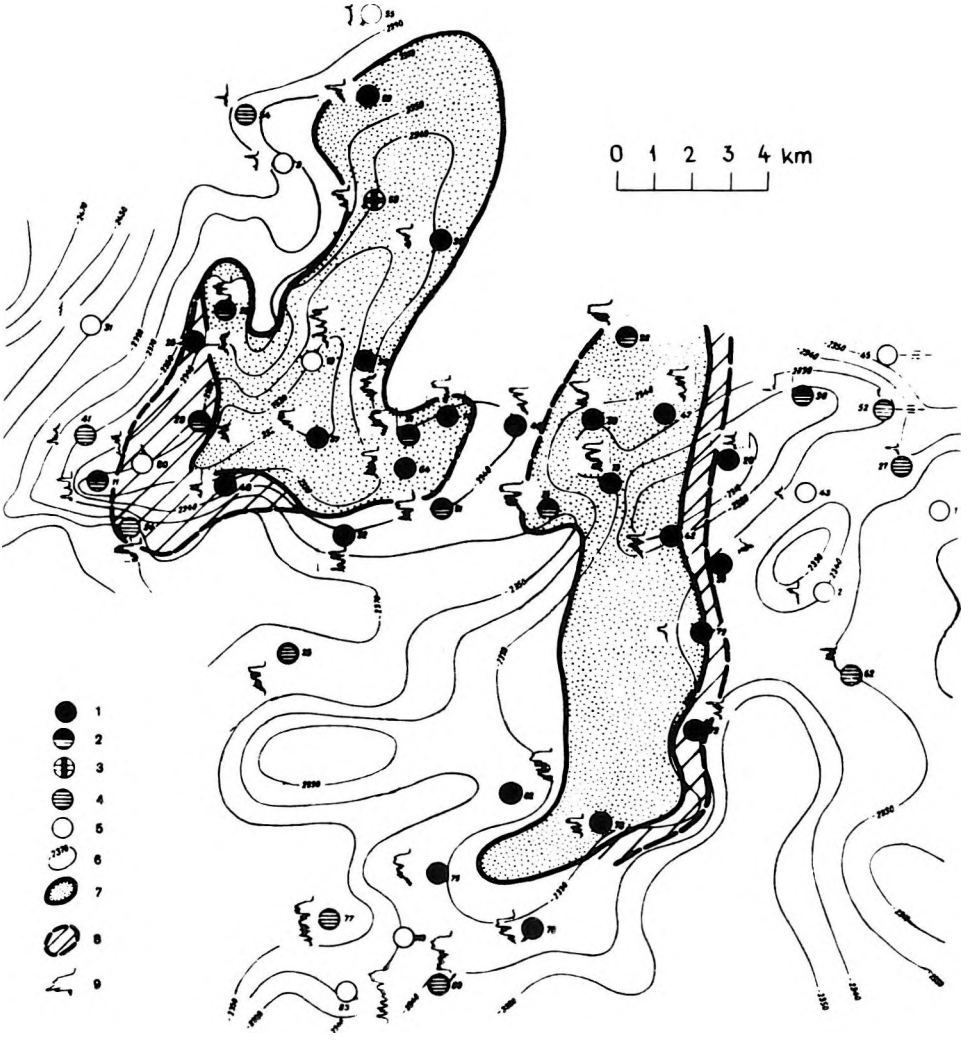

Fig. 7. Well log facies map for the interval, corresponding to the productive bed $БВ_8$
1 — oil-producing wells; 2 — mixed oil-water wells; 3 — wells giving water with oil film; 4 — water wells; 5 — dry wells; 6 — contour lines showing roof of payzone $БВ_8$; 7 — areas of development of accumulated bar sands; 8 — boundary zones of the accumulation of bar sands; 9 — SP patterns corresponding to bed $БВ_8$

7. ábra. A $БВ_8$ produktiv rétegnek megfelelő karotázs fácies-térkép:
1 — termelő olaj-kutak; 2 — olaj-víz keveréket adó kutak; 3 — olajfilmes vizet adó kutak; 4 — víz-kutak; 5 — száraz fúrások; 6 — a $БВ_8$ termelő réteg fedőjének izohipszái 7 — gát-homokkövek kifejlődési területei; 8 — gát-homokkövek határzónái; 9 — a $БВ_8$ rétegnek megfelelő PS-görbék

Рис. 7. Карта каротажных фаций по интервалу, связанному с продуктивным пластом $БВ_8$
1 — скважины, давшие нефть; 2 — скважины, давшие нефть с водой; 3 — скважины, давшие воду с пленкой нефти; 4 — скважины, давшие воду; 5 — скважины, где отсутствуют данные опробования; 6 — изогипсы по кровле отражающего горизонта «$БВ_8$»; 7 — области развития аккумулятивных песчаных тел барового типа; 8 — краевые зоны аккумулятивных песчаных тел барового типа; 9 — диаграммы ПС против пласта $БВ_8$

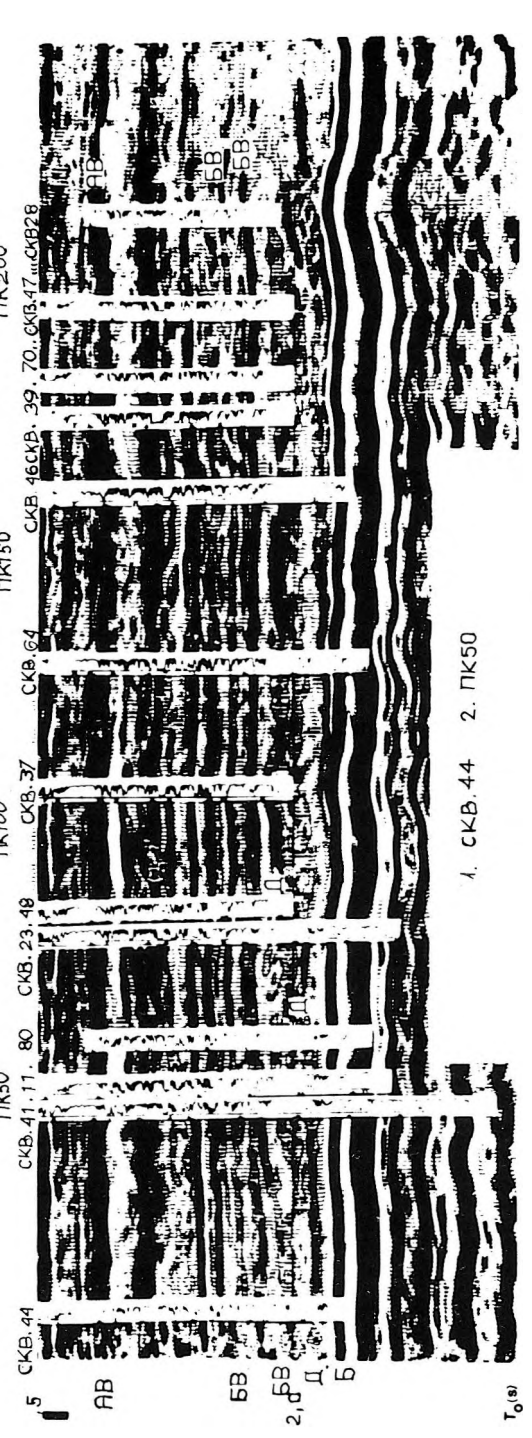

Fig. 8. Composite representation of the pseudo-acoustic section and the SP logs for Profile 3 of the Pokacheva area
1—borehole; 2—pegmark

8. ábra. A pszeudo-akusztikus szelvény és az PS adatok egyesített ábrázolása a Pokacseva—3 vonal mentén 1—mélyfúrás; 2—karószám

Рис. 8. Совместное представление псевдоакустического разреза и кривых ПС по профилю 3 Покачевской площади

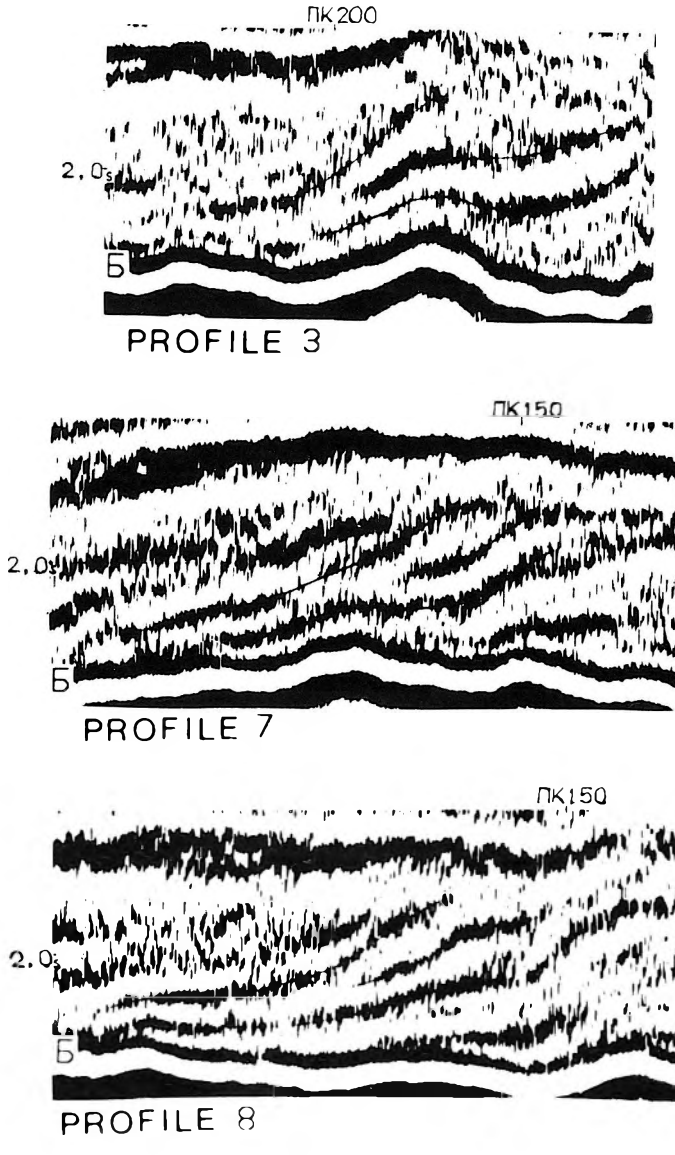

Fig. 9. Sigmoid seismic facies on a series of parallel profiles

9. ábra. Szigmoid szeizmikus faciesek néhány párhuzamos szelvényen

Рис. 9. Сигмовидные сейсмофации на серии параллельных профилей

The clearest representation of the geological information contained in seismic data can be achieved by the pseudo-acoustic transformation of the time sections. *Figure 8* shows the pseudo-acoustic section constructed from Profile 3, proceeding through the dome of the Pokacheva deposit. (The corresponding time section was shown in Fig. 2). When carrying out the pseudo-acoustic transformation the low-frequency components of the velocities had not been taken into account, and a constant density had been asumed, so that the black-and-white shades of the display show the relative changes of the acoustic impedances. In particular, in the given case darker colours signify decreased acoustic impedance values. The time window 1.9–2.1 s corresponds to the Megion Formation, in the upper part of this interval the succession of low acoustic impedance values around 1.9 s corresponds to the productive bed $БВ_8$. The Megion Formation is underlain by the argillites of the Bazhenovo Formation, represented by the marker horizon at 2.1 s.

Stratigraphically, the reflection horizons have been correlated by means of well shooting, acoustic logs and gamma–gamma logs; however, because of the limited number of such measurements, additional information had to be sought from the detailed analysis of the seismic and geological materials. We singled out the most striking changes of the geological section (sand/shale transition within the layer, significant changes in their thickness, fluid saturation of the productive layers, layers of anomalous acoustic impedances, etc.) and compared them with corresponding changes on the seismograms. The final step in the stratigraphic correlation of the reflection horizons took place when we superposed the time-scaled well log curves on the seismic and pseudo-acoustic section (Figs. 2 and 8).

As a result of the seismic stratigraphic analysis of the wave patterns within the time gate of the Megion Formation we could delineate two seismic sequences, differing in form: the clinoform (in Fig. 2 between 1.94 and 2.07 s), correlating with the Megion Formation, including the so-called Achimovy member. Higher up in the section appears the overlying complex (between 1.90 and 1.94 s), which corresponds to those strata where also $БВ_8$ belongs.

The interior structure of the clinoform sequence can be characterized by two types of seismic facies: sigmoid *(Fig. 9)* and oblique reflections *(Fig. 10)*. Based on the characteristics of the interior structure of the complex, the study site can be split into two parts: the back part, characterized by the presence of two zones of sigmoid facies, occupying the SE-half of the area; the front part, extending along the NW-part of the territory, exclusively built up of oblique reflections.

The interior structure of the overlying complex is characterized by lenticular bodies, these correlate from profile to profile and constitute a regularly arranged system *(Fig. 11)*. The lenticular facies is confined to the depression zones and is most wide-spread in the west part of the area characterized by the most complex structure. This stratigraphic analysis has been completed by the construction of seismic lithofacies sections, both in the comtemporary- and the

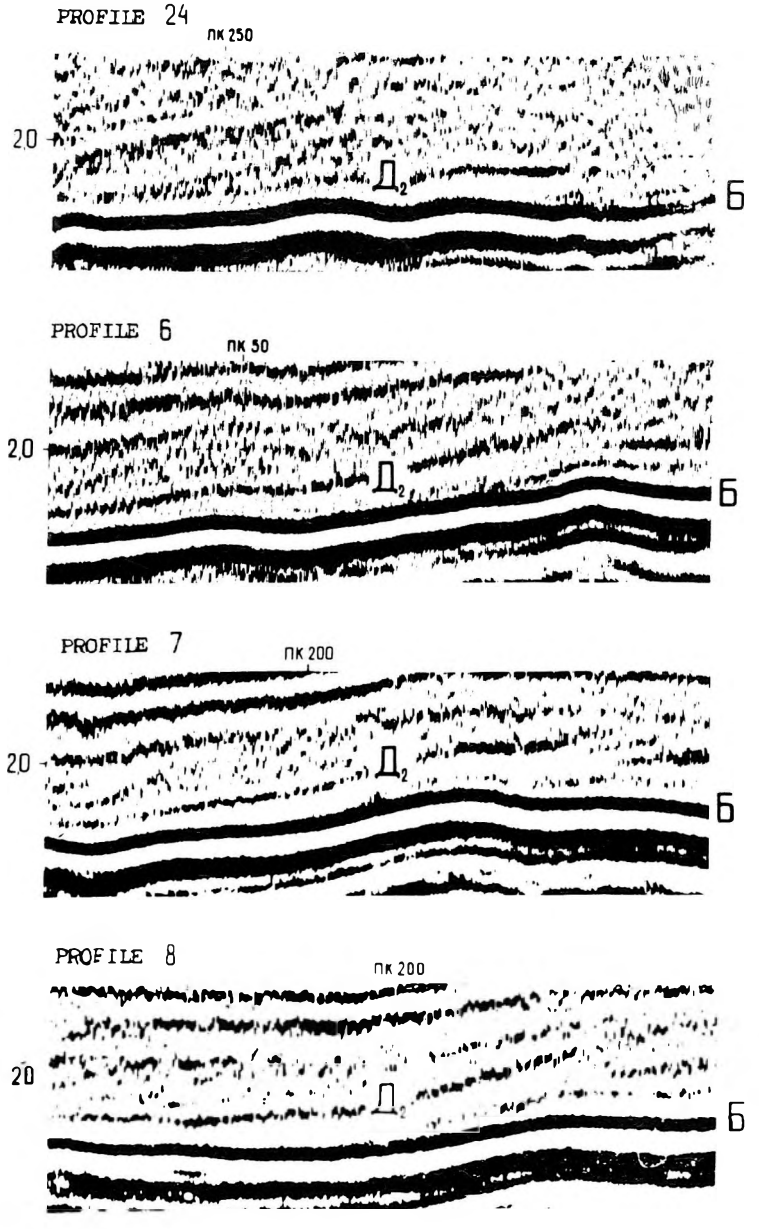

Fig. 10. Seismic facies characterized by oblique reflections on a series of parallel profiles

10. ábra. Dőlt reflektorokkal jellemzett szeizmikus faciesek néhány párhuzamos szelvényen

Рис. 10. Сейсмофации наклонных отражений на серии параллельных профилей

palaeoplans (Figs. 5 and 6), and by the well log facies map (Fig. 7). Thus we could genetically interpret the deposits of the Megion Formation.

4. Conclusions

The integrated analysis of the geological–geophysical materials, carried out as outlined above, has provided a sedimentation model of the Megion Formation. In the clinoform sequence of the Megion Formation one can distinguish regularly alternating sedimentation stages, characterized by different tectonic activities and different features of the generated geological bodies, which are considered statigraphic traps. In the initial stage of the formation of the clinoforms the fast lateral accretion of its back part took place passively, without the participation of tectonic movements. At the same time sigmoid lenses of varying aleurolithic–argillic composition whose cyclic structure is due to pulsations in the sediment transport, have been formed due to the prograding clinoforms, and the channel sands lying obliquely at the foot of the slopes having become argillaceous up-dip.

The sigmoid bodies and the sandstones at their feet have been hit by a number of wells. According to the stratigraphic correlation the sandstones have been identified with the dipping reflections, recorded from below the lower Megion Formation revealing six sandstone bodies, denoted in the figures as $Д_0$, $Д_2$, $Д_5$, $Д_6$, $Д_7$ and $Д_8$. *Figure 12* shows the composite map of the isochrons of oblique reflections, corresponding to sandstones of the Achimovy member. The formation of these sandstone bodies is connected with the activity of the bottom currents along the slopes.

The tiled structure of these bodies in the north-western part of the area is very likely due to the fact that the decelerated lateral advance into the basin of the noncyclic front parts of the clinoforms happened at the same time as a noticeable activation of the tectonic movements. In the final stage of development of the clinoforms, their shelf parts are characterized by vertical accretion of sediments. The features of the distribution of the corresponding shallow marine lithofacies are determined by the activation of the tectonic movements. In the depressions the lateral accretion of the clinoforms took place synchronously resulting in extremely varying lithofacies. In the depressions of the shelf, channel sands had been accumulated with lenticular seismic facies (Fig. 11), on the elevated parts there are sand bars (Figs. 6, 7). In the depression zones at the foot of the clayey slope, canyon sand bodies are formed due to the activities of the deep-water currents.

The sedimentation and the structural model of the deposits within the Megion Formation have been used to outline the basic prospective objects. For the obliquely deposited sandstone layers of the lower part of the Megion Formation (the Achimovy member) these are, first of all, nonanticlinal traps, connected with sand–shale transition up-dip. In the overlying complex we mapped the zones of channel sands and bars having the most favourable

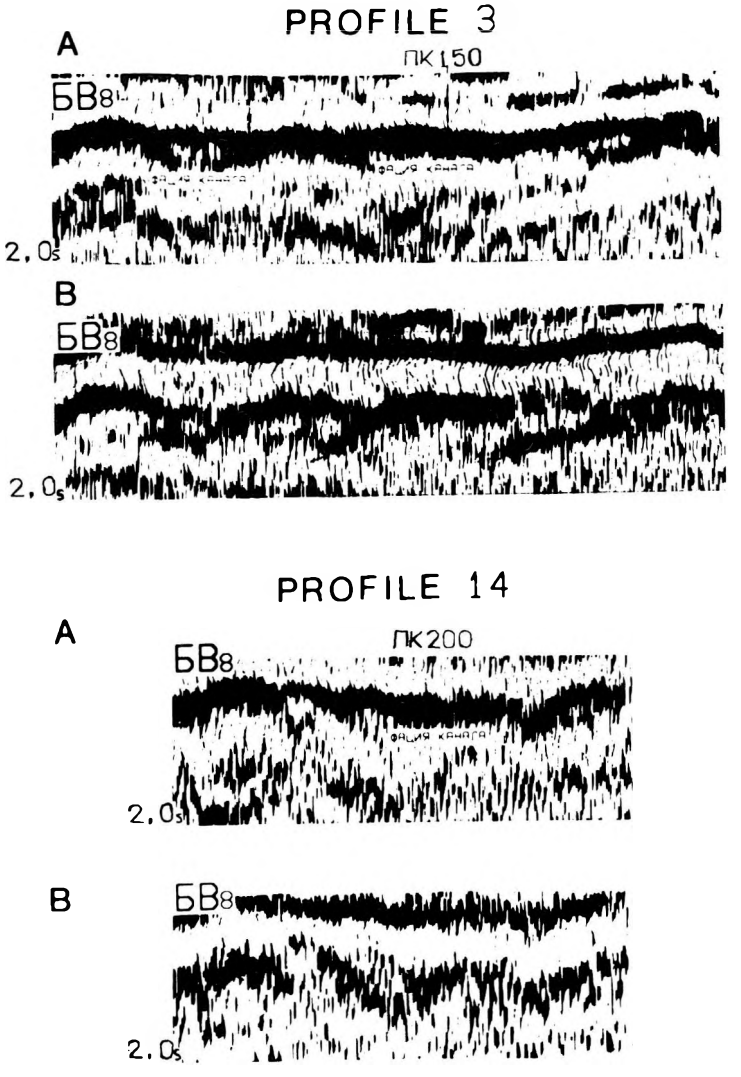

Fig. 11. Lenticular seismic facies, identified with the zone of channel sands
A — time section, direct polarity, B — time section, reversed polarity

11. ábra. Csatorna-homokkal azonosítható lencsés szeizmikus fáciesek
A — időszelvény egyenes polaritással; B — időszelvény fordított polaritással

Рис. 11. Линзовидные сейсмофации, отождествляемые с зоной развития канала
А — временной разрез прямая полярность; В — временной разрез обратная полярность

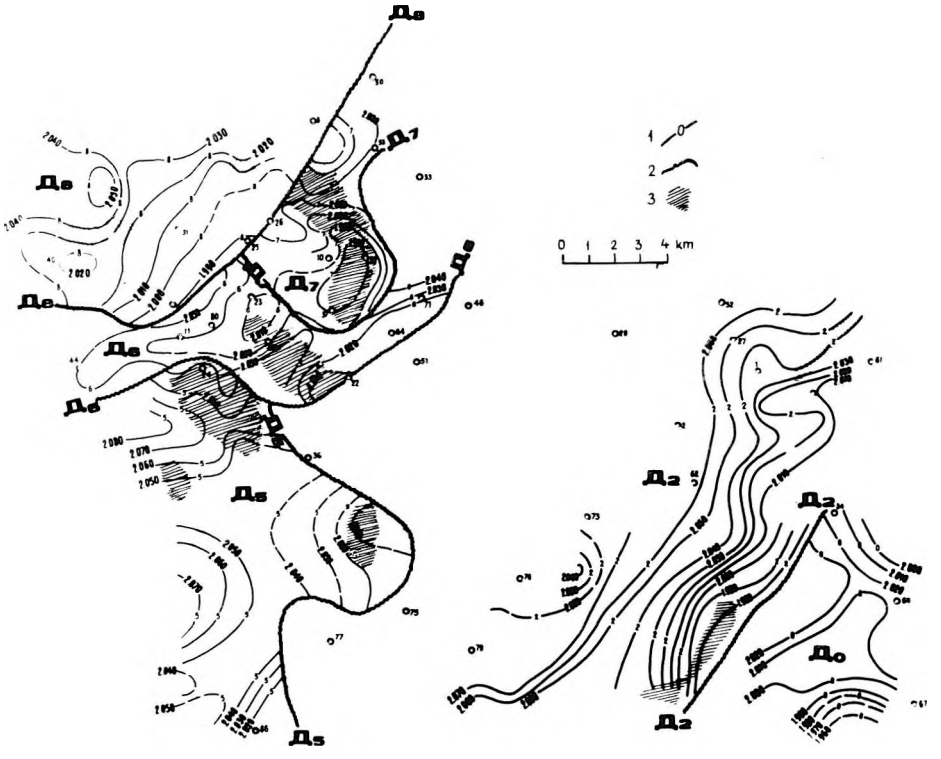

Fig. 12. Composite isochron map of the oblique seismic facies
1 — isochrons of the reflecting horizons corresponding to the roofs of the sand bodies $Д_0$, $Д_2$, $Д_5$, $Д_6$, $Д_7$, $Д_8$;
2 — sand/shale transition line; 3 — zones of decreased acoustic impedance within the beds

12. ábra. A ferde szeizmikus faciesek összetett izokron térképe.
1 — a $Д_0$, $Д_2$, $Д_5$, $Д_6$, $Д_7$, $Д_8$ homoktestek fedőinek megfelelő izokronok; 2 — homok–agyag átmenet vonala; 3 — a réteg belsejében levő csökkent akusztikus impedanciájú zónák

Рис. 12. Сводная карта изохрон наклонных сейсмических фаций
1 — изохроны отражающих горизонтов $Д_0$, $Д_2$, $Д_5$, $Д_6$, $Д_7$, $Д_8$, соответствующих кровлям песчаных пластов;
2 — линии глинизации разрезов пластов; 3 — зоны понижения акустической жесткости пластов

reservoir properties. Within the Pokacheva oil field the structural oil deposits are controlled by bars in the $БВ_8$ bed, while the nonanticlinal hydrocarbon traps are possibly connected with the pinch-outs in the zone of channel sands. High-productivity wells belong to uplifted zones of channel sands.

In order to get additional information on the nature of the changes of the petrophysical properties and of the fluid-saturation of the productive layers the quantitative estimations of the seismic wave-field parameters have been used. We computed, for all prospective objects detected during the construction of the sedimentation model, the velocity maps from pseudo-acoustic data and the instantaneous amplitude map based on the dynamic analysis of the complex traces. The highest inverse correlation has been established between the pseudo-acoustic velocities, on the one hand, and the thickness of the oil-bearing zone and the productivity of the wells, on the other. *Figure 13* shows a comparison of the pseudo-acoustic velocity map with the productivity map displaying the yield of the exploratory wells from the $БВ_8$ bed. Observe the fair agreement of the anomalously low pseudo-acoustic velocities with the highest yield of the wells in the north part of the Pokacheva field. By including all data into the analysis we could delineate the contours of the deposit within the productive bed $БВ_8$, we detected new structural traps and assessed the probable oil content.

In the sediments of the Achimovy member the analysis of the pseudo-acoustic sections and of other data revealed zones of decreased acoustic impedance, which correspond to the most elevated parts of the sand bodies, around the sand/shale transition line of the layers. Characteristic anomalies of the seismic parameters, corresponding to the development of the prospective object $Д_6$, are shown in *Fig. 14*. In zones like this, nonanticlinal hydrocarbon traps can be predicted. As an example *Fig. 15* shows the isochron map of object $Д_6$. On the same map we superimposed the respective intervals of the SP and apparent resistivity logs, characterizing the lithology of the geological body, which clearly show the accurate coincidence of the object $Д_6$ with the development of the sandstone layer. The sand/shale transition line was constructed on the basis of the dynamic analysis of the wave field and has been checked by the available well log data. The results of the integrated interpretation have rendered it possible to work out recommendations for the additional exploration of the oil field.

The investigation presented can be considered as a first step towards a novel technique in the geological exploration for oil and gas, which more fully relies on the up-to-date possibilities of seismic prospecting combined with all available geological–geophysical information. It should be noted that the solution of this task requires a new kind of research team as well, consisting of petroleum geologists, well log analysts and seismic interpreters. Only such team-work together with a thorough cross-analysis of the materials could lead to a synthesis of the ideas on the sedimentation history of the basins which would be in accordance with all available data and could thus be used for the detection of the prospective objects.

There is no doubt that the wide-spread use of the integrated approach of geological–geophysical interpretation—supported by sophisticated seismic techniques—in the detailed exploration and exploitation phase of oil and gas reservoirs would lead to a further increase in exploration efficiency.

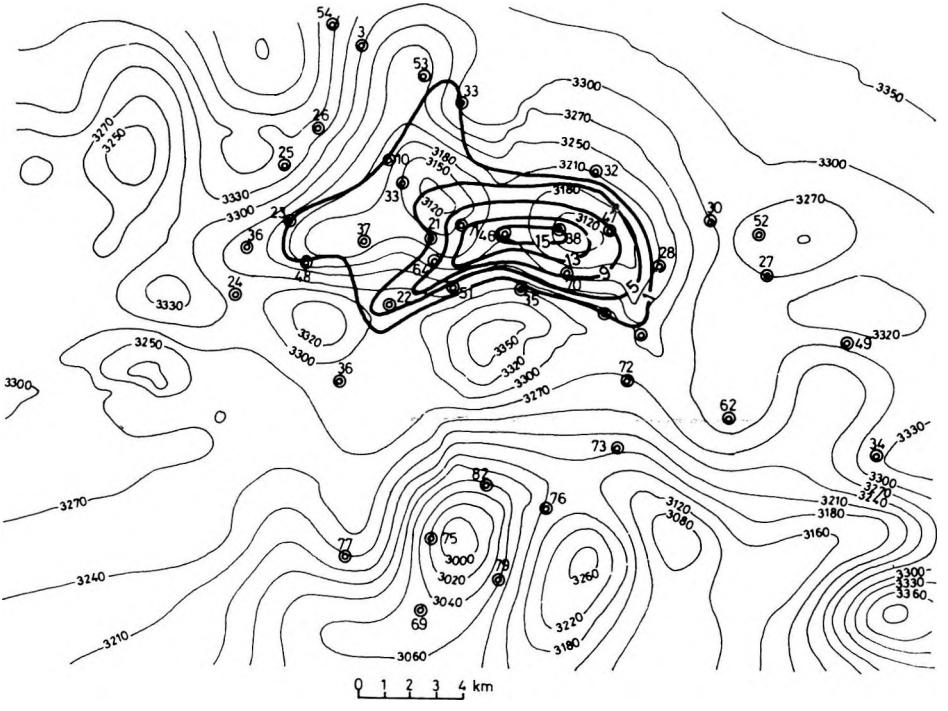

Fig. 13. Comparison of the map of interval velocities computed from pseudo-acoustic logs for the $БВ_8$ bed with the productivity isolines of the exploratory wells

13. ábra. A $БВ_8$ rétegben, a pszeudo-akusztikus szelvények alapján meghatározott intervallum-sebességek, valamint a kutató fúrások egyenlő hozam-görbéi

Рис. 13. Совмещение карты интервальных скоростей по кривым ПАК в интервале пласта $БВ_8$ и изолиний продуктивности разведочных скважин

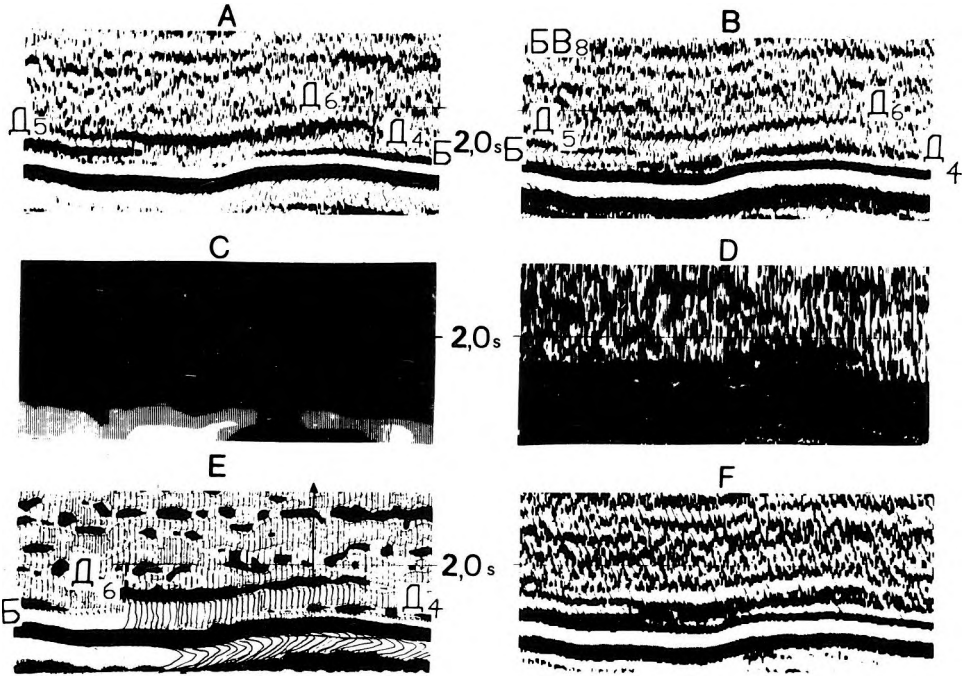

Fig. 14. Seismic wave-field characteristics for the range containing the prospective object $Д_6$ within the sediments of the Achimovy member
A — time section, direct polarity; B — time section, reversed polarity; C — instantaneous frequencies; D — instantaneous amplitudes; E — pseudo-acoustic section; F — instantaneous phases

14. ábra. A $Д_6$ homokkőtestet tartalmazó Acsimovi rétegsor szeizmikus hullámtér jellemzői
A — időszelvény egyenes polaritással; B — időszelvény fordított polaritással; C — pillanatnyi frekvenciák; D — pillanatnyi amplitúdók; E — pszeudo-akusztikus szelvény; F — pillanatnyi fázisok

Рис. 14. Характеристика волнового поля на участке выделения перспективного объекта в отложениях «ачимовской пачки» (объект $Д_6$)
A — временной разрез прямая полярность; B — временной разрез обратная полярность; C — мгновенные частоты; D — мгновенные амплитуды; E — псевдоакустический каротаж; F — мгновенные фазы

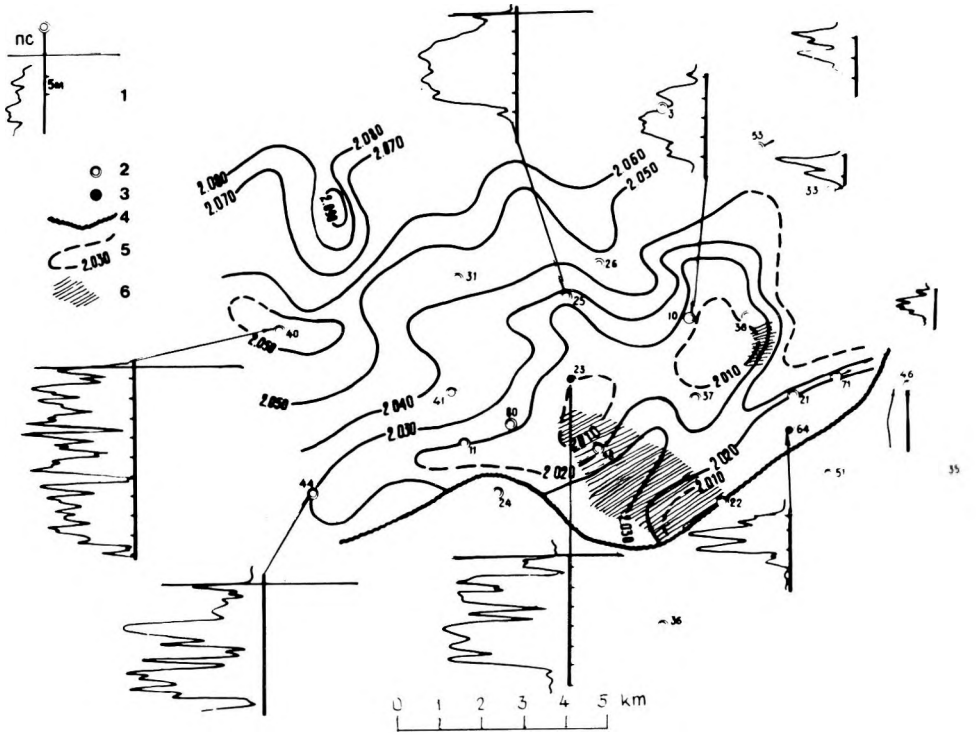

Fig. 15. Isochron map of the object $Д_6$ with characteristic well log patterns
1 — SP log; 2 — exploratory borehole; 3 — oil-producing well; 4 — sand/shale transition line; 5 — isochrons for horizon $Д_6$, corresponding to the roof of the sandstone body; 6 — zones of decreased acoustic impedance within the bed

15. ábra. A $Д_6$ homokkőtest izokron térképe, a jellemző karotázs felvételekkel
1 — PS-görbe; 2 — kutató fúrás; 3 — termelő olajkút; 4 — homok–agyag határvonal; 5 — a $Д_6$ fedőjének izokronjai; 6 — csökkent akusztikus impedancia-zónák a rétegben

Рис. 15. Карта изохрон по объекту $Д_6$ с фрагментами каротажных характеристик объекта
1 — результаты испытания пласта с указанием дебита нефти и воды; 2 — скважины; 3 — скважины, давшие нефть; 4 — линия глинизации разреза пласта $Д_6$; 5 — изохроны отражающего горизонта $Д_6$, соответствующего кровле песчанного пласта; 6 — зоны понижения акустической жесткости пласта $Д_6$

REFERENCES

AVERBUKH A. G., 1982: Seismic investigation of composition and properties of rocks (in Russian). Nedra, Moscow 227 p.

GOGONENKOV G. N., 1981: Prediction of geologic section on the base of seismic data (in Russian). Geologii nefti i gaza, **1**, pp. 48—55

GOGONENKOV G. N., 1981: Prediction of geological section for positioning of deep-drillings and for detailed delineation of pay-zones on the basis of seismic data (in Russian). Geologiya nefti i gaza, **2**, pp. 58—61

GOGONENKOV G. N., ZAKHAROV E. T., ELMANOVICH S. S., 1980: Prediction of detailed velocity-section by seismic data (in Russian). Prikladnaya Geofizika, **97**, pp. 58—72

KOZLOV E. T. GOGONENKOV G. N., 1980: Digital processing of seismic data (in Russian). Nedra, Moscow

PAYTON CH. E. (Ed.), 1977: Seismic stratigraphy—applications to hydrocarbon exploration. Am. Ass. Petr. Geol. Tulsa

PTETSOV S. N., GOGONENKOV G. N., 1982: Dynamic analysis of complex traces (in Russian). Prikladnaya Geofizika, **103**, pp. 37—45

TAYLOR G. K., 1980: Sandstone reservoirs. Results in oil geology (in Russian). Nedra, Moscow

SZEIZMIKUS ÉS KAROTÁZS ADATOK KOMPLEX ÉRTELMEZÉSE A SZÉNHIDROGÉN-KUTATÁS RÉSZLETES SZAKASZÁBAN

G. N. GOGONENKOV, S. S. ELMANOVICS, V. V. KIRSZANOV, Yu. A. MIHAILOV

Egy nyugat-szibériai olajmező kutatásának példáján bemutatjuk a szeizmikus sztratigráfia módszerének és a korszerű szeizmikus adatfeldolgozási eljárásoknak összekapcsolt alkalmazását. A geológiai információk, a karotázs-adatok, a szeizmikus és kőzetfizikai paraméterek integrált felhasználásával sikerült a területen található szénhidrogén-előfordulás megbizható becslése.

КОМПЛЕКСНАЯ ИНТЕРПРЕТАЦИЯ СЕЙСМИЧЕСКИХ И КАРОТАЖНЫХ ДАННЫХ ПРИ ДЕТАЛЬНОЙ РАЗВЕДКЕ НЕФТЯНЫХ И ГАЗОВЫХ МЕСТОРОЖДЕНИЙ И ПОИСКАХ НЕСТРУКТУРНЫХ ЛОВУШЕК

Г. Н. ГОГОНЕНКОВ, С. С. ЭЛЬМАНОВИЧ, В. В. КИРСАНОВ, Ю. А. МИХАЙЛОВ

В настоящей работе будут изложены методические основы комплексной интерпретации и на примере одной из разведочных площадей Западной Сибири проиллюстрирована эффективность ее применения на этапе доразведки месторождений углеводородов.

Основу рассматриваемых исследований представляет обработка сейсмических данных по комплексу программ прогнозирования вещественного состава геологического разреза ПГР и интерпретация полученных данных с применением принципов сейсмостратиграфического и сейсмофациального анализов, а также фациального анализа каротажных данных.

GEOPHYSICAL TRANSACTIONS 1984
Vol. 30. No. 2. pp. 201—211

VARIATION OF SPECTRAL PROPERTIES OF SEISMIC WAVES IN THE RANGE OF HYDROCARBON DEPOSITS

Stefan PRÖHL*

The usage of spectral properties of seismic waves for directly detecting hydrocarbon deposits is considered, VEB Geophysik Leipzig developed a special program for an ESR computer allowing the convenient calculation of several dynamic, i.e. mainly spectral, parameters. The method of calculating these parameters is explained, and the results of investigations along one profile across a known oil deposit are demonstrated.

d: direct interpretation, oil and gas fields, spectral properties, computer programs

1. Introduction

The detection of compositional changes of the subsurface using seismic reflection methods is an important task from many points of view. Of special importance among these methods is the direct detection of hydrocarbon deposits. In the range of deposits the change of the pore-content may give rise to alterations in seismic velocities and in the absorption of seismic waves. The magnitude of seismic waves depends on numerous factors — among others on the nature of the pore-content.

Additionally in the range of the deposits (e.g. on gas—water contact) changes of the reflection coefficient (mainly increments) may occur, which lead to amplitude anomalies (bright or dim spots) or to formation of horizontally arranged phase-axes (flat spots).

Besides direct CH detection the indentification of lithological changes offers information which is of great importance in geological investigations. Lithological changes can be verified with velocity and absorption parameters as well as with dynamic parameters, although their effect is in general too small; in other words their verification is successful only if the examined interval is sufficiently large.

At VEB Geophysik Leipzig a great deal of research work has been done in the last few years on the direct detection and on the verification of lithological changes. [PATZER and PRÖHL 1980] and [PRÖHL et al. 1978].

The use of digital recording- and processing techniques for seismic data provides favourable conditions for determining and processing the dynamic parameters of seismic waves. Digital data processing with high-speed computers

* VEB Geophysik, 7024 Leipzig, Bautzner Str. 67. GDR
Manuscript received: 25 January, 1984

applying Fast Fourier Transform (FFT) for computing the spectra enables us to determinate such parameters relatively cheaply.

The mentioned dynamic parameters deliver not only the desired information from the subsurface, but are influenced by numerous disturbances, as varying seismic source- and detection conditions, geometric effects in the range of overburden differences of stratification, interferences between signal and noise of different types as well as the effects of measuring geometry and data processing. In practice it is almost impossible to overcome effectively all conceivable disturbances. However results presented here show that positive results can be achieved even when the possible influence of individual factors is ignored.

In the following the possibilities of determining certain dynamic parameters will be mentioned and the results of investigations will be demonstrated along one profile across a known oil deposit.

2. Computation of dynamic properties

To determine dynamic parameters a special computer program called DYNA as well as a package of additional programs for an ESR computer were developed. These additional programs enable us to further process the data computed with the DYNA program which above all yields:

— samples of the amplitude spectrum between 0 and 100 Hz at a frequency increment of about 2 Hz
— properties derived from the amplitude spectrum (such as dominant frequency, spectrum width, maximum spectral amplitude, spectral amplitude at a given upper or lower frequency limit, etc.)
— time domain parameters such as mean amplitude, mean power, and mean period.

There are three variants for computing these parameters, viz.:

— within given time windows being shifted along the trace by given increments
— within time windows of a given width tracing a specific reflective horizon
— for two half-periods of a reflection.

The further processing of the results obtained by DYNA consists in the sorting of data, vertical and horizontal averaging, elimination of erroneous values, and data preparation for plotting. Thus, a convenient automatic system was implemented enabling a varied determination of dynamic properties from seismic traces at a low expense.

3. Practical example

The effectiveness of the program package was tested by means of direct hydrocarbon detection studies in several survey areas. In the following, the results of the processing of a 12-fold CDP profile crossing an oil deposit approximately perpendicular to the strike are presented. Stacking was carried out without deconvolution applying improved static and moveout corrections.

Figure 1 shows the stacked time section with the location of the deposits. The computation of dynamic properties was accomplished within a 300 ms long time window shifted by increments of 50 ms along the trace. The trace interval to be analysed was multiplied by a window function (hamming window) to avoid boundary effects. Thereafter, the computed data were averaged horizontally (15-fold) and vertically (3-fold).

When evaluating the connection between anomalies of several dynamic properties and the location of hydrocarbon deposits some peculiarities must be considered. Variations in absorption occuring in the range of deposits are — at least for thin reservoirs — usually not detectable and do not explain the amount of both the established change of that parameter and consequently of the dynamic properties derived therefrom. To interpret the effects obtained across the deposits, a seismically effective aureole of gaseous hydrocarbons produced by geochemical processes must be supposed above the deposit. This means that anomalies of seismic parameters may occur not only at the level of deposits but also at a limited distance above them. The fact that geochemical processes can be one of the reasons for the generation of anomalies of seismic parameters points to both the dependence of anomalies (e.g. tectonic faults) on the migration paths of hydrocarbons and also certain horizontal shifts of anomalies compared with the location of the deposit. This must be kept in mind

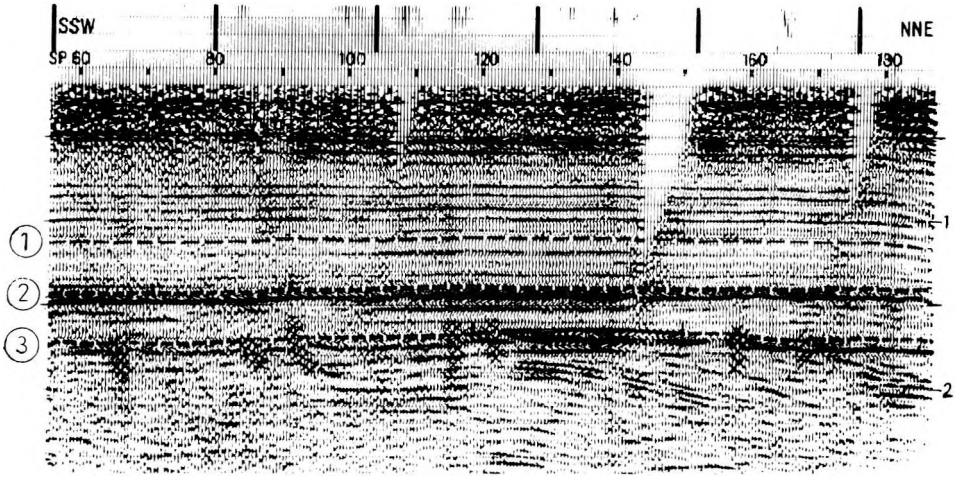

Fig. 1. Stacked section

1. ábra. Összegezett szelvény

Рис. 1. Накапливаемый разрез

when evaluating the measurement results. This means anomalies are also indicative of deposits when they are shifted somewhat vertically or horizontally compared with the deposit. Some selected examples are shown in Figs 2 to 5 in 2D-representation (x, t-plane).

Figure 2 involves a set of properties computed with the DYNA program from the amplitude spectrum. These are: dominant frequency f_v, halfwidth of spectrum f_b, maximum amplitude A_{max}, spectrum area F, and the upper cut-off frequency f_0 which corresponds to that frequency where the amplitude spectrum is decreased to 10% of its maximum value. This figure demonstrates that parameters f_v and A_{max} characterize the deposit quite well. The observed shift to the beginning of the profile which holds also for other parameters is caused by the specific conditions of that area. A small distance away from the profile an additional locally limited hydrocarbon accumulation was detected which contributes to the "shift" of anomalies over the outlined contour of the deposit. For properties f_b and f_0 a connection with the deposit is less clear but it does exist. However the spectrum area F shows no relation to the deposit.

In *Fig. 3* several time domain related parameters are shown additionally to the spectral properties: A_m is the mean amplitude (also determinded within the 300 ms time window being shifted by increments of 50 ms), E_m the mean power, E_{max} the mean energy derived from the peak values of the seismic trace occurring within the analysed time window, and T_m the mean period. The mean amplitude A_m clearly indicates the deposit, the same is valid with minor restrictions for E_m and E_{max}. Considerably less clear is the connection between the distribution of parameter T_m and the location of the deposit.

The most interesting results is the distribution of different samples of the amplitude spectrum (Figs. 4 and 5). These are presented in *Fig. 4* for the range between 10 and 20 Hz with a sampling interval of 2 Hz and in *Fig. 5* between 24 and 40 Hz (sampling interval 4 Hz) as well as for 60 Hz. From the results the following conclusions may be drawn:

- Already at a frequency of 10 Hz an anomaly occurs in the range of the deposit. The number of anomalies outside this range is low. This distribution occurs similarly at 12 and 14 Hz. The dominant element is the anomaly of the deposit.
- Changing over to 16 Hz the anomaly of the deposit remains but the number of anomalies outside the deposit is clearly increased. This situation is also encountered at 18 Hz, where the picture of anomalies and especially the anomaly of the deposit becomes smeared.
- In the range between 20 and 28 Hz the anomaly of the deposit no longer occurs. The picture is characterized by anomalies from outside.
- At 32 Hz the anomaly picture becomes totally smeared. The regular configuration attributed to the deposit or to reflectors is changed to a sporadic distribution which continues up to the high-frequency part of the spectrum. It is characteristic that the anomaly of the deposit is always located in an area of low-frequency values.

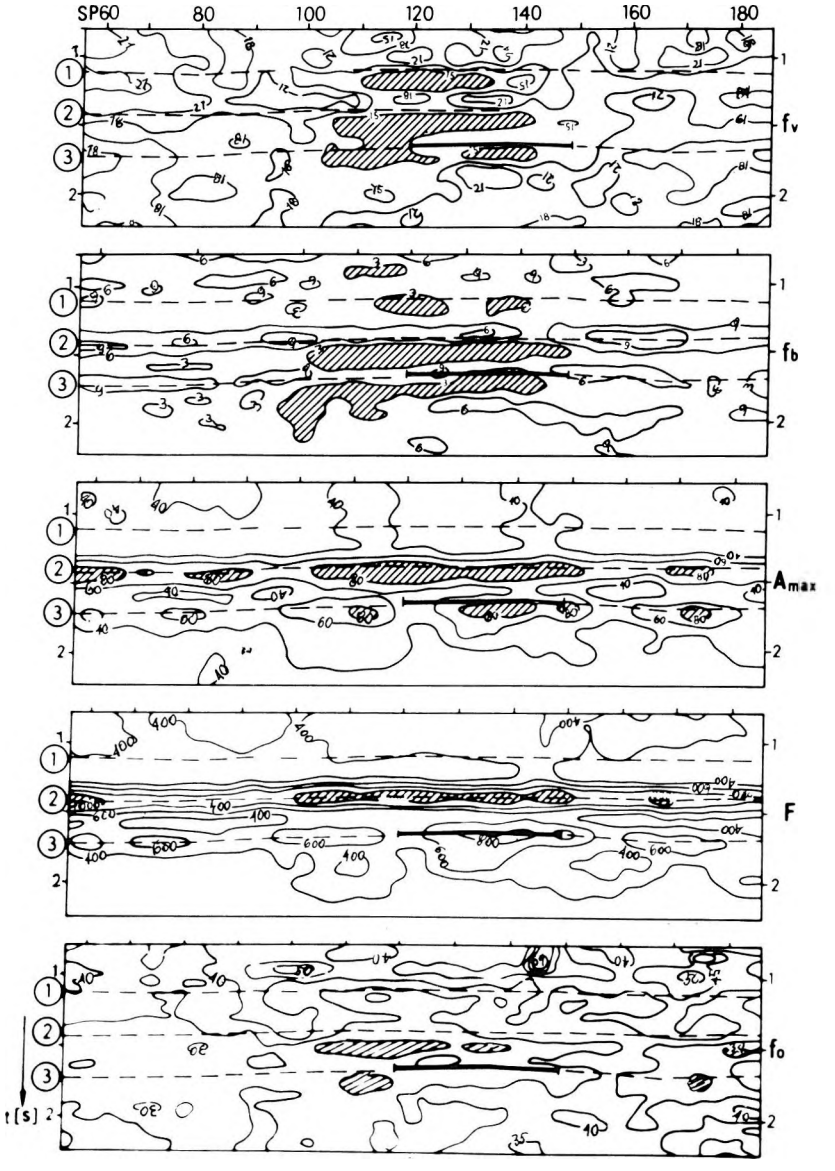

Fig. 2. x, t-plane distribution of selected properties derived from the amplitude spectrum

2. ábra. Az amplitudóspektrum kiválasztott mérőszámai az *x—t* síkban

Рис. 2. Распределение выбранных свойств, выведенных по амплитудному спектру, по плоскостям *x, t*

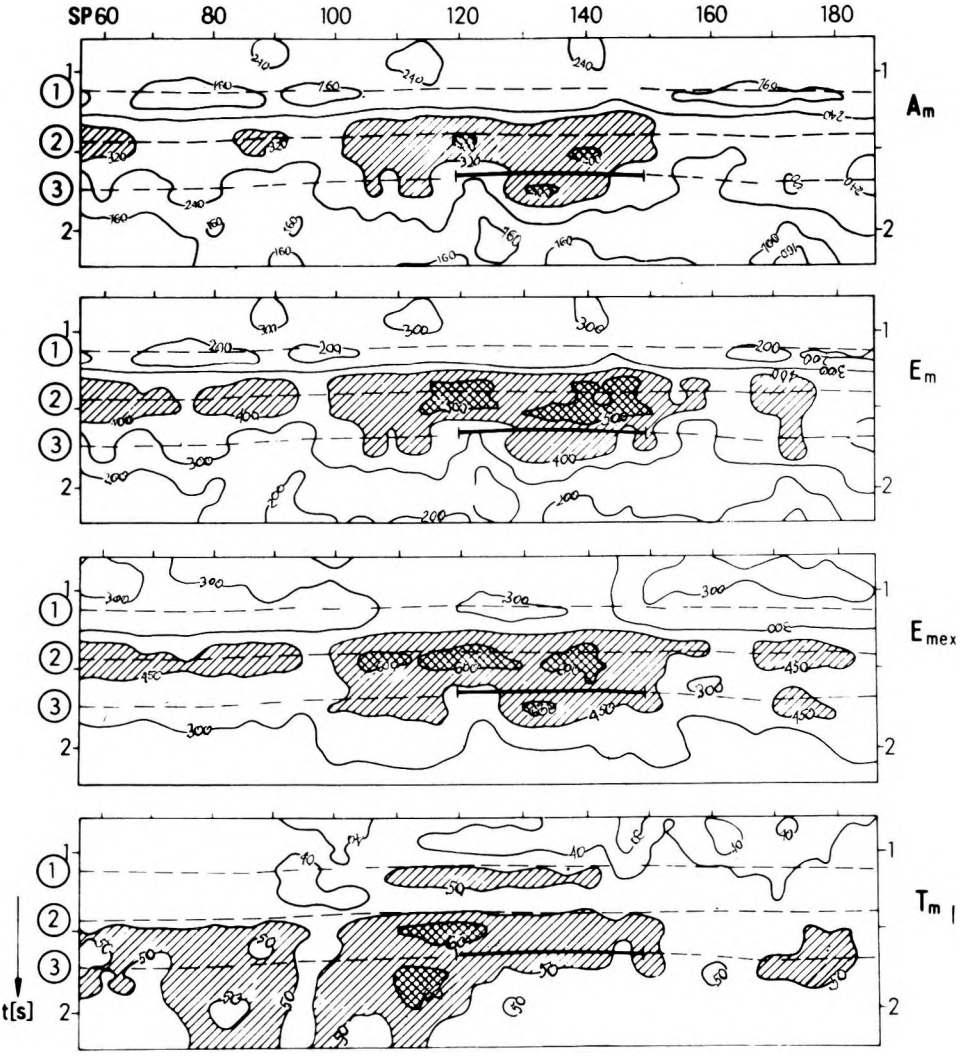

Fig. 3. x, t-plane distribution of time domain parameters

3. ábra. Időtartománybeli paraméterek eloszlása az x—t síkban

Рис. 3. Распределение параметров временной области по плоскостям x, t

These results demonstrate that a narrow low-frequency interval exists where the amplitudes of the spectrum can indicate a hydrocarbon deposit in the subsurface. This effect had been recognized at investigations of other deposits, and underlines the importance of the determination of these low-frequency components of the amplitude spectrum for the direct detection of hydrocarbon deposits under the given conditions. Additionally, it can be stated that the position of the interesting part of the amplitude spectrum varies from on survey area to the other depending on the magnitude of the mean dominant frequency obtained from the corresponding profile. In the present example the deposit is best reflected between 10 and 14 Hz. In other cases a good correlation between anomalies and the location of the deposit is also obtained at 18 Hz.

An interpretation of the relation between the distribution of dynamic properties — computed with DYNA — and the deposit seems possible when the following two effects occur — besides a velocity decrease — in the range of the deposit:

— In the deposit and especially above it (aureole due to geochemical processes) there is a directly computable increase of absorption which leads also to a change of the dynamic properties of seismic waves. From the parameters presented in Figs. 2 and 3 these are the dominant frequency f_v, the upper cut-off frequency f_0, and the mean period T_m.

— The range of the deposit is indicated by amplitude increases (bright spots). These are caused by a change of pore filling thereby generating an increase of reflectivity. Here the parameters A_m, E_m, and E_{max} (Fig. 3) are of interest.

— Both absorption and bright spots superimpose in an opposite sense. This superposition results in an increase of the low-frequency components of the amplitude spectrum as a consequence of the frequency dependence of attenuation. The distribution of the properties A_{max} and especially A_{10} to A_{16} must be attributed to this effect (see Figs. 2 to 5). The decay of the anomaly at frequencies above 18 Hz is considered as an overcompensation of the bright spot effect by attenuation. Model-computations verify these effects.

4. Conclusions

Dynamic properties of seismic waves may be changed characteristically in the range of hydrocarbon deposits due to absorption and variation of reflectivity or the combination of both effects. Hence, their evaluation is an essential element of direct detection techniques.

A very clear connection is revealed between the location of the deposit and the distribution of several low-frequency components of the amplitude spectrum. Due to the interaction of the two effects mentioned above some amplitude samples of the low-frequency part of the amplitude spectrum are increased only in the range of the deposit. This hitherto not described effect could be confirmed

by investigations of several objects; it explains the distribution of samples of the amplitude spectra presented in Figs. 4 and 5.

It seems to be expedient to accomplish the computation of dynamic parameters in the manner described above, i. e. within time windows shifted along the seismic trace. Against this, the results of parameter determinations along reflective horizons of for single reflections are less efficient.

In general, one can state that the use of the direct detection method makes a significant contribution to the verifiableness of reflection seismics. Given satisfactory initial values adaptation of this method makes it possible to get information about the presence of hydrocarbons in the subsurface. Depending upon the complexity of the model either statements on the general prospectiveness of one region or — as above demonstrated — additonal data on the localization as well as on the limitation of hydrocarbon deposits are possible. Uncertainties cannot be ruled out.

REFERENCES

PATZER U., PRÖHL S. 1980: Ein praktisches Beispiel für die Nutzung der Reflexionsseismik zum Direktnachweis von Kohlenwasserstoff-Lagerstätten. Geophysik und Geologie (Geophysikalische Veröffentlichungen der Karl-Marx-Universität), Leipzig, 2, pp. 107—115

PRÖHL S., PATZER U., REGENSBURGER H., LEIßRING B., 1978: Zur Anwendung der Reflexionsseismik für den Nachweis substantieller Änderungen. Schriftenreihe Geologische Wissenschaften, Berlin, 12, pp. 27—38

Fig. 4. x, t-plane distribution of the amplitude spectrum between 10 and 20 Hz

4. ábra. Az amplitúdóspektrum eloszlás függvénye 10 és 20 Hz között az x—t síkban

Рис. 4. Распределение выборок амплитудного спектра между 10 и 20 Гц по плоскостям x, t

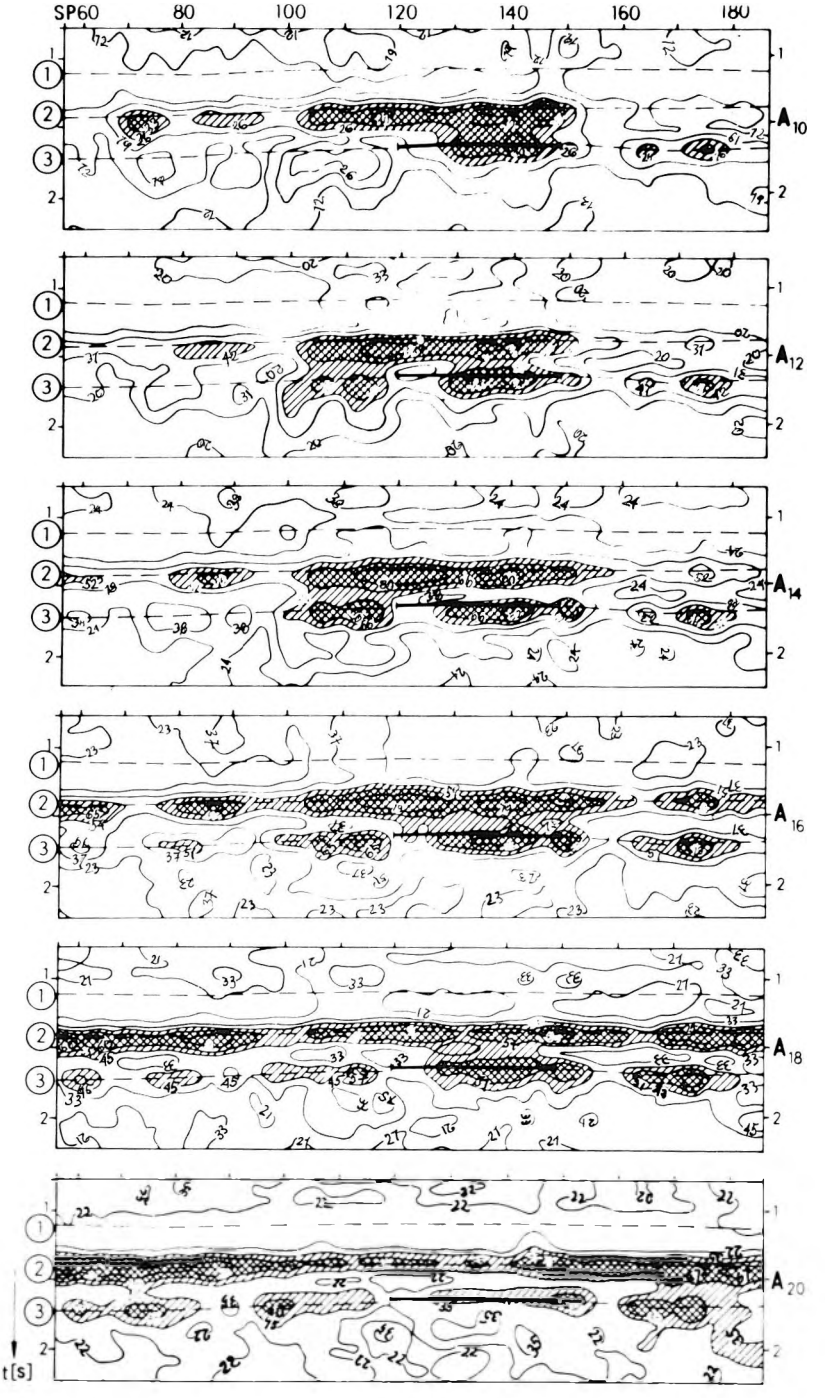
SP60
80
100
120
140
160
180
A10
A12
A14
A16
A18
A20
t[s]

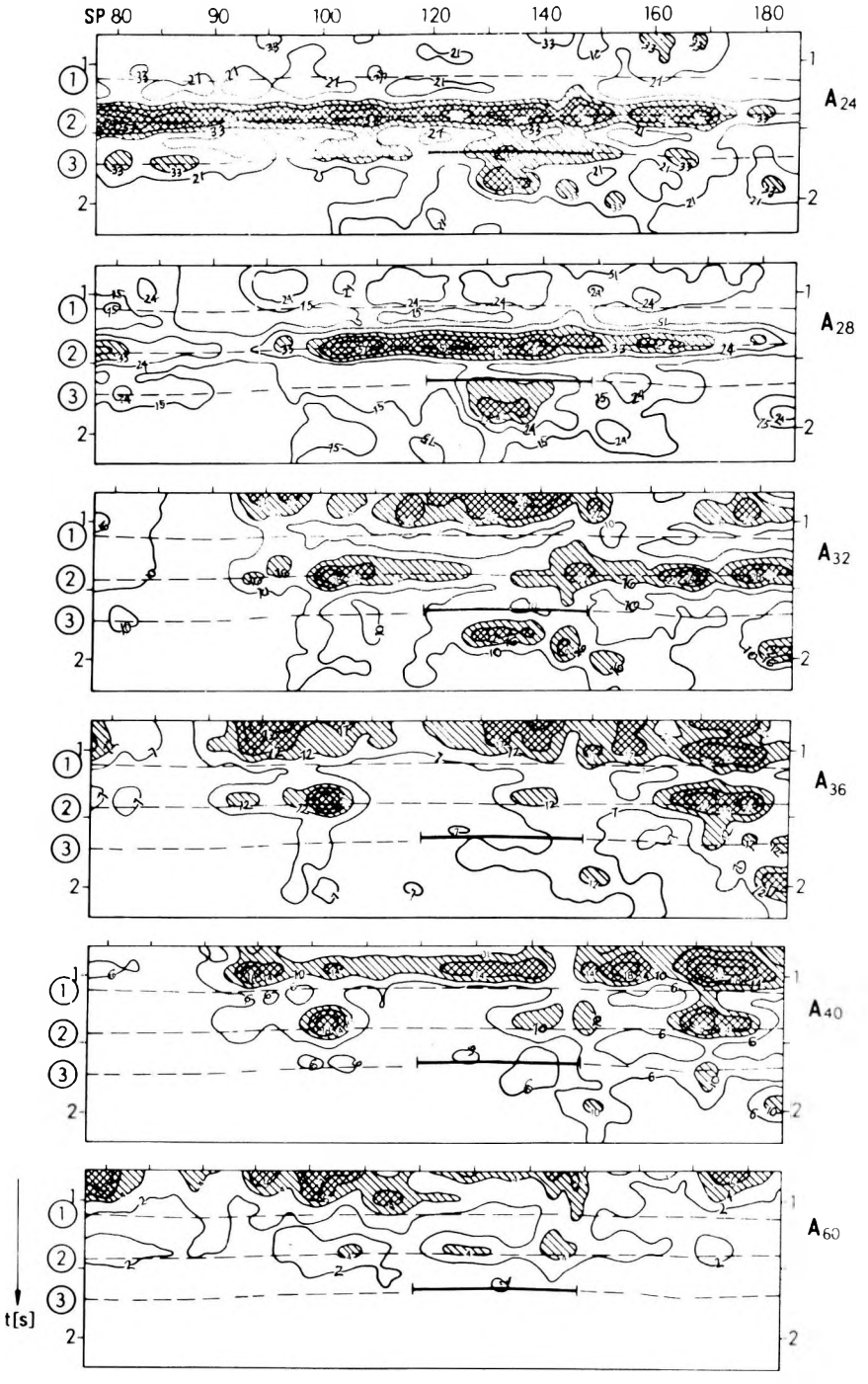
SP 80
90
100
120
140
160
180
A24
A28
A32
A36
A40
A60
t[s]

A SZEIZMIKUS HULLÁMOK SPEKTRÁLIS PARAMÉTEREINEK VÁLTOZÁSAI A SZÉNHIDROGÉN-ELŐFORDULÁSOK KÖRNYEZETÉBEN

Stefan PRÖHL

Áttekintést adunk arról, hogy a szénhidrogéntelepek közvetlen kimutatásában a szeizmikus hullámok spektrális paramétereinek milyen alkalmazási lehetőségei vannak. A lipcsei VEB Geophysik-nél ESzR számítógépre kidolgoztak egy programot, mely a különféle dinamikus mérőszámok, mindenekelőtt a spektrális paraméterek kiszámítására alkalmas. Ezen paraméterek kiszámításának módját ismertetjük és eredményeinket egy kőolaj-előfordulást keresztező szelvény feldolgozásának példáján mutatjuk be.

ИЗМЕНЕНИЕ СПЕКТРАЛЬНЫХ СВОЙСТВ СЕЙСМИЧЕСКИХ ВОЛН В ПРЕДЕЛАХ НЕФТЕГАЗОВЫХ МЕСТОРОЖДЕНИЙ

С. ПРЁЛ

В работе обсуждаются вопросы применения спектральных свойств сейсмических воли для прямых поисков месторождений нефти и газа. На предприятии ВЭБ Геофизика г. Лейпциг (ГДР) была разработана специальная программа для ЕС ЭВМ, которая позволяет удобно рассчитать некоторых динамических, в том числе спектральных параметров. Описывается метод вычисления этих параметров и приводятся результаты исследований, проведенных по профилю, пересекающему известные нефтяные залежи.

Fig. 5. x, t-plane distribution of the amplitude spectrum between 24 and 60 Hz

5. ábra. Az amplitúdóspektrum eloszlásfüggvénye 24 és 60 Hz között az *x—t* síkban

Рис 5. Распределение выборок амплитудного спектра между 24 и 60 Гц по плоскостям *x, t*

GEOPHYSICAL TRANSACTIONS 1984
Vol. 30. No. 2. pp. 213—223

INTEGRATED INTERPRETATION OF GEOPHYSICAL EXPLORATION DATA FOR DETECTING RESERVOIR-TYPE ANOMALIES

R. G. BERZIN, E. A. KOZLOV, O. A. POTAPOV, V. S. PAVLUSHIN, Y. A. TARASOV, S. S. CHAMO*

The efficiency of integrating geophysical methods for reservoir delineation and location of water lenses therein is demonstrated with reference to a hydrocarbon deposit in south-west Turkmenia. Although seismics is the most informative method, high-accuracy gravity and geoelectric prospecting yield important additional geophysical data thereby increasing the reliability of locating geological inhomogeneities, zones of lithofacies changes in reservoirs, and gas–water and oil–water interfaces.

d: oil and gas fields, oil–gas interface, oil–water interface, seismic methods, magnetotelluric methods, transient methods, statistical analysis

1. Introduction

As more and more complicated problems must be solved associated with the exploration and prospecting of deep-seated objects containing gas and oil, the identification of structural traps differing from anticlinal ones, gas—water —oil interfaces and zones of lithofacies changes in reservoirs, the necessity arises to integrate geophysical methods. Experience has recently been gained in the integrated use of geophysical methods enabling, in numerous cases, much more accurate and reliable identification of the objects being sought for and allowing problem solution at a higher geological and economic level.

This paper deals with integration as a method for the more reliable identification and tracing of the gas—water—oil interfaces of a large condensed gas field of unusual structure in south-east Turkmenia.

2. Description of region

As shown by the data of geophysical – primarily seismic – investigations and deep drillings carried out within the examined region, its structure is represented by two large dissimilar tectonic elements linked together: the deep-seated Murgab depression in the north and a zone of large swell-like structural

* NPO Neftegeofizika, 103062 Moscow, Chernyshevskogo 22, USSR
Paper presented at the 28th International Geophysical Symposium, Balatonszemes, Hungary, 28 September — 1 October, 1983

height forming the Badkhyz—Karabil—Maimanin elevated zone in the south. On closer examination, three zones can be distinguished within it: the top of the swell-like uplift in the south, monoclinal north-dipping beds in the centre, and an extensive terrace-like zone in the north.

The top of the swell-like uplift has a particularly complex tectonic pattern, as there is a series of local small-amplitude heights and zones of tectonic dislocations.

The zone of monoclinal north-dipping beds has a much simpler tectonic pattern. Judging by the results of the refraction correlation method (RCM), a large deep-seated fault zone is enclosed within it thus complicating the structure of the crystalline basement and the deeper layers of the earth's crust.

The terrace-like zone in the north is nearly flat-bedded with local small-amplitude heigths not very large in size.

The gas field itself has a most unusual structure due to two peculiarities of its spatial and areal situation. Firstly, the field is restricted to the Hauterivian sandstones and is very extended. Within its boundaries the depth of the pay zone changes from 2800 to 3600 m in a monoclinal manner, i.e. its localization is influenced somewhat by structural factors. Secondly, an extensive lens has been detected within the field that is characterized by higher water content and noticeable decrease or lack of gas-saturation.

3. Investigation

It may be expected that direct detection within such fields of unusual structure and considerable size (cross-sectional width is over 55—60 km) will be very difficult and not highly effective at the initial stage because of numerous factors, the principal ones being:

a) Extremely unfavourable seismogeological conditions on the surface and at lower depths (twice or three-times layered low velocity zone (LVZ) with a thickness ranging from 10—15 to 200 m) giving a low signal-to-noise ratio.

b) Complex tectonic pattern of the examined irregular object and specific structural conditions of its spatial localization (crowns, monoclinal dips, deep-seated zones with subhorizontal altitudes of bedding, etc.).

c) High probability of the presence of other irregularities within the section of such an extended field, associated both with water lenses (places of higher water content) and with lithofacies changes, fault zones, unconformities, pinching out, local changes in surface conditions, etc.

d) Lack of experience in prospecting giant fields of this kind.

The above peculiarities pointed to the need for high-facility geophysical investigations using advanced digital equipment to refine the structural details and to identify and trace within the area the contours of irregularities associated with the gas field and high water content lenses.

Geophysical investigations were performed in two steps. In the first step

all available seismic data (5000 km CDP profiles) were processed by a fast-analysing program to yield integral characteristics.

Characteristic shapes of plots for absorption parameters β and δ (local, not too long high-gradient zones) together with higher $R(t)$ values of the autocorrelation function helped to provide preliminary identification and trace a series of anomalous zones presumably associated with gas—water interfaces in the western, northern and southern parts of the area *(Fig. 1)*.

Lower absorption parameters in the central part of the area indicated a transition zone with possibly smaller gas content and with a high gradient zone inside it. Unambiguous interpretation of these data, however, did not seem possible without more reliable data of deep drillings and integrated geophysical methods including digital seismic prospecting. Therefore integrated field studies were carried out simultaneously, including CRP prospecting that ensures 24-fold coverage, high-facility areal gravity prospecting and modified methods of electric prospecting — magnetotelluric sounding (MT) and transient electromagnetic sounding (TEM).

The results of all these field studies were processed by computer using a standard graph and a set of programs for special-purpose data analysis.

4. Interpretation

The results are reported citing as an example one of the seismic sections crossing the whole gas field and the contained water lens in the near N—S direction.

If one analyses the basic characteristics of the wave field *(Fig. 2)* it can be seen that a series of key or characteristic seismic horizons can be singled out within the interval of interest on the geological section. Firstly there is a well-defined key reflecting horizon restricted to Bukhara limestones of the Lower Palaeogene, whose signal is recorded within 1.0—1.1 s. Then follows a carbonate bed dating back to the Lower Aptian—Upper Barremian ($t_0 = 1.8 - 1.9$ s) and a terrigenous carbonate layer of the Hauterivian ($t_0 = 1.85 - 2.0$ s). In addition, a number of characteristic horizons were recorded on the section, confined to the Middle Palaeogene ($t_0 = 0.7$—0.9 s) and Upper Cretaceous: $K_2^5(t \approx 1.35$—1.45 s), $K_2^1(t \approx 1.5$—1.6 s).

The pay-zone is confined to Hauterivian sandstones, which gives the Lower Cretaceous sand-and-carbonate complex and its geophysical characteristics great importance.

The detailed velocity analysis was made in the time interval of 1.0—2.4 s. Horizontal spectra give information on velocity characteristics V_{CRP} for four reflecting horizons: Bukhara limestones of the Lower Palaeogene, and sand-carbonate beds of the Barremian, Hauterivian and Upper Jurassic stages. Layer velocities V_l are characterizing the change of the properties in section intervals bounded by the indicated horizons.

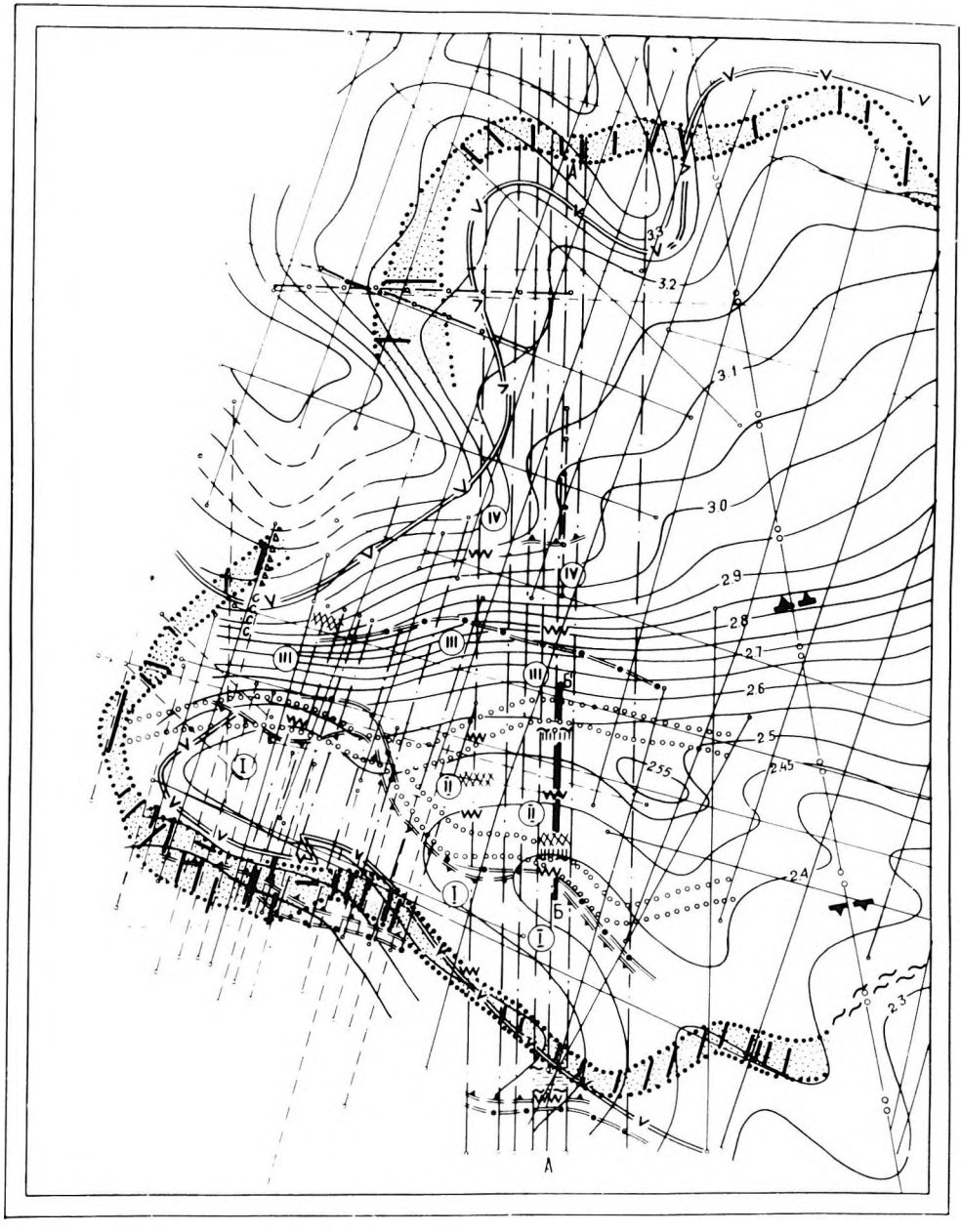

1 2 3 4 5 6 7
8 9 10 11 12 13 14
15 16 17 18 19 20

Fig. 1. Sketch map of anomalous zones in the investigated area
1 — contours of the bottom of the Hauterivian producing layer (IV); 2 — zone of greater values of absorption parameters, presumably associated with minor dislocations sorrounding the water lens; 3 — zones of large basement faults (from refraction survey); 4 — assumed tectonic dislocations (TEM data);
5 — reflection profiles; 6 — CDP profiles; 7 — refraction profiles; 8 — electric and gravity profiles; 9 — inner contour of gas reservoir from borehole data; 10 — band of abnormally high values of absorption parameters, presumably associated with gas–water interface; 11 — zones of high absorption parameter gradients resulting from gas–water interface irregularities;
12 — water lens; 13 — anomalous zones of seismic wave field ("flat spots") for the Hautervivian (upper mark) and for the upper Jurassic (lower mark); 14 — abnormally high absorption zones at traveltimes greater than 2.9 s (Jurassic); 15 — boundaries of transient electromagnetic anomalies; 16 — zone of higher values of summarized longitudinal conduction and vertical increments of apparent conduction using MT data, presumably associated with the water lens; 17 — anomalous zone of MT parameters presumably associated with gas–water interface; 18 — outer contour of gas presence from gravity data; 19 — boundaries of second order gravity zones; 20 — possible contour of gas–water contact

1. ábra. A kutatott terület anomáliáinak vázlata
1 — az hauterivi termelő réteg aljának izohipszái (IV); 2 — valószínűleg a vízlencse körüli kisebb diszlokációknak megfelelő magas abszorpciójú zónák; 3 — az aljzat töréseinek zónája (refrakciós mérésekből); 4 — feltételezett tektonikus diszlokációk (TEM-adatok); 5 — reflexiós szelvények; 6 — CDP-szelvények; 7 — refrakciós szelvények; 8 — elektromos és gravitációs szelvények; 9 — a gáztároló belső kontúrja, fúrási adatok alapján; 10 — valószínűleg víz—gáz határfelülettel kapcsolatos magas abszorpciójú anomáliák; 11 — feltehetőleg a gáz—víz határ egyenetlenségeivel kapcsolatos abszorpció-gradiens anomáliák; 12 — vízlencse; 13 — hauterivi (felső jel) és felső jura (alsó jel) összleteknek megfelelő szeizmikus anomáliák („flat spots"); 14 — 2,9 s-nál nagyobb menetidőknek (jura) megfelelő abszorpciós anomáliák; 15 — TEM anomáliák határa;
16 — feltehetően a vízlencsével kapcsolatos MT-anomáliák: az összegzett hosszirányú vezetőképesség és a vertikális látszólagos vezetőképesség megnövekedett értékeinek zónái; 17 — feltehetően a gáz—víz határral kapcsolatos MT-anomáliák; 18 — a gáztároló külső kontúrja, gravitációs mérésekből; 19 — a másodrendű gravitációs zónák határa; 20 — gáz—víz kontaktus valószínű határa

Рис. 1. Схематическая карта аномальных зон на площади исследований в сопоставлении с данными глубокого бурения
1 — стратоизогипсы подошвы продуктивного горизонта (IV) готеривского яруса; 2 — зона повышенных значений парметров поглощения, предположительно связанная с мелкими нарушениями, ограничивающими водяную линзу; 3 — зоны крупных разломов в фундаменте (по КМПВ); 4 — предполагаемые тектонические нарушения (данные ЗСМ); Сейсмические профили: 5 — МОВ; 6 — МОГТ;
7 — КМПВ; 8 — Электро и гравиразведочные профили; 9 — внутренний контур газоносности по геологическим данным; 10 — полоса аномально высоких значений параметров поглощения, предположительно связанная с ГВК; 11 — зоны максимальных градиентов (ЗМГ) параметров поглощения, обусловлен неоднородностями в полосе ГВК;
12 — площадь водяной линзы; 13 — участки аномальной структуры волнового сейсмического поля («плоские пятна»), характеризующего готеривский комплексы;
14 — зоны аномально выского поглощения, выделяемые на временах более 2,9 с (юра);
15 — границы электрических аномалий ЗСМ; 16 — зона повышенных значений суммарной продольной проводимости и вертикалных приращений кажущейся проводимости по данным МТЗ, предположительно связанная с водяной линзой; 17 — аномальная зона параметров МТЗ, возможно связанная с ГВК; 18 — внешний контур нефтеносности по гравиметрическим данным; 19 — границы гравитационных зон II порядка; 20 — возможное продолжение внутреннего контура ГВК на ЮВ площади

The results derived calculating V_l values between two Neocomian horizons K_1br—K_1h are of the greatest interest. Analysis of the $V_l(X)$ K_1br—K_1h curve and its comparison with the geological data show that no distinct and reliable correlation exists between velocity and section irregularities. For this bed within field boundaries a zone of low V_l values turns out to be rather wide, with three local maxima within it. The most well-defined maximum is attributed to the water lens *(Fig. 2)*; the nature of the other two maxima is unknown so far.

The V_l data fail to delineate clearly the gas—water interfaces as well. The V_l values tend to increase only at the southern end of the field.

Thus parameter (V_l) can hardly be a basic detector for identification of section irregularities of interest under the given seismogeological conditions (small pay zone thickness — not exceeding 25—40 m resulting in gross errors in velocity measurements, comparable with expected anomalies of 0.5—0.6 km/s; complex tectonic pattern of field and widely varying low velocity zone thickness, etc.). The data of this analysis, however, should not be neglected when starting complex data processing, since they make the statistical data set more complete.

Dynamic characteristics of reflected waves were studied by the corrected amplitude time section (CATS) and by analysing the amplitudes and quasi-periods for each horizon using a computer program. Analysis of corrected amplitude time section data for the Neocomian horizons indicates with fair certainty a water lens characterized by clearly visible general amplitude decrease of the wave reflected from the top of the pay zone.

Amplitude decrease is particularly abrupt within loci confined to shear zones. It is also quite distinct in the time section (Fig. 2). Summarized, the water lens is characterized by sudden level changes over short intervals on records of the reflected wave. Structural peculiarities of dynamic characteristics of waves from the Neocomian horizons, found on corrected amplitude time sections, conform fairly well with the calculated data on quantitative amplitude characteristics. Within the water lens, for example, a reduction of 6—8 dB was obtained for intensity of the wave from the top of pay zones and a significant lengthening of quasi-periods. Distinct quasi-period lengthening was also recorded within the southern gas—water interfaces and outside the section contours.

To analyse and study the dynamic parameters of reflected waves we used the computer program package "Command" for two types of seismograms, i.e. for the standard time section and for the corrected amplitude time section. The applied time window was 100 ms with 50 ms equalization in both directions related to the interval centre-line corresponding to the time of the basic phase of the horizon being analysed. As a result, the summarized dynamic parameter (Σ) for the wave from the top of the pay zone made it clear that an anomalous zone does exist within the water lens. The standard time section provided a well-recorded minimum of the parameter Σ within this zone, looking like a long band of negative values. The corrected amplitude time section also proved the existence of this minimum but the anomalous zone is even more recognizable by the dispersed values of the single and summarized parameters *(Fig. 3)*. By the minima of parameter Σ the off-contour parts of the gas field can be distin-

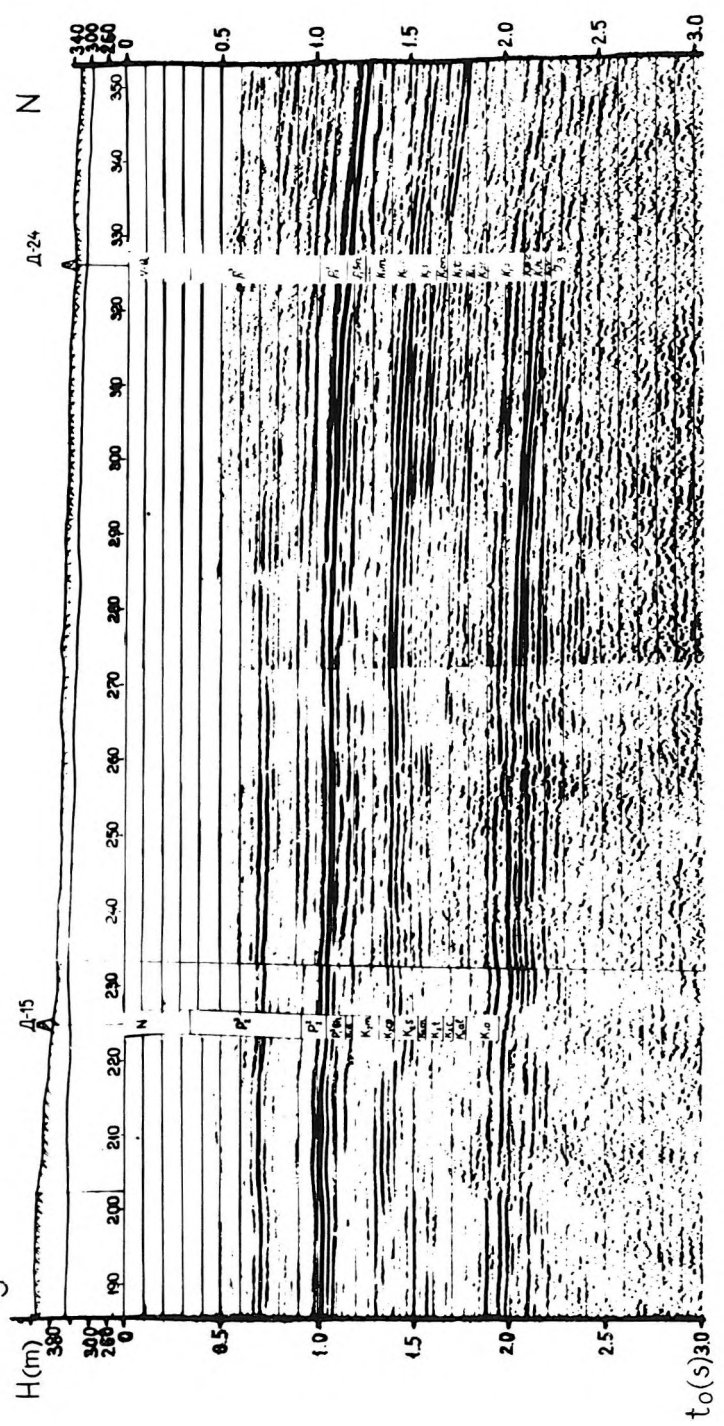

Fig. 2. Fragment of seismic time section (line Б—Б′ in Fig. 1)

2. ábra. Az 1. ára Б—Б′ vonala mentén felvett szeizmikus időszelvény részlete

Рис. 2. Фрагменты временного сейсмического разреза (линия Б—Б′ на рис. 1.)

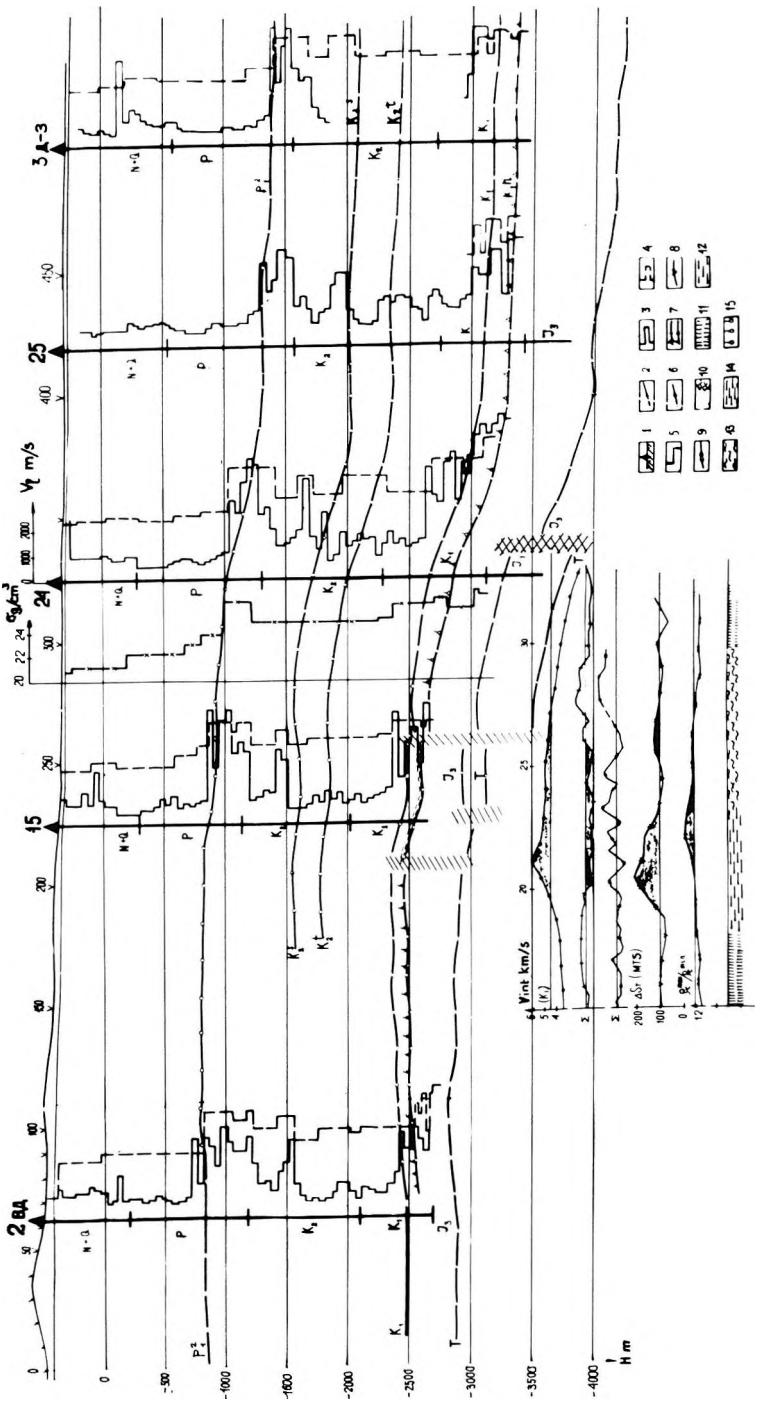
2 84
15
24
25
3 А-3
σ g/cm³
Vt m/s
Vint km/s
H m

guished with comparative certainty. Positive-to-negative transition of parameter values takes place in the vicinity of the gas—water interfaces.

The data of other geophysical methods are less informative but they supplement and refine the seismic prospecting data to a fairly high degree. MTS impedance curves, for example, have abnormal distortions within the water lens, recorded in the form of local minima indicating a lower impedance zone occurring on the section. In the field of vertical increments of apparent longitudinal conduction and in summarized longitudinal conduction the anomalous zones are identified by the maxima of these parameters. A similar maximum was recorded within the northern gas—water interfaces and outside the section contours. Judging from the transient magnetotelluric sounding data, the water lens coincides with the anomalous zone of the parameters (Fig. 3).

Fig. 3. Curves of geophysical parameters within the water lens (line Б—Б') as compared with the seismic section and drilling results (along line A—A')
1 — boreholes; 2 — marker horizons; 3 — resistivity; 4 — layer velocity; 5 — density; 6 — interval velocity; 7 — summarized dynamic parameter defined by standard time section (upper mark) and by corrected amplitude time sections (lower mark); 8 — increments of apparent ongitudinal conduction (according to MTS); 9 — $\varrho_\tau^{max}/\varrho_\tau^{min}$ curve (according to TEM); 10 — supposed teectonic dislocations (from seismic data). Local zones identified by the results of areal processing of the gravity data, showing; 11 — maximum probable presence of gas; 12 — maximum probable absence of gas; 13 — equally possible presence or absence of gas. 14 — Water lens; 15 — gas field

3. ábra. A vízlencsét metsző vonalon (Б—Б') végzett geofizikai mérések, és az A—A' vonalon kapott fúrási adatok összehasonlítása
1 — fúrás;2 — vezérszint; 3 — ellenállás; 4 — rétegsebesség; 5 — sűrűség; 6 — intervallumsebesség; 7 — összegzett dinamikus paraméter, standard időszelvény alapján (felső jel) és korrigált amplitúdójú időszelvény alapján (alsó jel); 8 — a látszólagos ellenállás longitudinális növekményei (MTS-adatok). 9 — $\varrho_\tau^{max}/\varrho_\tau^{min}$-görbe (TEM-mérések alapján); 10 — feltételezett tektonikus elmozdulások (szeizmikus adatokból). A gravitációs adatok területi feldolgozása alapján azonosított lokális zónák: 11 — gáz előfordulásának maximális valószínűsége; 12 — gáz hiányának maximális valószínűsége; 13 — gáz előfordulásának és hiányának egyenlő valószínűsége. 14 — Vízlencse; 15 — gázmező

Рис. 3. Графики геофизических параметров в пределах водяной линзы (линия Б—Б') в сопоставлении с глубинным сейсмическим разрезом и результатами глубокого бурения (по линии А—А')
1 — глубокие свкажины; 2 — опорные отражающие горизонты. Графики изменения с глубиной: 3 — электрического сопротивления; 4 — пластовой скорости; 5 — плотности. Графики геофизических параметров: 6 — интервальной скорости; 7 — суммарного динамического параметра, определенного: высший — по стандартному временному разрезу, низкий — по временному разрезу СОА; 8 — приращения кажущейся продольной проводимости (по МТЗ); 9 — график $\varrho_\tau^{max}/\varrho_\tau^{min}$ (по ЗСМ); 10 — предполагаемые тектонические нарушения (по данным сейсморазведки). Локальные зоны, выделенные по результатам площадной обработки гравиметрических данных, характеризующие: 11 — высокую вероятность присутствия газа; 12 — высокую вероятность отсутствия газа; 13 — равную вероятность присутствия или отсутствия газа. 14 — Область водяной линзы; 15 — поле газовой залежи

The data of high-facility gravitation studies enables the water lens and the adjacent zone of layers dipping north in a monoclinal manner to be considered as a unit, i.e. as a transition zone characterized by small-amplitude, sign-changing and not very extensive local anomalies most often recorded within small structures with a hydrocarbon deposit. The not very extensive mosaic structural pattern of local anomalous zones, the abrupt change of signs and the strike lines of anomalies, etc. all point to the complex structure of the transition zone. Its section may contain irregularities of various sizes and different in physico-geological characteristics. This concept is also confirmed by the distribution pattern of anomalous zones identified by means of directed narrow-band reception technique. The results produced after the data of high-facility gravitation prospecting processed by different methods have made it possible to imagine that the hydrocarbon deposit is not so widely spread over the transition zone but restricted to some localities of near N—S strike.

5. Conclusions

The results allow the following to be stated:

a) The most imformative data for studying the water saturated lens and reservoir contours are amplitude characteristics of reflections from the pay zone boundaries and interval velocities.

b) The data of precision gravity and electric prospecting supplement the seismic prospecting data and ensure more reliable identification of the water saturated lens, and the gas—water and water—oil interfaces.

c) Reliable information on structural peculiarities of objects having complex tectonic pattern can only be obtained by different geophysical methods and by integration of all these methods.

A GEOFIZIKAI KUTATÁSI ADATOK KOMPLEX ÉRTELMEZÉSE TÁROLÓ-TÍPUSÚ ANOMÁLIÁK KIMUTATÁSÁRA

R. G. BERZIN, E. A. KOZLOV, O. A. POTAPOV, V. S. PAVLUSIN, Y. A. TARASZOV, S. S. CSAMO

A tanulmány egy Délnyugat-Türkméniában fekvő szénhidrogén-lelőhely példáján bemutatja a geofizikai módszerek komplex alkalmazásának hatékonyságát a tároló határainak kijelölésében és a benne elhelyezkedő vízlencsék lokalizálásában. Jóllehet a legtöbb információt a szeizmikus módszerek nyújtják, a preciziós gravitációs és geoelektromos módszerek hasznos kiegészítő adatokkal járulnak hozzá a geológiai inhomogenitások, a tárolókat jellemző litofácies változások meghatározásához, valamint a gáz—víz és olaj—víz határfelületek lokalizálásához.

КОМПЛЕКСНАЯ ИНТЕРПРЕТАЦИЯ ДАННЫХ РАЗВЕДОЧНОЙ ГЕОФИЗИКИ С ЦЕЛЬЮ ВЫДЕЛЕНИЯ АНОМАЛЬНЫХ ЗОН

Р. Г. БЕРЗИН, Е. А. КОЗЛОВ, О. А. ПОТАПОВ, В. С. ПАВЛУШИН, Ю. А. ТАРАСОВ, С. С. ЧАМО

На примере одного из месторождений углеводородов Юго-Западной Туркмении показана целесообразность комплексирования геофизических методов как для уточнения контуров залежи, так и для выявления в пределах этих контуров водяных линз. Хотя наиболее информативным является метод сейсморазведки, но при изучении сложнопостроенных объектов разведки дополнительную и часто важную чию даёт высокоточная гравиметрия и электроразведка. Комплексная интерпретация данных разведочной геофизики обеспечивает повышение надежности выявления неоднородностей геологического разреза, обнаружения зон лито-фациального замещения коллекторов, ГВК и НВК.

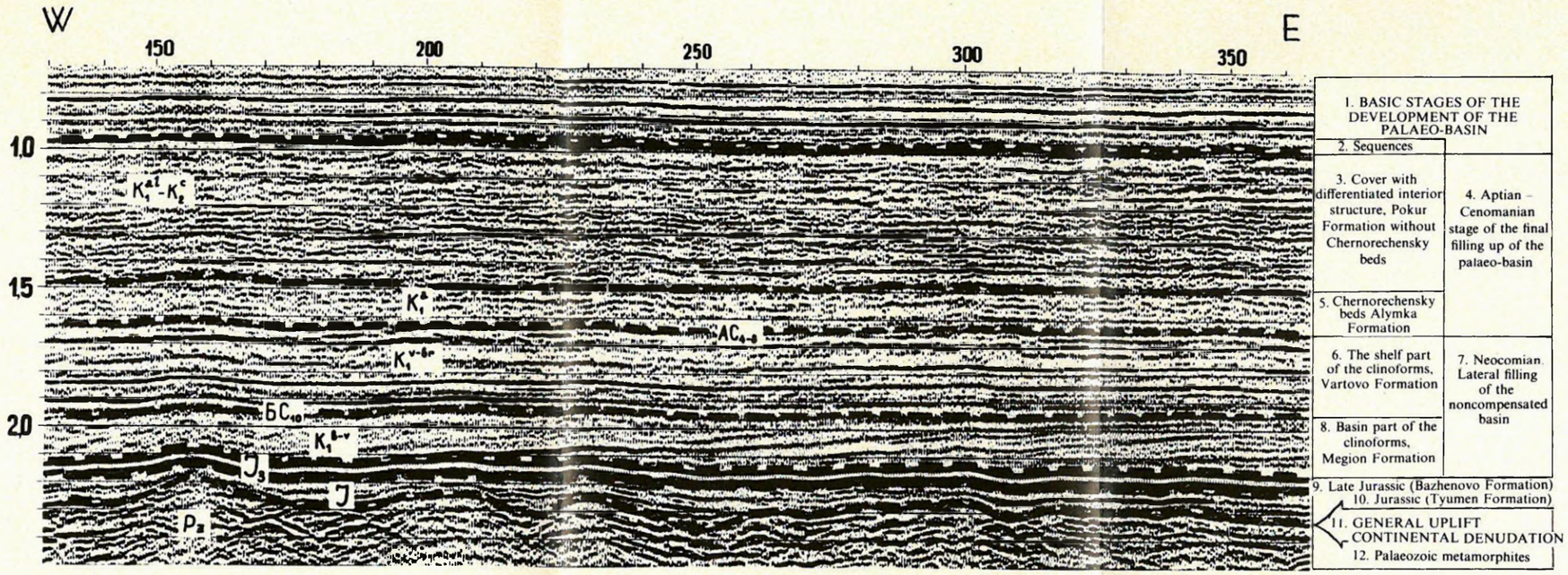

Fig. 3. Division of a seismic section of the Fedorovskaya area into seismic sequences

3. ábra. A Fedorovszkaja terület szeizmikus szelvényeinek felosztása szeizmikus rétegsorokra 1—A PALEO-MEDENCE FEJLŐDÉSÉNEK SZAKASZAI; 2—rétegsorok; 3—differenciált belső szerkezetű fedő (Pokur Formáció, Csernorecsenszki rétegek nélkül); 4—a paleo-medence apti-cenomániai feltöltődése; 5—fedőréteg differenciálatlan szekezettel, Csernorecsenszki rétegek, Alümka Formáció; 6—a klinoform összlet shelf-része, Vartovo Formáció; 7—nokom. A nem-kompenzált medence oldalirányú feltöltődése; 8—a klinoform összlet medence-része; 9—a zavartalan szedimentáció késő jura szakasza (Bazsenovo formáció); 10—jura, a feltöltődés kezdeti szakasza (Tyumeni Formáció); 11—ÁLTALÁNOS KIEMELKEDÉS, KONTINENTINÁLIS LEPUSZTULÁS; 12—paleozoós metamorfitok

Рис. 3. Выделение седиментационных сейсмических комплексов на временном разрезе Федоровской площади
1—ОСНОВНЫЕ ЭТАПЫ РАЗВИТИЯ ПАЛЕОБАССЕЙНА; 2—комплексы; 3—покров с дифференцированным внутренним строеннием, Покурская свита без чернореченской толщи; 4—апт-сеноманский этап конечного заполнения палеобассейна; 5—покров с недифференцированным внутренним строением, чернореченская толща, алымская свита; 6—покров — шельфовая часть клиноформы, вартовская свита; 7—неокомский этап бокового заполнения некомпенсированнои впадины; 8—депрессионная часть клиноформы, мегионская свита; 9—позднеюрский этап успокоения (Баженовская свита); 10—юрский этап начального заполнения (Тюменская свита); 11—ОБЩЕЕ ВОЗДЫМАНИЕ, КОНТИНЕНТАЛЬНАЯ ДЕНУДАЦИЯ; 12—палеозойский переходный этаж